

THE FORMATION OF RNA POLYMERS ON  
PRIMITIVE EARTH

# THE FORMATION OF RNA POLYMERS ON PRIMITIVE EARTH

By ALIX DUJARDIN, M.sc.

A Thesis Submitted to the School of Graduate Studies in Partial  
Fulfillment of the Requirements for  
the Degree Master of Science

McMaster University © Copyright by Alix Dujardin, April 2023

McMaster University

MASTER OF SCIENCE (2023)

Hamilton, Ontario, Canada (Chemistry and Chemical Biology)

TITLE: The formation of RNA polymers on primitive Earth

AUTHOR: Alix Dujardin  
M.sc. (Biogeosciences),  
Université de Rennes 1, France

SUPERVISOR: Dr. Maikel C. Rheinstädter and Dr. Ralph Pudritz

NUMBER OF PAGES: xxi, 124

# Abstract

One of the greatest scientific mysteries of all time is the Origin of Life on Earth. Life on Earth may have emerged with a unique molecule: Ribonucleic Acids (RNA). The RNA world for the origin of life is a theory that states that life started with RNA before DNA and proteins because RNA molecules can auto-replicate and store genetic information.

This thesis aims to expose how such RNA molecules could have been formed on a primitive Earth without the presence of other catalytic biomolecules such as enzymes. The model used in this thesis is the warm little ponds theory for the origin of life. RNA molecules could have been formed in these ponds thanks to wet-cold and warm-dry cycles. We used new experimental and computational technologies to try to answer this dilemma. Using a new machine, the *Planet Simulator*, which can mimic primitive environments by controlling five physical parameters, we found that extreme heat and low pH would destroy the building blocks of RNA. However, Molecular Dynamics computer simulations showed us that neutral pH could have led to the formation of RNA. Still, the presence of any surfaces and substrates would have decreased the polymerization rate due to the number of interactions between the RNA building blocks and the minerals substrates. We then found a new vision of where life could have come from: in super-saturated water droplets, which could

have been formed by geysers or springs on primitive Earth. We tested this theory experimentally using an acoustic levitator to levitate super-saturated droplets and study them in the laboratory. Our preliminary results showed that RNA could have been formed in such droplets on primitive Earth.

*To the people in my life who pushed me along the way,  
You made me stronger.*

# Acknowledgements

I would not have been here if it was not for the people that helped me along this path.

First, I want to thank my supervisors, Dr. Maikel Rheinstädter and Dr. Ralph Pudritz, who taught me a lot about science and research. You always pushed me to give the best of myself and gave me a lot of opportunities for growth and improvement. Thank you to my collaborators and committee members Sebastian Himbert, Jon Stone, Paul Higgs, and Paul Harrison. You helped me see with a new vision the research I did to make it better.

Thanks to my lab mates: Sanne, Taren, and Rachel. A special thanks to my person in the lab, the one who makes me laugh even though she does not know it, Hannah Krivic. You helped me have the light shine on me by singing along with me.

Also, thank you to the people who love me, my friends and family, as well as my new Canadian family; your support and understanding mean a lot to me.

Finally, I want to thank my partner in life who became throughout these two years my crush, my boyfriend, my roommate, and my fiancé. This would not have been possible without you.

# Table of Contents

<b>Abstract</b>	<b>iii</b>
<b>Acknowledgements</b>	<b>vi</b>
<b>Abbreviations</b>	<b>xxi</b>
<b>Declaration of Academic Achievement</b>	<b>xxii</b>
<b>1 Introduction</b>	<b>1</b>
1.1 The RNA world . . . . .	2
1.2 Activated nucleotides versus non-activated nucleotides . . . . .	6
1.3 RNA polymerization . . . . .	13
1.4 Life could have formed in Warm Little Ponds . . . . .	14
1.5 Outlines of thesis research . . . . .	18
<b>2 Acidic environment does not favor the formation of RNA polymers in a prebiotic salty Warm Little Pond.</b>	<b>19</b>
2.1 Preface for Acidic environment does not favor the formation of RNA polymers in a prebiotic salty Warm Little Pond. . . . .	20
2.2 Introduction . . . . .	21

2.3	Materials and Methods . . . . .	25
2.4	Results . . . . .	34
2.5	Discussion . . . . .	42
2.6	Conclusion . . . . .	45
<b>3</b>	<b>The formation of RNA pre-polymers in the presence of different prebiotic mineral surfaces studied by Molecular Dynamics simulations</b>	<b>46</b>
3.1	Preface for Paper I . . . . .	47
<b>4</b>	<b>The formation of RNA oligomers in supersaturated levitated droplets</b>	<b>76</b>
4.1	Preface for The formation of RNA oligomers in supersaturated levitated droplets . . . . .	77
4.2	Introduction . . . . .	79
4.3	Materials and Methods . . . . .	81
4.4	Preliminary Results . . . . .	85
4.5	Discussion . . . . .	88
4.6	Conclusion . . . . .	90
<b>5</b>	<b>Conclusions</b>	<b>91</b>
<b>A</b>	<b>Appendix</b>	<b>95</b>
A.1	Gel electrophoresis . . . . .	95
A.2	MD Simulations . . . . .	103

# List of Figures

1.1	A) shows the linkage between phosphate, sugar, and base (adenosine (A), uracil (U), guanosine (G), and cytosine (C)). Ribonucleic acid (RNA) is composed of a sugar-phosphate backbone linked via a phosphodiester bond between the <i>C3'</i> and the <i>C5'</i> of the sugar. B) shows the unfolded structure of RNA where this one can be translated but is not catalytic. C) shows the folded structure where RNA is catalytic but can not be translated. . . . .	5
1.2	Representation of a non-activated nucleotide in A) composed of a phosphate group, a pentose sugar, and a nucleobase. The different nucleobases are represented in B). The four RNA nucleobases are adenine (A), uracil (U), guanine (G), and cytosine (C). . . . .	7

1.3	<p>Example of a biochemical pathway of nonenzymatic template-directed RNA polymerization. An imidazole- (in red) activated nucleotide attacks another imidazole-activated nucleotide forming a dinucleotide intermediate linked via 5',5' imidazole. This dimer can bind to a template. The hydroxyl of a nucleotide primer bonds to a template and can attack the phosphate group of the intermediate dimer, extending the primer by one nucleotide and releasing an imidazole-activated nucleotide. Figure modified from [128]. . . . .</p>	9
1.4	<p>Different types of cycling nucleotides can be used for RNA polymerization research. A) shows a 2',3'-cyclic nucleotide. B) shows 3',5'-cyclic nucleotide. C) shows the biochemical pathway of the oligomerization of 2',3'-cyclic nucleotides and a nucleoside leading to the formation of an RNA dimer. Figure modified from [117] . . . . .</p>	11
1.5	<p>Biochemical pathway of the oligomerization of RNA, which starts with a nucleoside and a nucleoside triphosphate. Figure modified from [117]</p>	12
1.6	<p>Representation of the wet-dry cycles hypothesis for the origin of life on Earth. In the first phase, nucleotides would have been able to diffuse in the water in the pond. The heat would lead to water evaporation (beginning of the dry stage), leading to 2-dimensional confinement. The nucleotides would not have been able to diffuse. Two nucleotides in a <i>C3'-C5'</i> conformation would have been able to polymerize thanks to the activation energy brought by the heat (e.g., Sun). Water from rain (or other) would have remixed the nucleotides. . . . .</p>	17

2.1	Sketch of the Planet Simulator (Angstrom Engineering, Kitchener, Ontario, Canada). The simulator is composed of a closed chamber where a computer controls temperature, humidity, pressure, radiation, and gas. Temperature (from -20°C to +120°C) is controlled by a Peltier element and a silicone oil bath. The humidity (%RH) is formed via a bubbler. The rough pump controls the pressure (0 to 760 Torr). The radiation (from 100 to 1000 nm) are controlled by two light bulbs and two light-emitting diode -LED-. Three gas lines allow the choice of the type of environment wanted in the simulator. . . . .	23
2.2	Gel electrophoresis of AMP:UMP, AMP:UMP:NH <sub>4</sub> Cl, AMP:UMP:(NH <sub>4</sub> ) <sub>2</sub> SO <sub>4</sub> , and AMP:UMP:NH <sub>4</sub> NO <sub>3</sub> after 40 cycles. The coloration was inverted so that the results appear in black on the gel. . . . .	35
2.3	Mass spectrometry results obtained with HPLC- ESI-TOF. In A), DAD (Diode Array Detector) are the results obtained for a mix AMP:UMP:NH <sub>4</sub> Cl. The retention time was inferior to the retention time obtained with a known dimer. No peaks can be seen for longer polymers either. In B), the mass spectrum was extracted from the DAD (Diode Array Detector) for the 1-3.5 min peaks. Non-covalent (N-C) adducts are seen.	37

2.4	<p>Molecular Dynamics (MD) simulations were run in the presence of nucleotides (in grey), quartz (in yellow), ammonium ions (in purple), and calcium ions (in green) represented by snapshots at the top (MD with ammonium ions) and the bottom (MD with calcium ions) of the figure, at different percentage of hydration. Fully hydrated, nucleotides started forming clusters with ammonium ions far from the quartz slide, whereas calcium and nucleotides did not form clusters. When dehydrated the systems, tight clusters of ammonium and nucleotides were more and more present and closer to the slide, but this phenomenon is less present with calcium ions. The number of Hbonds between <math>C3' - C5'</math> of the nucleotides was calculated as a function of hydration. The number of Hbonds is small when fully hydrated for both systems (less than 5); this number started to increase in the presence of <math>NH_4</math> ions to finish at <math>\sim 15</math> but did not with calcium ions. . . . .</p>	39
2.5	<p>The radial pair distribution function <math>g(r)</math> was calculated in the presence of ammonium ions (top) and calcium ions (bottom) at 100% hydration, 0.5% at 30°C and 90 °C. No organization of the nucleotides can be seen with calcium ions, whereas nucleotides are organized at 0.5% in the presence of ammonium ions. . . . .</p>	42

4.1	Sketch of primitive Earth including warm little ponds. Geysers of water, or water ricocheting off rocks, could have formed tiny droplets containing nucleotides. The dehydration and confinement could have led to RNA formation. The experiment set-up using an acoustic levitator containing a droplet with nucleotides can be seen on the right. Videos were taken using a Raspberry Pi camera, and temperatures were recorded using a thermal camera. . . . .	80
4.2	Picture of the experiment set-up. The acoustic levitator was placed in front of the Raspberry Pi camera module as well as the thermal camera.	83
4.3	Preliminary results. A) shows the size of the droplet over time. At the beginning of the experiment, the size of the droplet is about $\sim 2.3$ mm. Once all the water evaporates, the pellet is about $\sim 0.75$ mm. B) display the temperature of the droplet over time. At the beginning of the experiment, the droplet is $20.4^{\circ}\text{C}$ . After 40 min, the droplet warms up until $29.6^{\circ}\text{C}$ which is the environment temperature inside the levitator. C) is a radio-labeling electrophoresis gel. At pH 9, a signal can be seen at 50 nt. At pH 2 dry at $25^{\circ}\text{C}$ and at pH 2 dry at $25^{\circ}\text{C}$ and once on the slide, heat-up at $85^{\circ}\text{C}$ , signals around 18 nt are observed. . . . .	87

- A.1 AMP:UMP after 40 cycles a), b). AMP:UMP after 4 days without cycles, at 25°C c),d). The distribution of polymers length is shown in the gel line in a), and c). The quantitative analysis is shown in b) and d). With cycles, degradation of AMP:UMP can be seen. Without the cycles, no degradation nor polymers are revealed by the gel analysis. Only noise can be observed in the quantitative analysis. . . . . 96
- A.2 Microscope images of an AMP:UMP:NH<sub>4</sub>Cl film before (a), b), c)) and after (d), e), f)) 40 hydration-dehydration cycles (scale: 250 μm). Before cycling, a film and a crystalline structure are seen in a), b). Nucleotides are concentrated on the crystals' surfaces, in c). After cycling, triangular-shaped crystals are observed in d), e). Nucleotides are concentrated at the periphery of the crystals (f)). The intensity through the gel is shown on the band in g). The gel's quantitative analysis (h)) indicates a substantial amount of degradation. Microscope images of an AMP:UMP:(NH<sub>4</sub>)<sub>2</sub>SO<sub>4</sub> film before (i), j), k)) and after (l), m), n)) 40 hydration-dehydration cycles (scale: 250 μm). Before cycling, a crystalline structure and an amorphous phase are seen (i), j)). Nucleotides are concentrated on the crystals and on the film (k)). After cycling, irregular structures are observed in the film (l)). Darkfield, in m) shows tiny crystals inside the film. Nucleotides are uniformly distributed in the film (n)). The overall intensity through the gel is strong which might indicate a higher degradation, as seen in o). . . . . 97

A.3 Microscope images of an AMP:UMP:NH<sub>4</sub>NO<sub>3</sub> film before (a), b), c)) and after (d), e), f)) 40 hydration-dehydration cycles (scale: 250 μm). Before cycling, crystalline structures are seen in the film (a), b)); nucleotides are concentrated on the crystals. After cycling, small crystals appear in (d). Nucleotides are concentrated on and around those crystals (f)). In the gel, a band is observed, indicating degradation (g)). Microscope images of an AMP:UMP:NH<sub>3</sub>COONH<sub>4</sub> film before (i), j), k)) and after (l), m), n)) 40 hydration-dehydration cycles (scale: 250 μm). Before cycling, a smooth film is observed on the slide (i), j)). Nucleotides are uniformly distributed inside the film even if the highest concentration is observed along the edge of the film (k)). After cycling, in l), the sample takes a rough clumpy structure. This mix does not form crystal (m)). Nucleotides are found to be everywhere throughout the sample (n)). The overall intensity on the gel line (o)) is minimal, and no large band can be seen. . . . . 98

A.4 Gel electrophoresis of AMP:UMP:(NH<sub>4</sub>)<sub>2</sub>SO<sub>4</sub> after 40 hydration-dehydration cycles. The coloration was inverted so that the results appeared black on the gel. The sample ran with 1:1 nucleotides:salt ratio, and mixed at the end of the experiment before precipitation (Materials and Methods, Electrophoresis gel preparation). The intensity is stronger when the ratio is higher. Nothing is detected with a ratio lower than 1:1. . . 99

A.5 Gel electrophoresis of AMP:UMP:(NH<sub>4</sub>)<sub>2</sub>SO<sub>4</sub> after 2, 4, 6, 8, 10, and 12 hydration-dehydration cycles. The coloration was inverted so that the results appeared black on the gel. After 2 and 4 cycles, the band is weak, and nothing appears on the gel. After 6 cycles, the bands' intensity is stronger. At 8 cycles, the migration shape is the same as after 6 cycles, but the overall intensity is stronger. . . . . 100

A.6 Gel electrophoresis of AMP:UMP:NH<sub>4</sub>Cl. Sequence 1 underwent 24 hours of high temperature and low humidity. Sequence 2 went through 24 hours of cycling and 24 hours of high temperature and low humidity. Sequence 3 shows the sample result that ran during 24 hours of high temperature and low humidity, plus the same parameters as sequence 2. The last sequence underwent 24 more hours of cycles at the beginning of the experiment compared to sequence 3. The overall intensity on the gel is vigorous. . . . . 101

A.7 Gel electrophoresis of AMP:UMP:NH<sub>4</sub>Cl. This experiment is the opposite of the one before. Instead of high temperature and low humidity, the effect of the humidity is tested, so the sample underwent high humidity and low temperature. Sequence 1 went through 24 hours of low temperature and high humidity. Sequence 2 had 24 hours of cycling and 24 hours of high temperature and low humidity. Sequence 3 underwent 24 hours of high temperature and low humidity, plus the same parameters as sequence 2. The last sequence ran 24 more hours of cycles at the beginning of the experiment compared to sequence 3. When samples underwent more cycling than the other samples, the degradation is more intense, like indicate by a longueur and larger band on the gel. . . . . 102

A.8 Computer simulations of AMP:UMP (in gray) in the presence of  $(\text{NH}_4)_2\text{SO}_4$  in water. Only  $\text{NH}_4$  ions are represented (in purple). a), b), c) represent the position of the nucleotides in presence of  $\text{NH}_4$  ions at 0.1 ns, 5 ns, and 100 ns respectively. The graphic d) indicates the number of Hbonds between the nucleotides over time. The average was found to be 30. e) represents the number of Hbonds between  $\text{NH}_4$  ions and the nucleotides over time. During the first 5 ns, the number increases and stabilized at  $\sim 475$ . The graphic f) shows the evolution of the number of Hbonds between  $\text{NH}_4$  ions and  $C5'$  of nucleotides. As same as e), the number of Hbonds increases during the first 5 ns and then stabilized at  $\sim 350$ . The number of Hbonds between  $C2'/C3' - C5'$  is indicated in g). The average number was estimated at 4. The Hbonds are represented in blue, the phosphate group in brown, and the  $C2'$  and  $C3'$  groups in pink. . . . . 103

A.9 Computer simulations of AMP:UMP (in gray) in water. a), b), c) show the nucleotide distribution at 0.1 ns, 5 ns, and 100 ns respectively. The nucleotides are homogeneously dispersed over time. The graphic d) represents the number of Hbonds between nucleotides over time. The average number of H-bonds is  $\sim 20$ . The graphic e) indicates the number of  $C2'/C3' - C5'$  Hbonds over time. The average number is  $\sim 8$  Hbonds. The Hbonds are represented in blue, the phosphate group in brown, and the  $C2'$  and  $C3'$  groups in pink. . . . . 104

A.10 Computer simulations of AMP:UMP (in gray) in the presence of  $\text{CaCl}_2$  in water. Only Ca ions are represented (in green). a), b), c) show the evolution of the nucleotides in presence of Ca ions in solution at 0.1 ns, 5 ns, and 10 ns respectively. The graphic d) represents the number of Hbonds between nucleotides over time. The average number of Hbonds is  $\sim 30$ . The graphic e) indicates the number of  $C2'/C3' - C5'$  Hbonds over time. The average number has been found to be  $\sim 4$  Hbonds. The Hbonds are represented in blue, the phosphate group in brown, and the  $C2'$  and  $C3'$  groups in pink. . . . . 105

A.11 Computer simulations of tRNA in the presence of  $(\text{NH}_4)_2\text{SO}_4$  in water. Only  $\text{NH}_4$  is represented (in purple) in a), b), and c). The graphic shows the number of Hbonds between nucleotides and  $\text{NH}_4$  ions over time (ns) (f). a) shows a homogenous distribution of the ions in water, at 0.1 ns. After 5 ns, ions clusters start to form but not inside the tRNA. The same phenomenon is observed after 100 ns. The number of Hbond between tRNA and ions is stable over time ( $\sim 20$ ). . . . . 106

A.12 Number of Hbonds between  $C3'$  and  $C5'$  within  $7 \text{ \AA}$  close to the quartz. The overall number of Hbonds is lower than observed in the entire simulation box meaning that the quartz does not affect the formation of Hbonds between the nucleotides. . . . . 107

# List of Tables

2.1	Planet Simulator settings for the different steps. All steps were conducted in a 100% nitrogen atmosphere. . . . .	28
A.1	List of all solutions prepared and their concentrations. . . . .	95

# Abbreviations

## Abbreviations

<b>AMP</b>	Adenosine monophosphate
<b>DNA</b>	Desoxyribonucleic Acid
<b>Hbonds</b>	Hydrogen bonds
<b>MD</b>	Molecular Dynamics
<b>nt</b>	nucleotides
<b>RH</b>	Relative humidity
<b>RNA</b>	Ribonucleic Acid
<b>T</b>	Temperature
<b>UMP</b>	Uridine monophosphate
<b>WLP</b>	Warm Little Ponds
<b>WM</b>	Water molecules

# Declaration of Academic Achievement

I, Alix Dujardin, declare that this thesis entitled “The Formation of RNA Polymers on Primitive Earth” and the work presented here are my own. The results addressed in this thesis are the fruit of my own work in collaboration with others.

The entire research thesis has been reviewed and edited by my supervisors, Ralph and Maikel.

I displayed at the beginning of chapters 2, 3, and 4 the contribution of each author.

Chapter 1, which is an introduction to the field, and Chapter 5, which regroups the main conclusion of the work done, have been written by myself.

Chapter 2 has been, for the most part, written by myself, except the *2.4.1. Mass Spectrometry* part, which was written in collaboration with Avinash Dass.

Chapter 3 presents my first paper, published in *Life*. This paper was written by me and edited by Maikel and Ralph.

Chapter 4, has been composed by myself, with the exception of *4.3.4* where the experimental protocol has been written by Jake Brill.

# Chapter 1

## Introduction

The quest to find the Origins of Life has become an expanding field in the last few decades. Numerous research groups are trying to answer the question “how did life begin on Earth?”. Since Charles Darwin’s observations which led to the famous theory of evolution by natural selection in 1859 [30], what we define as living needs to be able to evolve. Louis Pasteur (1822-1895) proved that life has to come from life [8]. Alexander Oparin (1894-1980), in his book “The origin of life” [101], proposed that life could have started in a “prebiotic soup” in the ocean, where non-biological molecules could have assembled through chemical reactions to form biological molecules such as RNA or cells. With these two ideas, life comes from life and the prebiotic soup; Stanley Miller (1930-2007) and Harold Urey (1893-1981) created an experiment to replicate the Early Earth, with water, atoms, and electricity to mimic lightning, bringing energy. When they analyzed the “primitive soup”, they found amino acids [85, 89]. That was the starting point of the origin of life experimental research. With today’s space conquest (e.g., the Perseverance rover on Mars [55] and the James Webb Space Telescope [3] that has the mission to find a second Earth), founding how life

started on Earth has become more crucial than ever. The formation of life on Earth research and results may be expanding and applied to other planets and the Universe.

## 1.1 The RNA world

The origin of life field has two general theories to explain the formation of life on primitive Earth. The first involves the creation of a stable metabolism for the beginning of life on Earth. This view is proposed by the hydrothermal vents hypothesis, where pH and temperature gradients near undersea vents provide energy for life. Thanks to the different gradients, stable and autocatalytic cycles could have been present to provide energy for chemical reactions to happen [81, 126, 118, 110, 5, 100, 80]. This theory, however, does not explain in detail how cells could have been formed in such conditions or how information polymers would have arisen. And in water, molecules are constantly diffusing which would have made the concentration of molecules difficult, in addition to hydrolysis.

The other theory is based on “information first”. Life may have started with ribonucleic acid (RNA) molecules. This theory was produced in 1967 by Carl Woese [130]. The time period where life exists mainly in the form of RNA is called the “RNA world”, a term introduced by Walter Gilbert in 1986 [54].

RNA plays a crucial role in modern biology and life. RNA is a polymer composed of four different units: adenosine monophosphate (AMP), uridine monophosphate (UMP), cytidine monophosphate (CMP), and guanosine monophosphate (GMP). Those molecules are linked together between their carbon 3' and 5' (Fig 1.1A)) via a phosphodiester bond. In biological cells today, DNA is transcribed using DNA polymerase and other proteins to form what is called messenger RNA (mRNA). Once this

mRNA is formed, it is translated to form proteins using another molecule called ribosome which is composed of RNA molecules called transfer RNA (tRNA) and proteins. So to start transcribing DNA, a protein and RNA are needed. But in order to make proteins, DNA is needed. So what came first: DNA or proteins? The answer might be neither. Indeed, RNA can play the role of both proteins and DNA. Like DNA, it encodes information in a form of genetic code. But, the RNA molecule, because it is a single strand, can fold on itself to have a 3-dimensional structure like proteins and can have many of the same properties and functions as proteins.

The RNA world hypothesis for the origin of life is based on seven pieces of evidence:

- (1) RNA is a catalytic molecule which is capable of making a copy of another RNA strand if nucleotides are present in the direct environment [113, 18];
- (2) the probability of forming molecules from just one auto-catalyst is higher than finding two different molecules at the same place at the same time, such as a nucleic acid and a protein. Furthermore, proteins can not act as templates for replication, but they could have stabilized an RNA [15, 50];
- (3) The ribosome, tRNAs, and a common genetic code are found in all organisms [74];
- (4) proteins use ribonucleotide coenzymes which contain nucleotides. Nucleotides are not necessarily the reactive part, but this suggests that the nucleotides need to be there to bind the coenzyme to a ribozyme [129];
- (5) deoxyribonucleotides are derived from oxyribonucleotides synthesis, meaning that DNA came after RNA;
- (6) it is easier to start a life with RNA because we know that it continues with DNA transferring information from RNA to DNA by hybridization [19, 67];

(7) it has been shown that RNA is capable of evolution *in-vitro* [73, 9, 10, 114, 6, 124, 43]. This shows that ribozymes can be generated in a laboratory and can have a variety of functions. It suggests that the range of functions in an RNA world is larger than what biological ribozymes currently do (which have only a few roles, such as hammerheads or ribosomes).

One of the major problems is that RNA can not be translated and thus play its genetic carrier role and be catalytic simultaneously. To be replicated, the RNA molecules need to be unfolded (Fig. 1.1B)), while they need to be folded to be catalytic (Fig. 1.1C)). The RNA folded structures are held together via hydrogen bonds interaction between the base of the nucleotides in Watson and Crick conformation. The nucleobase adenine forms two hydrogen bonds with uracil and guanine forms three hydrogen bonds with cytosine. Such hydrogen bonds can be broken with high temperatures or, like in our modern cells, with a helicase enzyme that uses the energy stored in a coenzyme adenosine 5'-triphosphate. RNA polymerases can partially solve this problem. RNA polymerases are similar to DNA polymerases that are used in modern cells to form mRNAs. RNA polymerases are folded, thus catalytic, and bind to the end of an RNA strand. While traversing the strand, they attach the appropriate nucleotide found in its immediate environment to the previous nucleotide. In the RNA world hypothesis for the origin of life, if RNA polymerases had been present, they would have formed a double-stranded RNA. The mechanism of splitting the double helix into one strand is not yet known, but research suggests that heat would have been necessary [75].

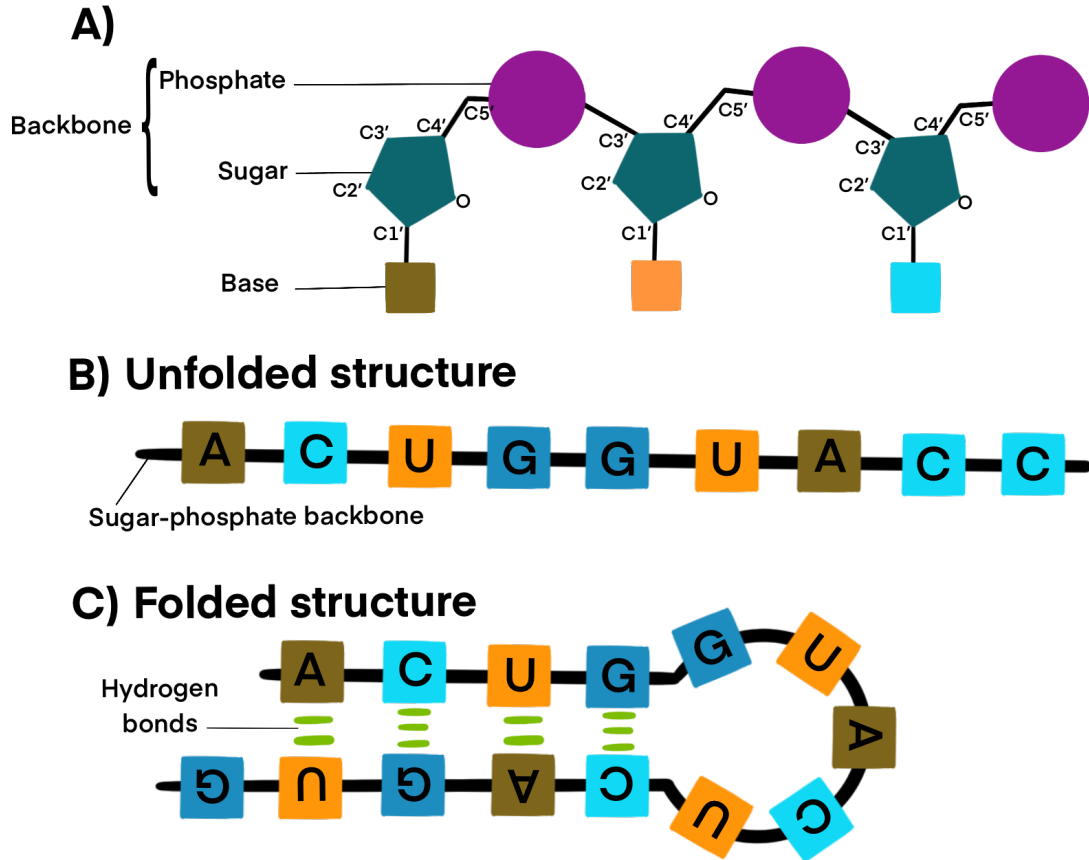


Figure 1.1: A) shows the linkage between phosphate, sugar, and base (adenosine (A), uracil (U), guanosine (G), and cytosine (C)). Ribonucleic acid (RNA) is composed of a sugar-phosphate backbone linked via a phosphodiester bond between the  $C3'$  and the  $C5'$  of the sugar. B) shows the unfolded structure of RNA where this one can be translated but is not catalytic. C) shows the folded structure where RNA is catalytic but can not be translated.

## 1.2 Activated nucleotides versus non-activated nucleotides

In the origin of life research today, researchers use two different types of nucleotides: activated and non-activated. Activated nucleotides give good results regarding RNA polymerization in a prebiotic world; however, it has not yet been found how such molecules could have been polymerized on a prebiotic Earth. On the other hand, different processes of non-activated nucleotide formation on primitive Earth have been brought to light, but these nucleotides did not give such positive outcomes.

### 1.2.1 Non-activated nucleotides

A non-activated nucleotide is a term that refers to a nucleotide that is present in modern RNA and DNA today. They comprise a phosphate, linked to a pentose sugar's 5<sup>th</sup> carbon. Two oxide groups are linked to the second and third carbon of an RNA nucleotide. The first carbon is linked to a nitrogenous base, also called nucleobases: adenine (A), uracil (U), guanine (G), or cytosine (C), as shown in Fig 1.2. Those nucleotides are not reactive by themselves and thus can not form bonds without an external energy source.

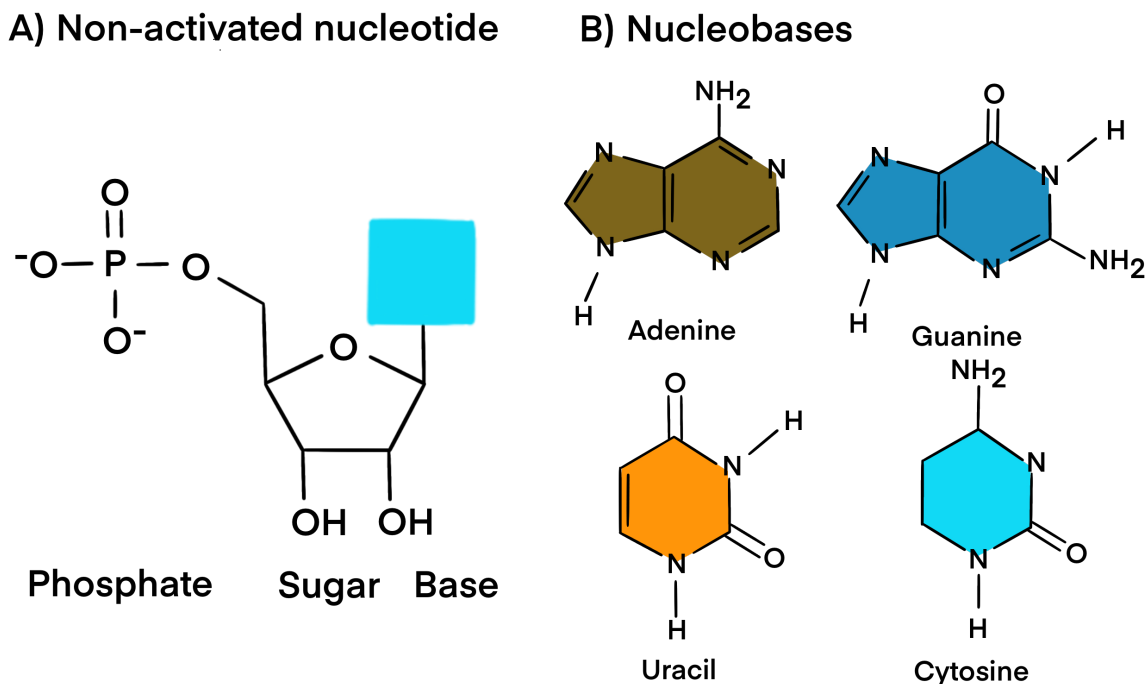


Figure 1.2: Representation of a non-activated nucleotide in A) composed of a phosphate group, a pentose sugar, and a nucleobase. The different nucleobases are represented in B). The four RNA nucleobases are adenine (A), uracil (U), guanine (G), and cytosine (C).

Some groups used those molecules in the optic of synthesizing RNA polymers [112, 93, 26, 99].

Their components (nucleobase, sugar, phosphate) must first form to polymerize such nucleotides. Three different pathways could have led to nucleobase formation on primitive Earth [104]. The first one, the Fischer-Tropsch-type reaction, consists of the formation of nucleobase by mixing dihydrogen, carbon monoxide, and ammonia in contact with minerals of iron, aluminum, and silica [84, 104]. Another possible pathway would have been based on hydrogen cyanide that could react with other molecules to form the nucleobases [105, 104]. The last one consists of reacting formamide in the presence of titanium, aluminum, or silica to form the nucleobases with

the exception of guanine [105, 104].

Once that is done, one of the solutions is to mix all the compounds together and wait for the reaction to happen. This is the Lego block approach [86, 107, 108, 106, 52, 58, 104]. The second pathway of the formation of nucleotides is based on four components: cyanamide, cyanoacetylene, glycolaldehyde, glyceraldehyde, and inorganic phosphate. The inconvenience is that these reactants need to be introduced in a specific order. But, it is unlikely that primitive Earth would have followed the rigorous steps of scientific [110, 104].

## 1.2.2 Activated nucleotides

Activated nucleotides are modified chemically to create additional bonds linked to the sugar. The degradation of these bonds allows the release of energy that can be used to form a phosphodiester bond between nucleotides. It exists different types of activated nucleotides.

### Imidazole as a leaving group

The most common activated nucleotides that are used are imidazole-activated nucleotides. Imidazole is linked to the phosphate of a nucleotide. When the phosphate and imidazole bond is hydrolyzed, the energy release allows the formation of a phosphodiester bond. The biochemical pathway is quite complex to pass from the first to the final product, including three different steps, other molecules such as peptides, and other steps on the side to form derived products [2]. Nucleotides linked with imidazole are much more reactive and do not need an external enzyme to polymerize [120].

Imidazole can also be used for nonenzymatic template-directed RNA polymerization. The imidazole group from a first nucleotide can attack the imidazole group from a second nucleotide to form a dinucleotide intermediate. This dinucleotide, linked to a template, can bond to a third non-activated nucleotide (primer), extending it by one nucleotide, and leaving an imidazole-activated nucleotide starting a nonenzymatic template-directed RNA polymerization, as seen in Fig 1.3 [128].

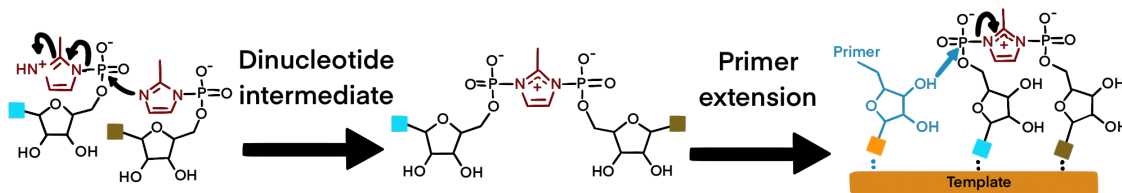


Figure 1.3: Example of a biochemical pathway of nonenzymatic template-directed RNA polymerization. An imidazole- (in red) activated nucleotide attacks another imidazole-activated nucleotide forming a dinucleotide intermediate linked via 5',5' imidazole. This dimer can bind to a template. The hydroxyl of a nucleotide primer bonds to a template and can attack the phosphate group of the intermediate dimer, extending the primer by one nucleotide and releasing an imidazole-activated nucleotide. Figure modified from [128].

Many groups used imidazole to polymerize RNA in the context of the origin of life [48, 45, 68, 46, 119, 131].

Using side compounds, Oró *et al.* [102] have shown that forming imidazole-nucleotide molecules would have been possible under prebiotic conditions. Two different pathways were found. The first one used an aldehyde, glyoxal, and ammonia as precursor agents. The second one started with a carbohydrate and ammonia [102].

### Cyclic nucleotides

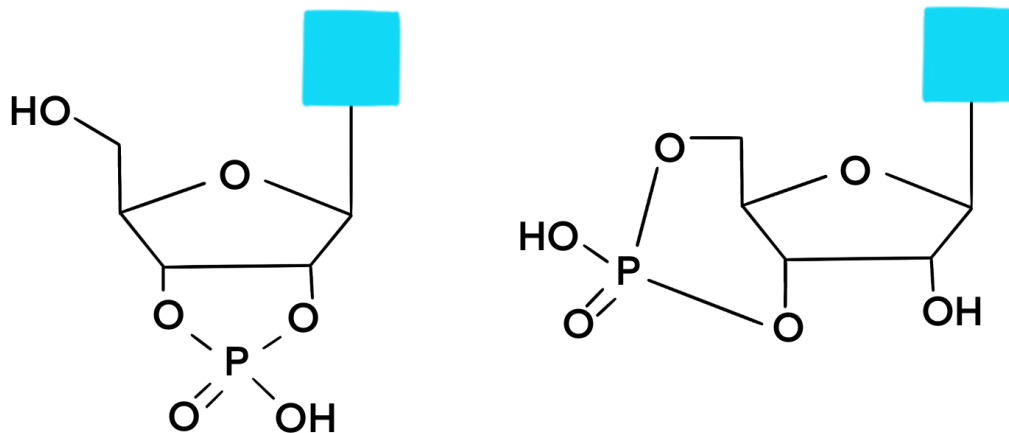
Different types of cyclic nucleotides exist and can be used for the origin of life research. Some groups used 2',3'-cyclic nucleotide (Fig. 1.4A)) for RNA polymerization [31],

while other favored 3',5' cyclic nucleotides (Fig. 1.4B)) [24, 25, 91].

Hydrolyzing the bond between 2' and the phosphate of the 2',3'-cyclic nucleotide, or 3'-phosphate bond for the 3, 5' cyclic nucleotides, will allow freeing the phosphate, in addition to the liberation of energy, which can be used to form another phosphodiester bond with the *C3'* (if using the 3', 5' cyclic nucleotides) or the *C5'* (if using the 2', 3'-cyclic nucleotide) as seen on Fig. 1.4C).

But such molecules would have been difficult to use to promote polymerization on primitive Earth due to a small  $\Delta G$  which is a consequence of the two non-stabilized reactions which happen forward and backward of 2',3'-cyclic phosphodiester and 3',5'-phosphodiester. This suggests that RNA polymerization would have been less favorable using such cyclic molecules [117]. Scott *et al.* argued that this assumption could have been wrong, and the biochemical pathways were necessary to revise. They discussed that a three-state reaction would have been necessary (and feasible on primitive Earth) to stabilize the final product and suppress the back reaction. Stabilization of the final product in Fig. 1.4 could have been possible by nucleotide stacking interactions and base-pairing which increased the energy barrier between the final production and intermediate product. Those two combined would have driven RNA helix formation, leading to a kinetically favored product and preventing the back reaction from occurring [117]. They did not, however, do any experiments to support these assumptions.

**A) 2', 3' - cyclic nucleotide    B) 3', 5' - cyclic nucleotide**



**C) Polymerization reaction**

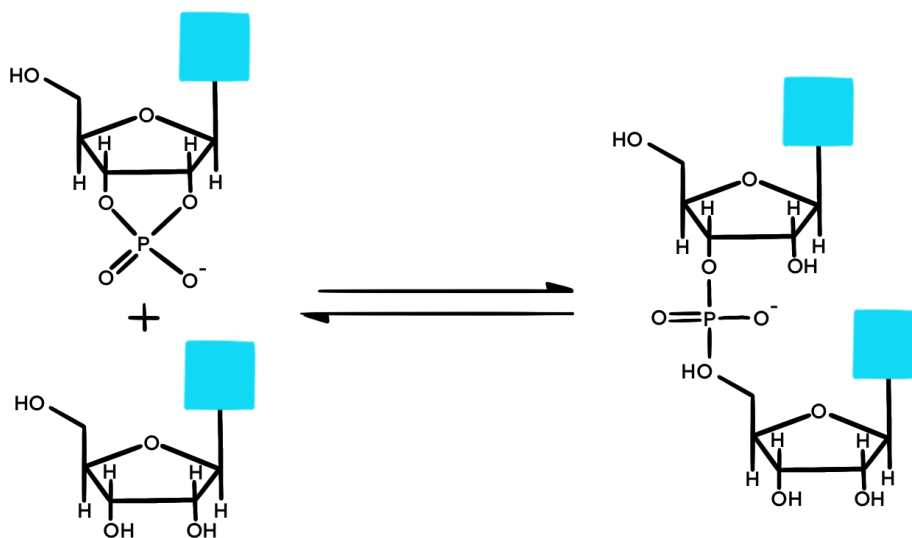


Figure 1.4: Different types of cycling nucleotides can be used for RNA polymerization research. A) shows a 2',3'-cyclic nucleotide. B) shows 3',5'-cyclic nucleotide. C) shows the biochemical pathway of the oligomerization of 2',3'-cyclic nucleotides and a nucleoside leading to the formation of an RNA dimer. Figure modified from [117]

## Nucleosides triphosphates

Nucleosides are molecules precursors of nucleotides, thus, nucleoside triphosphate would have been the precursor of a nucleotide. Some groups used such molecules for their prebiotic experiments [42, 70].

In a prebiotic polymerization using these types of molecules, a nucleoside (composed of a sugar and a base) would have reacted with a nucleoside triphosphate in a highly exothermic reaction similar to reactions catalyzed by modern RNA polymerase where the departure of the phosphate leaving group is crucial for the RNA polymerization, releasing an important amount of energy allowing the formation of a phosphodiester bond (Fig. 1.5) [117].

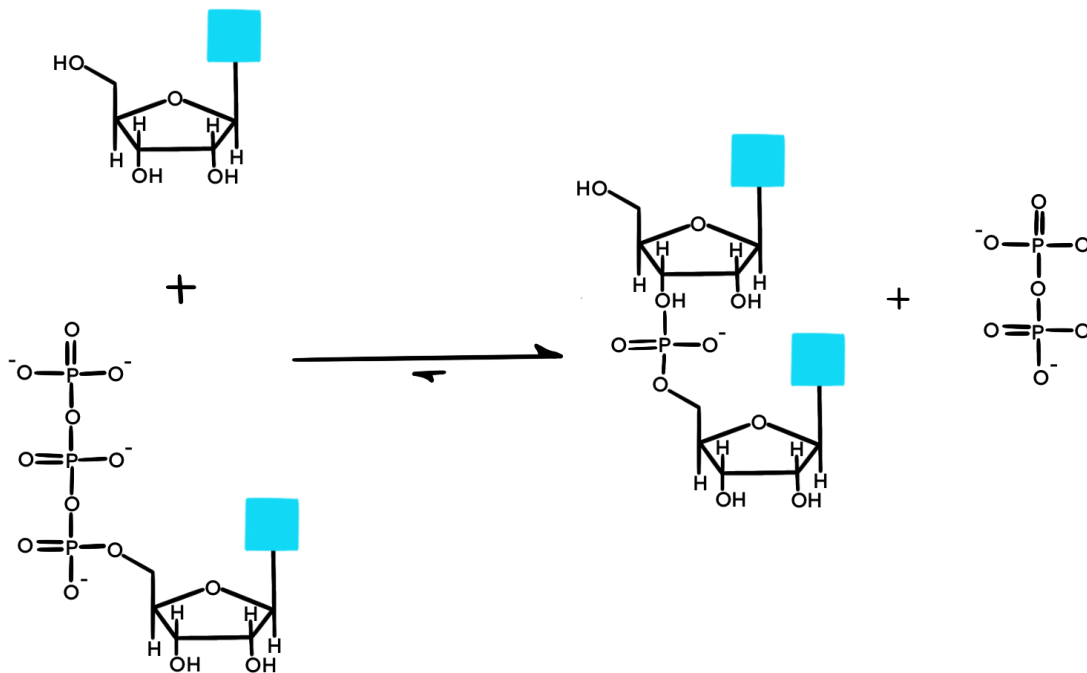


Figure 1.5: Biochemical pathway of the oligomerization of RNA, which starts with a nucleoside and a nucleoside triphosphate. Figure modified from [117]

Thermodynamically, this reaction could have been feasible because the  $\Delta G$  is large and negative [117]. Orgel and colleagues had, however, stated that nucleoside triphosphate needs to be used with complex enzymes to catalyze the reaction that would have been unlikely present on primitive Earth. Without such enzymes, the reaction would have been too slow for RNA polymerization to occur [79].

### 1.3 RNA polymerization

Polymerizing RNA, without enzyme, in a primitive atmosphere is not trivial. Throughout the research, different techniques have been established, but all of them included activated nucleotides, and it is not clear how such molecules would have been formed on primitive Earth. [82, 48, 70, 31]

But it is possible to form a phosphodiester bond between two nucleotides via a condensation reaction between two non-activated nucleotides in a world without enzymes.

Kinetics simulations have shown that oligomer synthesis is fast after dehydration, while hydrolysis is slow. Ross *et al.* [115] had shown that with a  $\Delta G' = -10$  kcal/mol, the reaction is energetically favorable, and the time to equilibrium is short (a few tens of seconds, versus 10 h when they tried with  $\Delta G' = -3.5$  kcal/mol). Each oligomer in the evaporite is more stable than its immediate precursors. Furthermore, at 85°C,  $\Delta G'$  and the water activity decrease when the size of the cavity decrease (the cavity refers to where nucleotides are trapped, such as pores). This form of Kelvin equation can approximate the effects, where  $a_w$  is water activity,  $\lambda$  is the surface tension, and  $V_m$  is the molar tension of water at  $T$  temperature, the size of the cavity is

representing by  $d$ , and  $R$  is the universal gas constant:

$$\ln a_w = -\frac{2\lambda V_m}{dRT}. \quad (1.3.1)$$

The re-hydration will drive the initial high-value diffusion rates. However, according to Equation (1.3.2), for high diluted value,  $\tau = 1/k_{-1}$  which is about 100 hours for pool conditions but with evaporation,  $k_1$  will be the main term in the denominator so  $\tau$  will decrease by a similar amount. In contrast, the polymerization reaction takes place in  $\sim 10$  s. Oligomers can grow thanks to hydration-dehydration cycles: where  $a$  refers to the activity of nucleotides monomers  $m$  and  $n$  at equilibrium  $eq$ ,  $k_1$  refers to the rate of polymers formation whereas  $k_{-1}$  is the rate of nucleotides breakdown, and  $\tau$  refers to the relaxation time, echo to the recovery time from abrupt perturbation, disturbing the system from equilibrium [115]

$$\tau = \frac{1}{(a_m^{eq} + a_n^{eq})k_1 + k_{-1}} \quad (1.3.2)$$

So to reach the activation barrier of non-activated nucleotides and be able to form phosphodiester bonds between two carbons, one would say it is necessary to have hydration-dehydration cycles.

## 1.4 Life could have formed in Warm Little Ponds

Many different theories exist about what type of environment life may have beginning on Earth. Some groups tested cold environments with ice [123, 87, 4, 90]. Ice contains pores that could have trapped molecules. Ice has been used to form RNA polymers because of the possibility to find mineral particles, salty liquid water, and gas bubbles

trapped in it. Thus, electrical potential, ions densities, and a pH gradient can appear [123, 87]. But the activation barrier for non-activated nucleotides would be difficult to reach in ice due to the low temperature.

Other groups are looking deep in the oceans near hydrothermal vents for the searching answers to the “metabolism first” theory [81, 126, 118, 110, 5, 100, 80].

Finally, warm little ponds (WLP) could have been where life had started [122, 64, 33, 34, 36, 32, 60, 115, 28, 26, 59, 35, 27, 37]. Anecdotally, Charles Darwin wrote a letter to one of his friend in 1871, where he mentioned that he had this idea that life could have started in “*some warm little ponds with all sort of ammonia and phosphoric salts, -light, heat, electricity present*” [29].

In ponds today, scientists have found many different molecules like salts and minerals [33]. Because a pond is not deep, it is easy for the water to evaporate quickly (Fig. 1.6). As the water evaporates, less and less water is present, and the molecules such as amphiphiles, nucleotides, and solutes would become more and more concentrated. Finally, molecules would not be able to diffuse anymore and would have been stuck in contact with an inorganic surface, such as minerals present in the pond. The heat of the Sun could have brought enough energy to activate the nucleotides, and thus, phosphodiester bonds would have been created thanks to a condensation reaction [115, 27, 63]. Because of the rain, the nucleotides would not be stuck on the minerals and would be able to diffuse again. Water is also important to diffuse nucleotides and polymers synthesized, but also to form proto-cells and to allow proper functioning of ribosomes [27, 63]. During a second period of dryness, nucleotides could again concentrate on the rocks, but in another conformation than the first time, leading to the growth of RNA chains [46, 47, 66, 26].

In this thesis, we are focusing on the WLP theory for multiple reasons like fatty-acid self-assembly or polymerization reactions [34, 28]. Furthermore, biosignatures were found in ancient hot springs showing that life may have begun in this type of environment [38]. Finally, this idea was tested on homologous sites, showing that condensation reaction to form ester bond between two nucleotides can appear outside of a laboratory [33].

But the experiments have a hard time matching the theory when using non-activated nucleotides, and results are often controversial, usually blaming the lack of different techniques to prove the results.

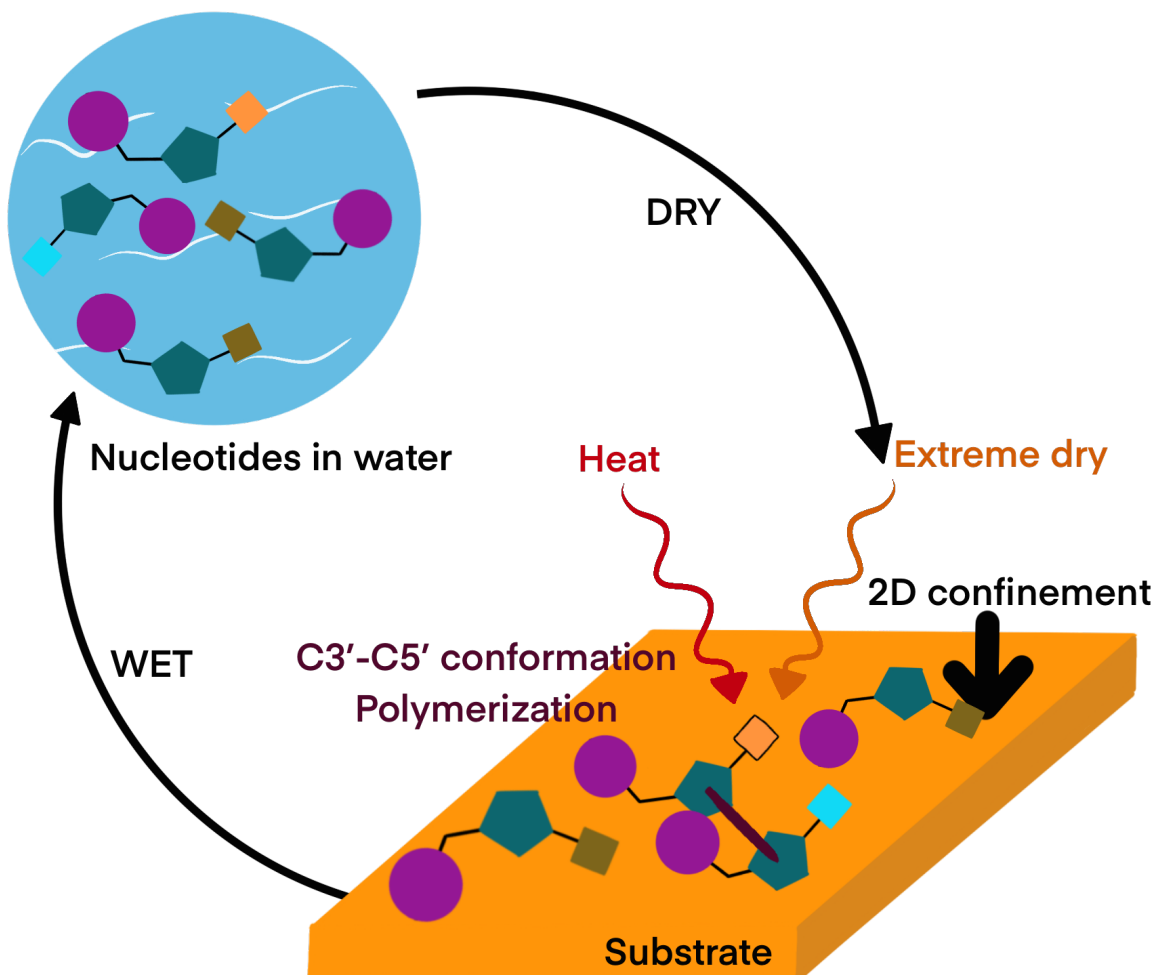


Figure 1.6: Representation of the wet-dry cycles hypothesis for the origin of life on Earth. In the first phase, nucleotides would have been able to diffuse in the water in the pond. The heat would lead to water evaporation (beginning of the dry stage), leading to 2-dimensional confinement. The nucleotides would not have been able to diffuse. Two nucleotides in a  $C3'-C5'$  conformation would have been able to polymerize thanks to the activation energy brought by the heat (e.g., Sun). Water from rain (or other) would have remixed the nucleotides.

## 1.5 Outlines of thesis research

This thesis focuses on the formation of a complex molecule: Ribonucleic Acid (RNA), using non-activated nucleotides in the context of the origin of life on Earth.

Chapter 2 shows that pH plays an essential role in the origin of life research. We experimentally investigated acidic pH with ammonium salts to form RNA polymer using non-activated nucleotides. We worked with a unique machine, only present at McMaster University, the *Planet Simulator*. We also examined the role of the salts at neutral pH using MD simulations under wet-dry cycles.

In Chapter 3, we focused on the interactions of nucleotides with different substrates materials that can be used as RNA polymerization catalysts studied by Molecular Dynamics (MD) simulations. We reviewed the literature to collect information about the different types of minerals which may have been present on primitive Earth and what types of minerals research groups used for their experimentation. We presented a new model for where RNA polymerization could have occurred on primitive Earth. This paper was published in a peer-reviewed journal *Life* (13(1):112) in 2022 by myself, Alix Dujardin, Sebastian Himbert, Ralph Pudritz, and Maikel Rheinstädter

In Chapter 4, we used the new model presented in the previous chapter to form RNA polymers experimentally without the use of enzymes or activated nucleotides.

Finally, in Chapter 5, we summarized the main conclusions from the three previous chapters.

## Chapter 2

# Acidic environment does not favor the formation of RNA polymers in a prebiotic salty Warm Little Pond.

*Alix Dujardin*<sup>1,2</sup>, *Avinash Vicholous Dass*<sup>1,2,3,4</sup>, *Renée-Claude Bider*<sup>1,2</sup>, *Sebastian Himbert*<sup>1,2</sup>,  
*Ralph Pudritz*<sup>1,2</sup>, *Maikel Rheinstädter*<sup>1,2</sup> <sup>1</sup>Origins Institute, McMaster University,  
Hamilton, ON, Canada

<sup>2</sup>Department of Physics and Astronomy, McMaster University, Hamilton, ON, Canada

<sup>3</sup> Systems Biophysics, Ludwig Maximilian University Munich, München, Germany

<sup>4</sup> Center for NanoScience (CeNS), Ludwig Maximilian University Munich, München,  
Germany

## 2.1 Preface for Acidic environment does not favor the formation of RNA polymers in a prebiotic salty Warm Little Pond.

These researches were conducted to understand the formation of RNA polymers using different types of salts. For more than six months, we were optimistic about the results obtained; gel electrophoresis showed bands using certain types of salts ( $\text{NH}_4$  ions salts) but none with others. We then conducted Molecular Dynamics computer simulations to understand why we had such good results with the salts. But we found, using mass spectrometry technique, that our bands were not RNA but a result of decomposition of the nucleotides into sugar due to the acidic pH and high temperature. Research on this specific subject has been on standby since.

**Status:** Because of the final mass spectrometer results, research on this subject has been left on standby. Research needs to be continued.

### **Author Contributions:**

Sample Preparation: Alix Dujardin, Renée-Claude Bider, Maikel Rheinstädter

Matlab Coding For Electrophoresis Gel Analysis: Sebastian Himbert

Planet Simulator Design: Maikel Rheinstädter, Ralph Pudritz

Gel Data Analysis: Alix Dujardin, Maikel Rheinstädter, David Deamer

Mass Spectrometer: Avinash Dass

MD Model Development: Maikel Rheinstädter

MD Analysis: Alix Dujardin

### **Special Acknowledgments:**

We wanted to give a special thanks to Angstrom Engineering, Maikel Rheinstädter, and Ralph Pudritz for the design and the conception of the machine, the *Planet Simulator*.

## **2.2 Introduction**

Wet-dry cycles in warm little ponds for the origin of life is now a theory that is being spread through the scientific community. Different groups have tested the effect of hydration-dehydration (HD) cycles on polymerization. DeGuzman *et al.* [37], and Rajamani *et al.* [112] used lipids as an organized matrice in their experiments. Nucleotides formed polymers after cycling, from 10 to >50 nucleotides long [37], and from 25 to 100 nucleotides long [112] respectively, by analyzing with nanopore and gel electrophoresis. The presence of a secondary structure was proven by polymers exhibiting hyperchromicity and intercalating dye. Hassenkam *et al.* [60] have noticed viroid size ring-like structure by AFM, showing that nucleotides formed secondary structures. Instead of lipids, DaSilva *et al.* [26] used salts as an organized matrice. Four different monovalent salts were tested (LiCl, NaCl, KCl, and NH<sub>4</sub>Cl). According to nanopore and gel electrophoresis results, ammonium chloride (NH<sub>4</sub>Cl) was found to be the best salt to promote RNA polymerization.

Himbert *et al.* [64] have shown via X-ray diffraction technique that nucleotides can be organized on elements surface such as lipids or salts. Depending on the environment, the rate of polymerization is different. X-ray diffraction reveals that some environments are better for organizing nucleotides and procuring two-dimensional

confinement. Lipids had formed a liquid crystal film confining nucleotides where they can diffuse and react without organic molecules, anhydrous or charge surface. Ammonium chloride and clay provide a large surface area where nucleotides can be confined between salt crystallites and the clay layers. Nevertheless, these environments do not give the same amount of ordered structures. Clay improves UMP organization, whereas salt is better with the mix AMP:UMP. However, the structure of minerals depends on different parameters such as pH, concentration, and nature of molecular solutes and electrolytes. Interactions between solutes and minerals can inhibit the development of crystals [61]. The polymerization of RNA-like polymers was unsuccessful but produced backbones of sugar-phosphate with a pH around 2, at  $\sim 80-90^{\circ}\text{C}$  [93]; indeed, it has been found later on that under these conditions, the base was lost [93].

Different experimental techniques are used to mimic the primitive environment with hydration-dehydration cycles. For the dehydration part, DaSilva *et al.* (2015) [26] used a hot plate heated to the desired temperature ( $85^{\circ}\text{C}$ ) under carbon dioxide to obtain an oxygen and water-free environment. The samples were dispersed in  $100\mu\text{L}$  of  $1.0\text{ mM HCl}$ . Other groups built automatic machines. DeGuzman *et al.* [37] created their homemade simulator chamber. This chamber is equipped with an aluminum disk containing vials with the reactions. They used carbon dioxide and heated it at  $85^{\circ}\text{C}$  as well. Water was used to re-hydrate the mixture. Fox *et al.* (2019) [49] designed another type of apparatus. They used a chemical system of condensation. A Schlenk flask is warmed up via an oil bath. The flask is attached to a heat-insulated glass riser linked with a reservoir. This part is attached to the low part riser with a time-controlled valve. During the dehydration phase, the flask is

heated. The nitrogen carries the water out. In the dehydration phase, the previously stocked water vapor condensed in a reservoir is introduced into the hot flask via the valve.

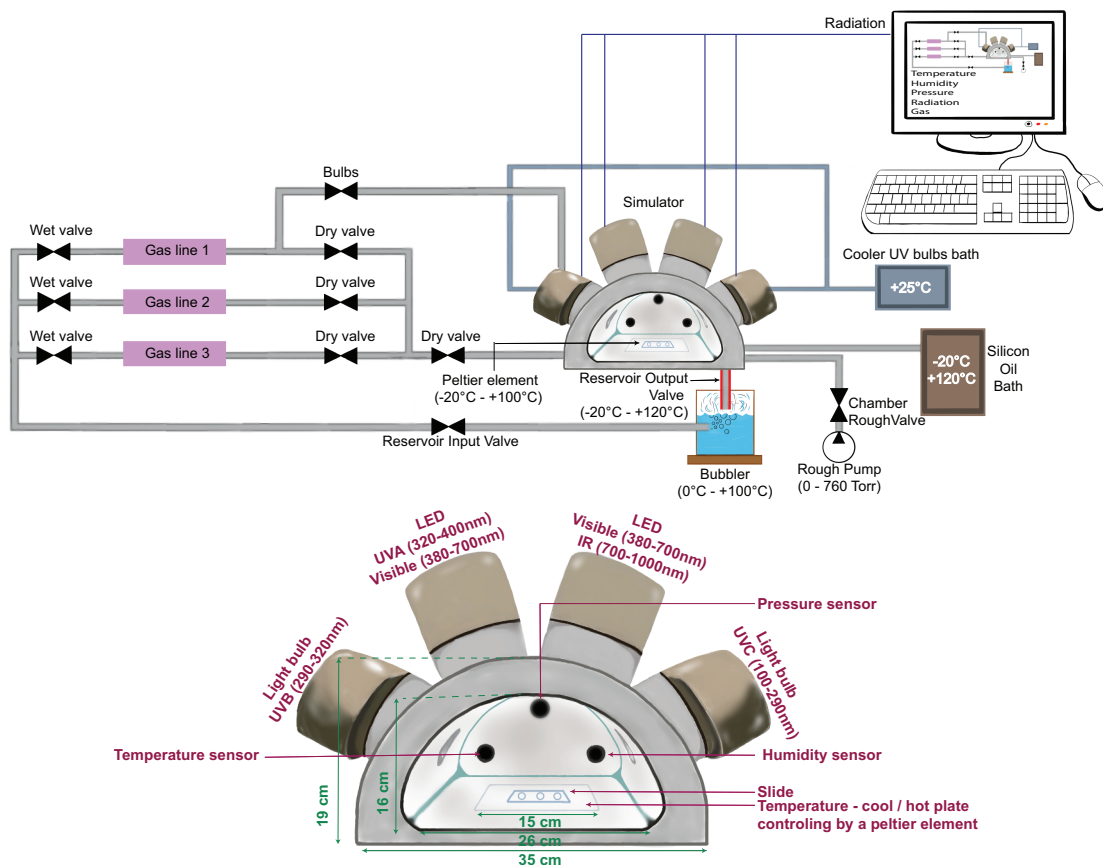


Figure 2.1: Sketch of the Planet Simulator (Angstrom Engineering, Kitchener, Ontario, Canada). The simulator is composed of a closed chamber where a computer controls temperature, humidity, pressure, radiation, and gas. Temperature (from  $-20^{\circ}\text{C}$  to  $+120^{\circ}\text{C}$ ) is controlled by a Peltier element and a silicone oil bath.

The humidity (%RH) is formed via a bubbler. The rough pump controls the pressure (0 to 760 Torr). The radiation (from 100 to 1000 nm) are controlled by two light bulbs and two light-emitting diode -LED-. Three gas lines allow the choice of the type of environment wanted in the simulator.

In this study, we used a novel simulation chamber to mimic hot-cold and hydration-dehydration cycles with unprecedented resolution and duration called the *Planet Simulator*, shown in Fig. 2.1. The Planet Simulator can modify five different parameters (temperature, humidity, gas, pressure, radiation). It has the advantage of being wholly automatized and computer-controlled. The parameters are regulated thanks to the sensors present inside the chamber, and measurements can be saved and followed in real-time. A full description of its capacity is described in the *2.3 Materials and Methods* part under *2.3.2 The Planet Simulator*.

The RNA world proposed by Gilbert [54] in 1986 envisions that the first genetic polymers that formed on the pre-biotic Earth were based on RNA polymerization and replication. In this study, we investigated the formation of RNA using non-activated nucleotides and hot-cold and hydration-dehydration cycles (HD cycles) under acidic pH experimentally and neutral pH using Molecular Dynamics (MD) simulations in the presence of different ammonium salts that have been reported or suggested for their catalytic function. This study uses a novel simulation chamber to create unprecedented resolution and duration cycles.

Using this simulator to mimic the HD cycles, we found that the pH of the solution plays an important role in the polymerization of non-activated nucleotides. Under acidic pH, the nucleotides are destabilized and then fragmented by hydrolysis. At neutral pH, bonds would be more stabilized because of the titration of the polar groups responsible for hydrogen bonding between the base pairs in RNA. Thus, nucleotides would not degrade. Adding ammonium salt increased the number of positive charges without changing the pH of the solution. From Molecular Dynamics (MD) computer simulations, the  $\text{NH}_4^+$  ions form hydrogen bonds with the nucleotides in the aqueous

phase, forming nucleotide clusters. When the water is removed successively, these clusters' nucleotides start forming 3'-5' hydrogen bonds. In a dry (2 water molecules per nucleotide and 90°C) state, we observe the formation of hydrogen-bonded stacks of up to six nucleotides. The ability to form these hydrogen bonds makes ammonium different from other inorganic salts. We speculate that these pre-polymers are a prerequisite for forming RNA polymers. In summary, we present a plausible molecular model of how HD cycles in warm little ponds can lead to the formation of RNA polymers in a prebiotic environment using non-activated nucleotides.

## 2.3 Materials and Methods

### 2.3.1 Sample Preparation

Solutions of AMP:UMP nucleotides (Sigma) and salts were prepared. Nucleotides were mixed with  $\text{NH}_4\text{Cl}$ ,  $(\text{NH}_4)_2\text{SO}_4$  in a 1:1 molar ratio. A  $\sim 10$  mg/ml stock solution of AMP (Sigma-Aldrich), initially in powder form was made with ultra-pure ( $18.2 \text{ M}\Omega\cdot\text{cm}$ ) water. Subsequently, solutions were sonicated for approximately 15 min using a tip sonicator (10 s pulse, 15 s off), assuring complete dissolution. Complete dissolution was indicated by a shift from a cloudy translucent solution to a transparent solution by eye. This protocol was repeated for CMP and GMP (both from Sigma-Aldrich). A  $\sim 9$  mg/ml stock solution of UMP (Sigma-Aldrich), initially in crystal form was prepared. The solution was vortexed for 10 s, until crystals were completely dissolved and the solution appeared homogeneous when observed through a flashlight. AMP and UMP solutions were then mixed in a 1:1 molar and volumetric ratio and vortexed for 10 s to form a homogeneous solution. Though some

experiments were conducted with CMP and GMP, AMP:UMP solution was the main source of nucleotides in these experiments. AMP and UMP were selected as they are complimentary which facilitates bonding [111].

A  $\sim 1.5$  mg/ml stock solution of ammonium chloride (99.5% purity, Caledon) was prepared by combining ammonium chloride crystals with ultrapure water which was subsequently vortexed for 10 s to dissolve any remaining crystals. The same protocol was repeated to prepare stock solutions of ammonium sulfate, ammonium nitrate, and ammonium acetate. Stock concentrations are listed in Table A.1.

Working under a biosafety enclosure, a glass slide was cleaned in dichloromethane for  $\sim 20$  min. The slide was  $75\text{ mm} \times 25\text{ mm} \times 3\text{ mm}$  with three wells, each of which could hold  $\sim 300\ \mu\text{l}$  of liquid (United Scientific supplies, Inc). The slide was subsequently rinsed by alternating  $\sim 5$  ml of methanol, and ultrapure water, ending with methanol. The slide was then dried under a stream of nitrogen gas and placed on a hot plate heated to  $85^\circ\text{C}$ . Typically  $250\ \mu\text{m}$  of the solution was pipetted into each sample well, such that each experiment had three replicates.

### 2.3.2 The Planet Simulator

The samples were then placed in the Planet Simulator (Angstrom Engineering, Kitchener, Ontario, Canada), a custom-built simulation chamber in McMaster University's Origins of Life Laboratory. The simulator is sketched in Fig. 2.1. The Planet Simulator can control temperature ( $-20$  to  $120^\circ\text{C}$ ), humidity (0 to 100% RH), atmospheric composition (four unique gas lines), radiation (155 to 1000 nm), and pressure (0 to 750 Torr). The Planet Simulator can intake multi-step recipes controlling these parameters, which can be looped to repeat steps. The simulator was first calibrated to

a 40% RH, and 30°C for both chamber and plate temperature. A simple cycle was comprised of a dehydration phase and a hydration phase. To achieve dehydration phases, the plate temperature was elevated to 90°C, and the chamber temperature was elevated to 85°C, while the humidity was decreased to 10% RH. In this state, nucleotides are thought to have sufficient energy to bond, while the lack of water would minimize hydrolysis and restrict nucleotide movement so that nucleotides aligned during the drying phase can bond. To achieve a hydration phase, the humidity was increased to 90% RH while the plate temperature was decreased below the chamber temperature, set at 20°C to 15°C. Placing the sample temperature below the dew point induced condensation on the sample. Dehydration and hydration steps were repeated, creating cycles. Throughout the experiment, pressure remained ambient while the atmosphere was flooded by nitrogen gas to prevent any oxidation reactions from occurring. Programmed cycle parameters can be seen in Table 2.1. The first step presented in the table was an initial step to calibrate the temperature, humidity, and gas in the chamber. At the end of step four, the cycles resumed at step two. Samples were cycled for 40 cycles. After each hydration-dehydration cycle, a short re-calibration occurred, where the plate and the chamber temperature were returned to 30°C, and the humidity to 40%. This ensured the simulator's maximum and minimum humidity did not change as the experiment progressed.

Step	Chamber (°C)	Plate (°C)	Humidity (% RH)	Time (hours)
1	30	30	40	2
2	30	10	40	0.66
3	98	90	10	1
4	30	30	40	1

Table 2.1: Planet Simulator settings for the different steps. All steps were conducted in a 100% nitrogen atmosphere.

### 2.3.3 Microscopy

Fluorescent and optical microscopy were conducted using an Eclipse LV100 ND Microscope from Nikon in the Origins of Life Laboratory at McMaster University. The instrument is equipped with a Tu Plan Fluor BD 50 $\times$  objective with a numerical aperture of 0.8. Images were recorded using a Nikon DS-Ri2 Camera with a resolution of 4908  $\times$  3264 pixels and a pixel size of 7.3  $\times$  7.3  $\mu\text{m}^2$ . The camera is mounted via a 2.5 $\times$  telescope to the microscope. All images were recorded in episcopic illumination mode using a halogen lamp. Due to the high numerical aperture, the objective has a small depth of focus between 0.7  $\mu\text{m}$  and 0.9  $\mu\text{m}$ . To record a uniform sharp image, the Nikon control software (NIS Elements, Version 4.60.0) was used to record an Extended Depth of Focus (EDF) image by combining multiple images with different focal planes. brightfield, darkfield and fluorescent images were taken for all samples.

A B-2A long-pass emission filter cube was used with an excitation wavelength of 450–490 nm, and a long-pass analyzing filter with a barrier wavelength of 520 nm. Due to their auto-fluorescence, nucleotides light up in the fluorescent picture. Conversely, salts barely emit a fluorescent signal such that nucleotide-enriched regions can be identified on the fluorescent image.

### **2.3.4 UV-Visible Spectroscopy**

UV-visible spectroscopy was conducted using a Nanophotometer (IMPLEN NP80). Water was used as a blank, and five 1.2  $\mu$ l sample measurements were taken for each compound. Complete wave scans were measured and normalized for a wavelength range from 200 nm to 800 nm. These scans were used to determine nucleotide concentrations, which were returned by the nanophotometer in ng/ $\mu$ l. Working with very short RNA strands, this step was key in confirming the presence of nucleotides before running the gel. The nanophotometer was often saturated, indicating a high concentration of nucleotides. Given this information, if a gel was returned with little to no results, it could be determined that the experimental parameters had not promoted RNA synthesis.

### **2.3.5 Electrophoresis Gel Preparation**

DNA or RNA precipitation followed by Polyacrylamide gel electrophoresis is a standard practice determining the length of DNA and RNA strands. Ethanol RNA or DNA precipitation typically requires a two-hour freezing in  $-20^{\circ}\text{C}$  before centrifuging. Glycogen is typically added to the ethanol solution if concentrations of RNA or DNA are low. Glycogen (Glycogen for Mol. Biol., Roche), a highly branched glucose

polymer, is insoluble in ethanol and forms a precipitate in the presence of salts. As it precipitates, it traps nucleic acids, acting as a carrier and increasing precipitation yield. Glycogen also forms a visible pellet which aids in further handling. Polyacrylamide gels for RNA or DNA visualization are typically prepared with concentrations ranging from 5-10%. This protocol is designed for visualizing long strands of genetic material, such as entire genes, and was not found to be sufficient for the visualization of very short RNA strands.

Therefore, the electrophoresis gel preparation protocol used in these experiments was optimized to increase gel resolution in the range of short strands [57]. When precipitating the gel, the freezing step was increased to  $\sim 12$  h at  $-20^{\circ}\text{C}$  to increase the yield of short-strand precipitation. Though nucleotide concentrations were much higher than typical precipitated solutions, glycogen was added to the ethanol solution to account for low polymerization yields. Gel concentration was increased to 20% polyacrylamide, increasing the separation of different strand lengths and short strand visibility.

Sample was first extracted from the Planet Simulator processed samples to perform RNA gel electrophoresis. To remove the sample from the glass well, 100  $\mu\text{l}$  of a 70% ethanol solution was deposited on the sample in the well. The sample surface was delicately disturbed with the pipette tip. The ethanol solution was then extracted along with any dissolved sample and deposited in a 1.7 ml Eppendorf tube (Diamed). This procedure was repeated approximately three times until the well appeared clear. 70% ethanol was then added to the Eppendorf tube to bring the volume to a total of  $\sim 700$   $\mu\text{l}$ . In order to precipitate the RNA, 20  $\mu\text{l}$  of 3M sodium acetate and 1  $\mu\text{l}$  of glycogen were added to an Eppendorf tube. After that, samples were vortexed and

placed in the freezer at  $-20^{\circ}\text{C}$  for 12 hours.

Samples were centrifuged at 13000 rpm and  $-2^{\circ}\text{C}$  for 20 min, precipitating the RNA. The supernatant was removed and replaced with 100  $\mu\text{l}$  of 70% ethanol to dissolve any remaining salts. The samples were centrifuged in the same settings for 5 min, and the supernatant was removed again, such that only the RNA pellet remained. Samples were dried under a nitrogen stream until the ethanol had completely evaporated.

To prepare samples for gel electrophoresis, 20  $\mu\text{l}$  of water, 2  $\mu\text{l}$  of gel loading dye, and 1  $\mu\text{l}$  of a 30% glycerol solution were added to each Eppendorf tube containing an RNA pellet. Samples were vortexed to redissolve the RNA. In order to denature the RNA and eliminate secondary structures, each sample was heated in a water bath at  $90^{\circ}\text{C}$  for 1 min and allowed to cool for 5 min.

A 20% polyacrylamide gel was prepared. 28.8 g of Urea (BioShop) was mixed with 6 ml of TBE Buffer (BioShop) 10 $\times$  and 30 ml of acrylamide 40% (29:1 crosslink ratio) (BioShop) and placed on the hot plate at  $50^{\circ}\text{C}$  with a mixing rod set to 450 rpm to dissolve urea. Once the urea was dissolved, 199.2  $\mu\text{l}$  of APS (Ammonium persulfate) and 24  $\mu\text{l}$  of TEMED (Tetramethylethylenediamine) (BioShop) were added to the solution, which was carefully mixed and poured between the two plates. Once the gel had filled the plates, a 20-well comb was added (each well measured  $\sim 4.5$  mm). The gel was then left to solidify for approximately 20 min. Once solidified, the gel and plates were clamped onto the vertical polyacrylamide electrophoresis machine (C.B.S scientific), and an aluminum plate was clamped to the back to distribute the heat, ensuring that RNA in all lanes encountered equal resistance and therefore migrated at the same speed. The comb was removed, and TBE 1 $\times$  was placed in the top and

the bottom bath, filling the wells and covering the bottom of the gel. A syringe was used to rinse the wells with TBE 1× to flush out any excess polyacrylamide solution which could deform the wells.

Finally, the gel was pre-run for 15 min with 3000 V, 400 mA, and 20 W. Preheating the gel allows the gel to stabilize and ensures that RNA strands move uniformly and do not accelerate as the gel warms. Before adding the samples to the gel, wells were once again rinsed with TBE 1× via a syringe to remove any urea accumulation in the lanes.

20  $\mu$ l of each sample was placed in each well with 200  $\mu$ l corning flat 0.4 mm thick gel-loading pipette tips (Sigma-Aldrich), such that there was a unique experiment in each well. Two ladders, dsRNA NO363S (BioLabs Inc), were added to two wells, and one well contained a control sample of a non-cycled AMP:UMP stock solution. Samples were run at 20 Watt constant power for approximately 1.5 h.

### 2.3.6 Electrophoresis Gel Analysis

To analyze the results, the gel was released from the electrophoresis plates and placed in a bath with 300 ml of TBE 1× and 3  $\mu$ l of SYBR Gold nucleic acid gel stain (Life Technologies Corporation; 10.000X concentrate in DMSO), for 10 min. Syber gold was used for these experiments as it provided the highest resolution. The gel was photographed under UV light (302 nm) using an Azure C400.

Once the gel has been photographed, our MATLAB script can map out the intensity of the entire gel. The black and white gel is converted to a jet color gel to visualize intensity better. Due to the acceleration of the polymers within the gel, the length of the polymers is exponentially spread out. We calibrate what value on

the y-axis corresponds to the length of the nucleotide chain using our two ladders and fit the correspondence with an exponential. Each well is analyzed by selecting and applying Gaussians to the most prominent peaks. The Gaussian peaks were chosen to correspond with the features seen in most or all gels with the same physical parameters (salts, AMP:UMP, etc.).

A noteworthy drawback of our analyzing process is the degree of the exponential needed to fit the calibration - because we chose to have greater precision for the smaller chains. The peaks at low polymer chain lengths are much clearer than those at higher nucleotide lengths. At those higher lengths,  $>100$ , RNA chains are highly compressed and difficult to discern via our current method. The appearance of ‘tails’ at the end of highly saturated gels is due to the compression of all of our data points after a particular mark on the gel.

### 2.3.7 Molecular Dynamics Simulations

MD simulations were also run to visualize the behavior of the nucleotides in our experiments. The simulation box contained 100 molecules of AMP and UMP respectively, a quartz substrate representing the slide, and different salts depending on the simulation run. Molecules were taken from the CHARMM-GUI archive-small molecules library using CHARMM-GUI multi-component assembler [71, 77, 16]. The simulation box was  $90 \text{ \AA}^3$  in size. GROMACS 2016.3 on MacSim was utilized to run the simulations, a GPU-accelerated computer workstation [1]. This computer is equipped with a 40 Core central processing unit (CPU, Intel(R) Xeon(R) CPU E5-2630 v4 @ 2.20GHz), 130 GB random-access memory (RAM), and three graphic processing units (GPU, 2 NVIDIA 1080 TDI + 1 GeForce GT 730). Simulations can

only be run at pH 7.

The systems were first energy minimized and then equilibrated for 100 ps using an NVT ensemble before being simulated for 10 ns at 100% hydration. All simulations used a 2 fs time step, a periodic boundary cutoff of 1.2 nm, the particle-mesh Ewalds method using a real-space cutoff of 1.2 nm, fourth-order interpolation, and 0.16 nm grid spacing to solve for long-range electrostatics. The parallel LINCS (P-LINCS) algorithm was used to determine bond constraints [62]. Temperature and pressure were maintained at 303 K and 1.0 bar using a Nose-Hoover thermostat [97, 98, 65] at 30°C ( $\tau = 1.0$  ps) and Parrinello-Rahman isotropic weak coupling ( $\tau = 1$  ps) [103]. All analyses were performed on the entire simulations.

Water was removed successively during the simulations to mimic dehydration and a wet-dry cycle, following the same protocol as explained in [41].

### 2.3.8 Mass Spectrometry

A HPLC was combined with a ESI-TOF. The detailed protocol of the mass spectrometry can be found in the Dass *et al.* (2023) paper [31]

## 2.4 Results

### 2.4.1 At pH 2, non-activated nucleotides are degraded

#### Gel electrophoresis

The gel electrophoresis results observed in Fig. 2.2 were not the same as what we could expect when looking at RNA polymers [78]. Indeed, no distinct bands are seen,

only a continuous band throughout the gel which is similar to what can be observed with polyphosphate [92].

After 40 cycles at pH 2 (Fig. 2.2), AMP:UMP mix reveals a weaker intensity on the gel than the mixes AMP:UMP:salt. It was noticed that AMP:UMP:ammonium sulfate had the strongest intensity on the gel, compared to the mixes with ammonium chloride or ammonium nitrate.

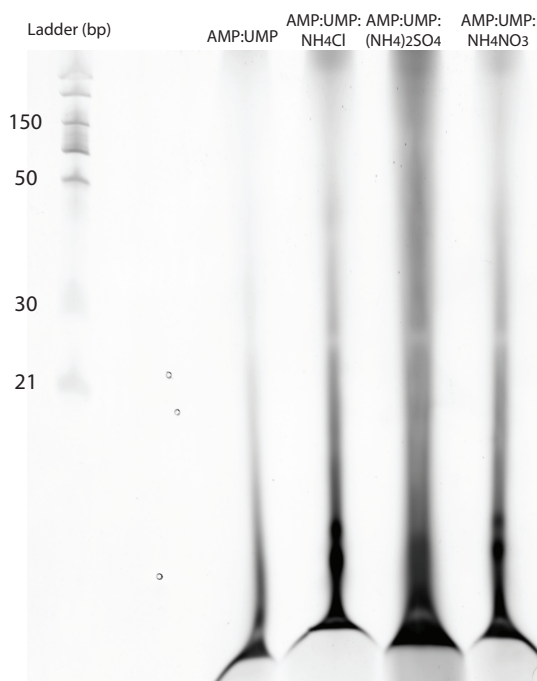


Figure 2.2: Gel electrophoresis of AMP:UMP, AMP:UMP: $\text{NH}_4\text{Cl}$ , AMP:UMP: $(\text{NH}_4)_2\text{SO}_4$ , and AMP:UMP: $\text{NH}_4\text{NO}_3$  after 40 cycles. The coloration was inverted so that the results appear in black on the gel.

A sample containing AMP:UMP was also run at  $25^\circ\text{C}$  without cycles. The results can be seen in Fig A.1. These results were generated using our MATLAB code. This code allowed us to create an intensity map of each gel's line (Fig A.1a), c)) and to convert it into the number of nucleotides in nanomole (quantity of nucleotides added in each well) in the function of the size of the polymers (calibration with the ladder

present on the gel electrophoresis) (Fig A.1b), d)). The results presented in Appendix A.1 show that cycling at high temperatures generates the degradation of nucleotides (due to the absence of peaks). However, room temperature without cycling does not help the formation of polymers, but they are not degraded either. These results suggest that high temperature is the main factor for the degradation of nucleotides.

Microscopy images of the mix AMP:UMP:salts have been taken before and after cycling to see the microscopy evolution of the salts crystals structure and the distribution of the nucleotides (seen in the fluorescent filter in Fig. A.2,A.3 in c), f), k), n)). On the microscopy images in Fig. A.2,A.3 in d), l) is the brown color resulting from the caramelization of the nucleotides. The degradation of the nucleotides looked more important with the ammonium sulfate salt as seen in Fig. A.2o), p).

The number of nucleotides:salts added to the gel was also tested (Fig A.4. Increasing the number of elements in the mix did not help prevent the degradation of nucleotides.

The number of cycles was also reduced to see after how many cycles the degradation of nucleotides started (Fig. A.5. A clear degradation started after 6 cycles. Even though no degradation is visible on the gel before 6 cycles, no polymerization is seen either.

Finally, long periods of dryness and humidity were tested. A long period of heat seems to accentuate the degradation of nucleotides (Fig A.6), while low humidity inhibits this degradation (Fig A.7).

## Mass spectrometry

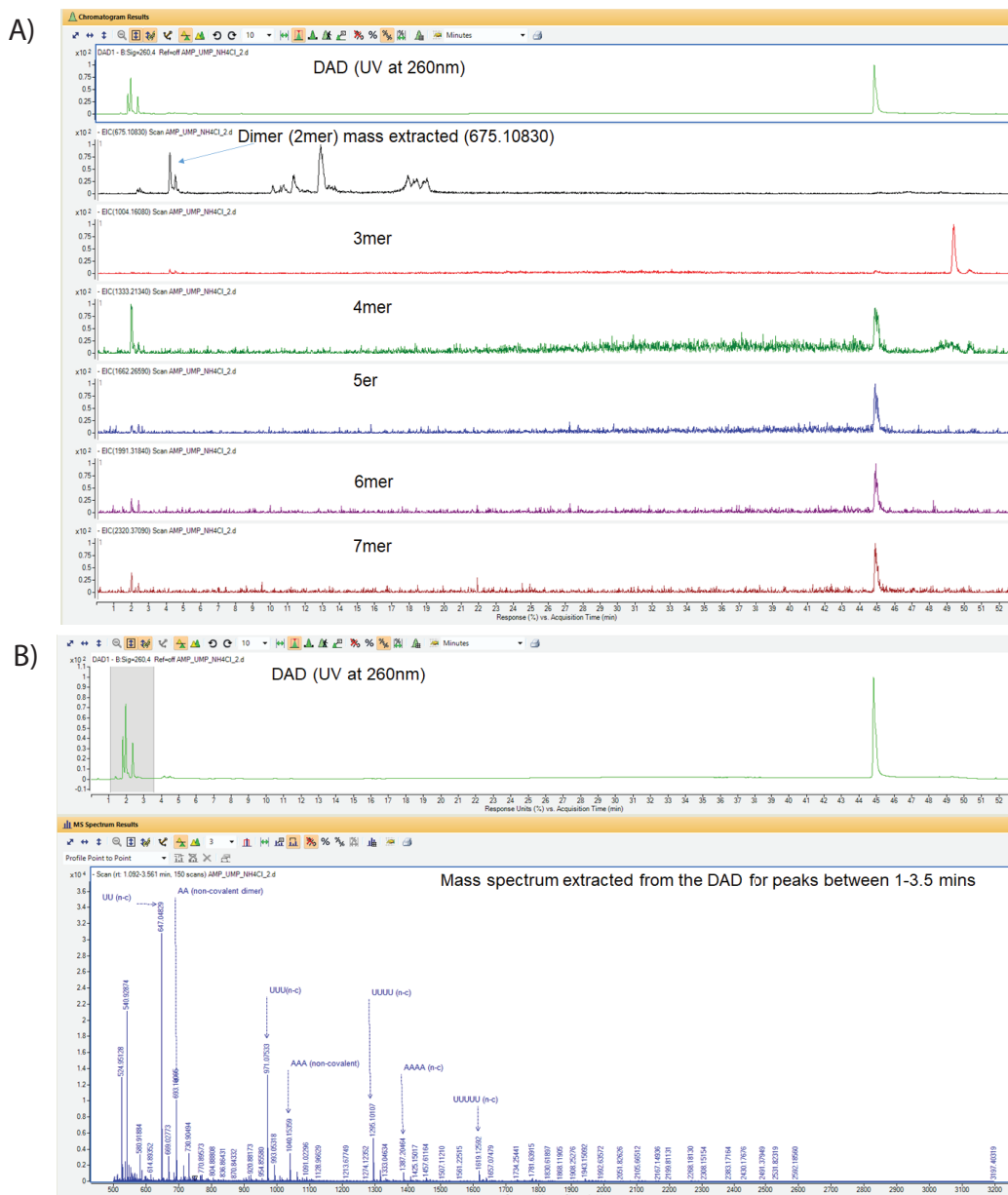


Figure 2.3: Mass spectrometry results obtained with HPLC- ESI-TOF. In A), DAD (Diode Array Detector) are the results obtained for a mix AMP:UMP:NH<sub>4</sub>Cl. The retention time was inferior to the retention time obtained with a known dimer. No peaks can be seen for longer polymers either. In B), the mass spectrum was extracted from the DAD (Diode Array Detector) for the 1-3.5 min peaks. Non-covalent (N-C) adducts are seen.

Mass spectrometry was performed on the different samples AMP:UMP and AMP:UMP:salts. The retention time of standard oligomers from 2-10 mers was obtained as seen in Dass *et al.* (2023) [31]. However, for AMP:UMP:NH<sub>4</sub>Cl after ethanol precipitation, there appear to be no oligomers as seen by lack in DAD (Diode Array Detector) (Fig. 2.3A)). The DAD showed possible dimer dimers. But on the inspection of corresponding mass spectrometry in Fig. 2.3B), the masses found were of non-covalent (n-c) adducts formed by the mass spectrometer analysis. The masses corresponding to oligomers 2-10 were extracted from EIC spectra, but none were observed (Fig. 2.3A)).

#### **2.4.2 At pH 7, Molecular Dynamics simulations reveal the formation of clusters in the presence of ammonium ions**

We wanted to understand how the nucleotides behaved in the presence of salt in the context of our experiment, and thus, we ran MD simulations. We ran the simulations before obtaining the mass spectrometry results. We wanted to understand why we had such “good results” with the presence of ammonium salts. We mimicked our experiments in the simulations by mixing 100 molecules of AMP and UMP AMP:UMP and NH<sub>4</sub> ions while drying the system slowly to reproduce the dehydration process. These simulations were run using the protocol in Dujardin *et al.* (2022) paper [41] (Chapter 2 of this thesis).

#### **Dehydration drives adsorption and 2-dimensional confinement of nucleotides and formation of pre-polymers in the presence of ammonium ions**

As defined in Dujardin *et al.* (2022) [41, 64], pre-polymers are nucleotides aligned in the good conformation C3'-C5' linked via hydrogen bonds but have not yet been

linked via phosphodiester bonds.

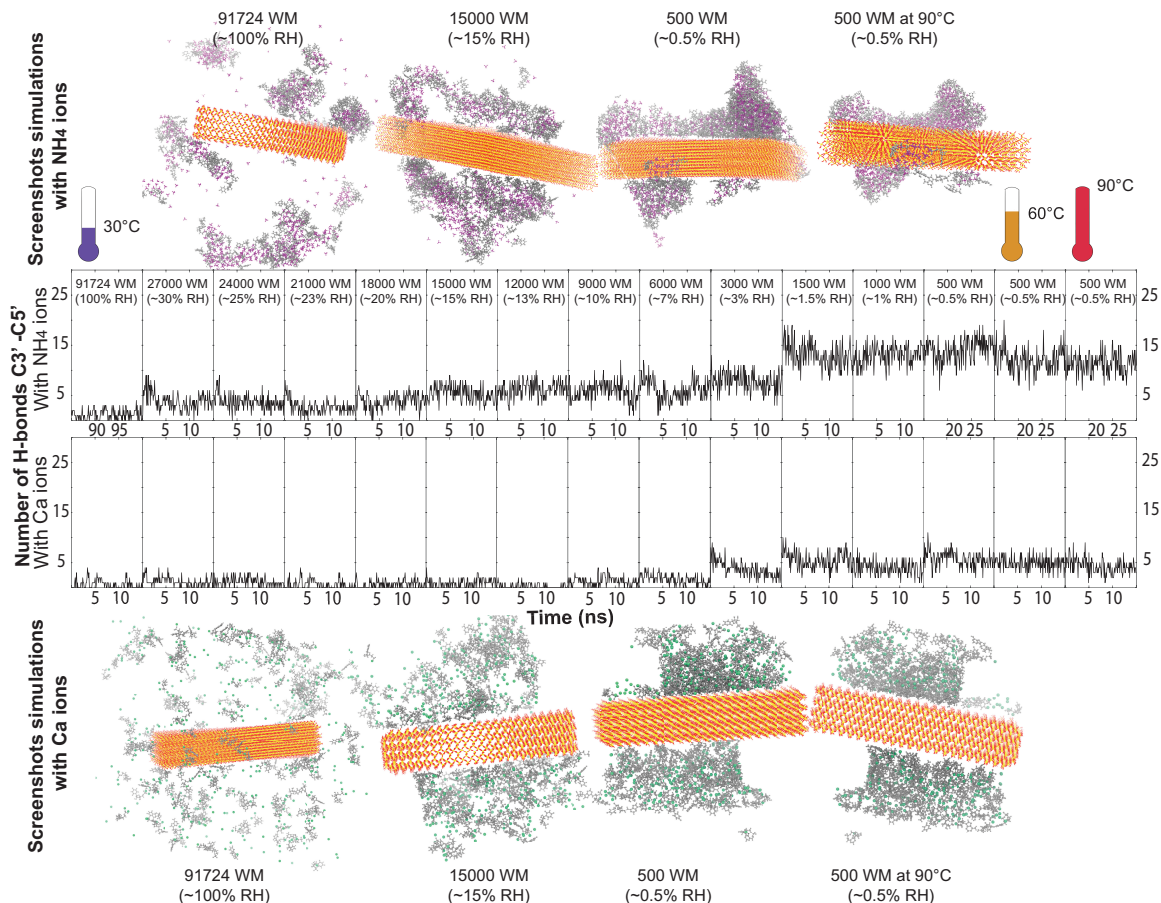


Figure 2.4: Molecular Dynamics (MD) simulations were run in the presence of nucleotides (in grey), quartz (in yellow), ammonium ions (in purple), and calcium ions (in green) represented by snapshots at the top (MD with ammonium ions) and the bottom (MD with calcium ions) of the figure, at different percentage of hydration. Fully hydrated, nucleotides started forming clusters with ammonium ions far from the quartz slide, whereas calcium and nucleotides did not form clusters. When dehydrated the systems, tight clusters of ammonium and nucleotides were more and more present and closer to the slide, but this phenomenon is less present with calcium ions. The number of Hbonds between  $C3'$  –  $C5'$  of the nucleotides was calculated as a function of hydration. The number of Hbonds is small when fully hydrated for both systems (less than 5); this number started to increase in the presence of  $NH_4$  ions to finish at  $\sim 15$  but did not with calcium ions.

Computer simulations were run with  $(NH_4)_2SO_4$  and AMP:UMP in water (Fig 2.4).

Nucleotides are represented in gray,  $\text{NH}_4$  ions in purple, and the quartz is shown in yellow on the top half of the figure. Snapshots were taken at three different hydration levels: 100%, 15%, and 0.5%. 0.5% was also run at 60°C and 90°C in addition of the 30°C. When fully hydrated, the nucleotides and ions do not cluster. When decreasing the humidity level, nucleotides and ions started to cluster on the quartz. It has been shown before that the interaction between the quartz and the nucleotides is negligible [41]. We also simulate without the quartz at 100% hydration (Fig.A.8a), b c)). After 100 ns, nucleotides and  $\text{NH}_4$  ions started to cluster. MD simulations were also run with nucleotides only at 100% hydration (Fig. A.9). After 100 ns, nucleotides do not form clusters.

The number of Hbonds was then calculated between the  $C3'$  and  $C5'$  of the nucleotides in the simulation. The number of Hbonds increased while the hydration level decreased. The variation of temperature does not affect the number of Hbonds formed. At 0.5%, the average was 15 Hbonds. The temperature slightly affected the number of Hbonds, changing from an average at 15 Hbonds at 30°C to 11 Hbonds at 90°C. For the simulation without the quartz, we calculated the number of Hbonds between the  $C2'/C3' - C5'$  with an average of 4 Hbond (Fig.A.8g).

We also ran a dynamic simulation with tRNA and ammonium sulfate to see if the ions intercalate between the bases (Fig.A.11). It appears that after the RNA formation, the ions do not play a role anymore and only form clusters between themselves. Indeed, only a few Hbonds can be seen on the graph, up to  $\sim 40$ , in contrast to  $\sim 475$  for AMP:UMP:( $\text{NH}_4$ )<sub>2</sub>SO<sub>4</sub> simulation (Fig. A.8e)).

### **There is no clustering in the absence of hydrogen bonding**

MD simulations were run with another ion than  $\text{NH}_4$ , Calcium (Ca) ions. Ca was chosen because it can not form Hbonds with the nucleotides. On Fig 2.4 bottom half, Ca ions are represented in green, nucleotides in gray, and the quartz in yellow. While looking at the simulation over time, nucleotides do not form tight clusters on the quartz slide. A representation of the simulation at 100% without the quartz slide can be seen in Fig. A.10.

The number of Hbonds between  $C3' - C5'$  of the nucleotides in the presence of Ca ions is 5 Hbonds at 0.5%, which is 33% fewer Hbonds than with  $\text{NH}_4$  ions.

### **Formation of pre-polymers is driven by dehydration, not by the surface**

To be sure that the quartz was not playing any role in the formation of the pre-polymers, the number of Hbonds was calculated the  $C3'$  and  $C5'$  of the nucleotides within 7 Å to the quartz (Fig. A.12). At 0.5% hydration, whether it be with  $\text{NH}_4$  or Ca, the average has been found to be 3 Hbonds.

### **Ammonium ions organized nucleotides up to six nucleotides**

The radial pair distribution function  $g(r)$  between two nucleotides' bases has been calculated in the presence of ammonium ions and calcium ions and is presented in Fig.2.5. At 100% hydration, whether with  $\text{NH}_4$  ions or Ca ions, nucleotides are not organized more than two bases pair. At 0.5% hydration at 30°C, ammonium ions helped form longer chains of nucleotides up to 5 nucleotides, even though the signal is noisy. The signal is even noisier with calcium ions, and peaks are more challenging to determine. Moreover, the quantity of the chains is less than with  $\text{NH}_4$  ions. At 0.5%

hydration at 90°C, the signal is less noisy, and the peak can be clearly determined in the simulation with ammonium ions, which led to the formation of chains up to 6 nucleotides, with a distance of  $\sim 2.5$  Å between the base. With the calcium, the signal at 90°C is similar to the one at 30°C.

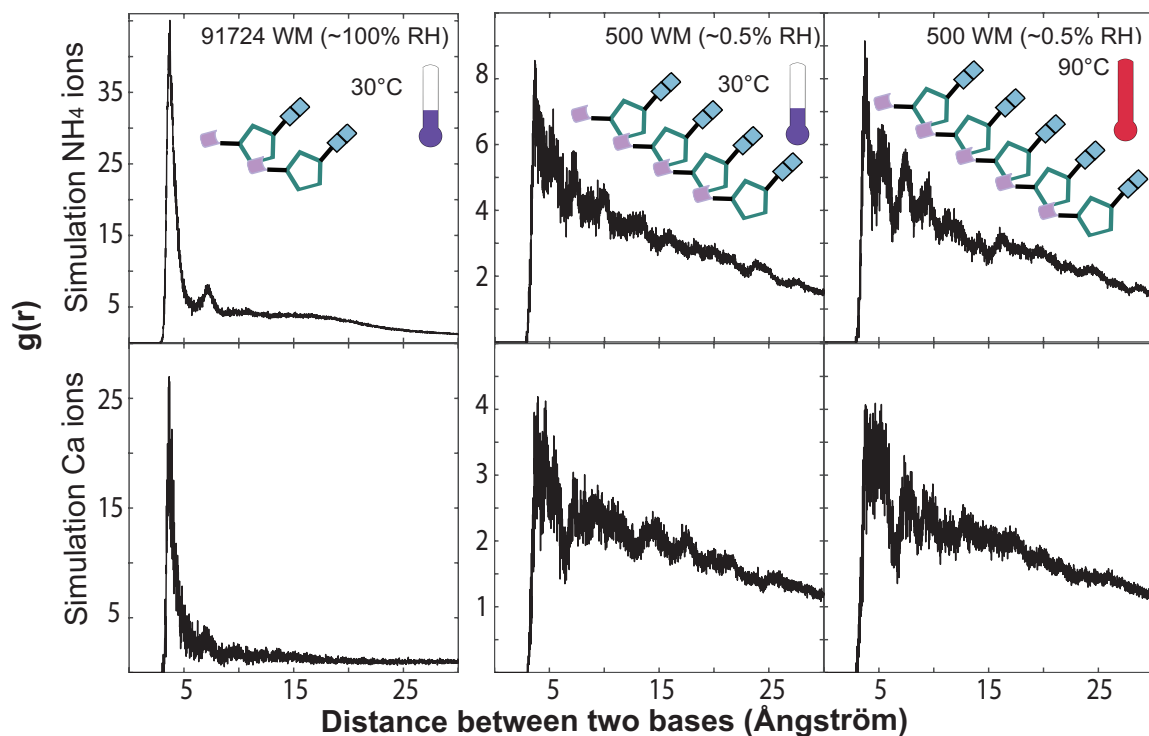


Figure 2.5: The radial pair distribution function  $g(r)$  was calculated in the presence of ammonium ions (top) and calcium ions (bottom) at 100% hydration, 0.5% at 30°C and 90 °C. No organization of the nucleotides can be seen with calcium ions, whereas nucleotides are organized at 0.5% in the presence of ammonium ions.

## 2.5 Discussion

This research aimed to find a way to form phosphodiester bonds between non-activated nucleotides using wet-dry cycles and salts as catalysts. Unfortunately, our results showed us a different route. Our first results revealed that the combination of acidic

pH plus high temperature accelerates the decomposition of nucleotides. Indeed, gel electrophoresis results displayed large and thick bands and mass spectrometry did not expose covalent bonds between the nucleotides. Furthermore, we found that without high temperatures, there is no decomposition of the nucleotide.

After some cycles, the color of the mixture started to change from a translucent color to a brown color. A phenomenon of caramelization occurred there due to the degradation of the nucleotides, similar to a Maillard reaction. However, caramelization differs from a Maillard reaction for the absence of amino acids and the pyrolytic aspect of the caramelization reaction [69]. Indeed, Mungi and Rajamani (2015) [93] have shown that under low pH and high-temperature conditions, the nucleotides became abasic, meaning that the nucleotide lost their nucleobases. Moreover, it has also been shown that under acidic conditions (e.g., pH 2) and high temperature (e.g., 100°C), 50% of the RNA phosphodiester bonds were cleaved after only 50 min [14]. This reaction can be due to nucleophilic substitution, where the atom linked to the sugar is substituted by another chemical. This leads to a split of the sugar and the phosphate group.

It is, however, unclear through these results what the products of degradation are. Indeed, the only products we can observe with the gel might be related to polyphosphate. But it is possible that we formed a backbone of polymers with a loss of base like Mungi and Rajamani (2015) [93] saw during their experiments. One experiment that can be done is to add borate to the mix to stabilize the pentose. As Benner [7] showed in his paper, borate might stabilize the sugar in the nucleotide molecules. Another method we can use to verify our results is nanopore sequencing, like Deamer and his group did in their research on the origin of life [26]. Furthermore,

the number of cycling used in our experiments could be reduced to match DaSilva *et al.* experiments [26].

No precise results can be detected from these results, and before continuing further, it is essential to understand the behavior of the nucleotides at different pHs and temperatures. Using Nuclear Magnetic Resonance (NMR) technique, a phase diagram can be done to understand the stability of the nucleotides under different temperatures and pHs.

To understand the link between the pH coupled with temperature and their effects on nucleotides, it would be interesting to run Nuclear Magnetic Resonance (NMR) to characterize the different products formed when nucleotides are degraded.

Molecular Dynamics simulations have shown that pH 7 and wet-dry cycles could be a potential source of RNA polymerization. MD simulations revealed that ammonium ions reduce the distance between the nucleotides by the formation of Hbonds between  $\text{NH}_4$  ions and the nucleotides. The decreasing distance led to the increasing number of pre-polymer, Hbonds formation between the  $C3'$  and the  $C5'$  of the nucleotides when decreasing the hydration rate. Even more, the nucleotides are organized periodically, every  $\sim 3 \text{ \AA}$ , when the system is dehydrated. Another important point to note is that the heat does not destroy this pre-polymer; even better, it allows a slightly better organization of the nucleotides. This phenomenon is not observed with other types of salt, such as calcium chloride. This suggests that these Hbonds would have been necessary on a prebiotic Earth to form later on phosphodiester bonds [41].

## 2.6 Conclusion

The formation of RNA from non-activated nucleotides using wet-dry cycles is not an easy process. The planet simulator allowed us to have wet-dry cycles with unprecedented resolution. However, the low pH, in addition to the extreme heat necessary to form the phosphodiester bonds, is not a good combination to preserve the integrity of the nucleotide molecules. Adding certain types of salts, such as ammonium ones, accelerates this decomposition. Neither gel electrophoresis nor mass spectrometry revealed the formation of phosphodiester bonds between nucleotides. Nevertheless, Molecular Dynamics simulations revealed that at pH 7, in the absence of water,  $\text{NH}_4$  ions help form Hbonds between the  $C3'$  and the  $C5'$  of the nucleotides by clustering. These pre-polymers may have been necessary for RNA formation on prebiotic Earth. These findings suggest that a neutral environment in a warm little pond in the presence of ammonium ions could have led to the formation of RNA polymers from non-activated nucleotides on an early Earth.

## Chapter 3

The formation of RNA

pre-polymers in the presence of

different prebiotic mineral surfaces

studied by Molecular Dynamics

simulations

## 3.1 Preface for Paper I

This paper aimed to have a deeper understanding of the nucleotide (AMP, UMP, CMP, GMP) interactions with different substrates using Molecular Dynamics (MD) simulations, in the context of the origin of life. We investigated the different properties of nine types of minerals. We wanted to find a link between the minerals' properties and the interactions with the nucleotides which may have led to the formation of RNA. Thus, we forced dehydration by removing manually after each simulation molecules of water mimic RNA formation in warm little ponds.

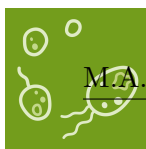
**Status:** published in Life

**Author Contributions:**

MD Model Development and Analysis: Alix Dujardin, Maikel Rheinstädter, Sebastian Himbert

Data Analysis: Alix Dujardin, Maikel Rheinstädter

Manuscript Preparation: Alix Dujardin, Maikel Rheinstädter, Ralph Pudritz



Article

---

# The Formation of RNA Pre-Polymers in the Presence of Different Prebiotic Mineral Surfaces Studied by Molecular Dynamics Simulations

---

Alix Dujardin, Sebastian Himbert, Ralph Pudritz and Maikel C. Rheinstädter

## Special Issue

The Origin and Early Evolution of Life: Prebiotic Systems Chemistry Perspective

Edited by

Dr. Michele Fiore and Dr. Emiliano Altamura



Article

# The Formation of RNA Pre-Polymers in the Presence of Different Prebiotic Mineral Surfaces Studied by Molecular Dynamics Simulations

Alix Dujardin <sup>1,2</sup>, Sebastian Himbert <sup>1,2</sup>, Ralph Pudritz <sup>1,2</sup> and Maikel C. Rheinstädter <sup>1,2,\*</sup> <sup>1</sup> Department of Physics and Astronomy, McMaster University, Hamilton, ON L8S 4M1, Canada<sup>2</sup> Origins Institute, McMaster University, Hamilton, ON L8S 4M1, Canada

\* Correspondence: rheinstadter@mcmaster.ca; Tel.: +1-(905)-525-9140-23134; Fax: +1-(905)-546-1252

**Abstract:** We used all-atom Molecular Dynamics (MD) computer simulations to study the formation of pre-polymers between the four nucleotides in RNA (AMP, UMP, CMP, GMP) in the presence of different substrates that could have been present in a prebiotic environment. Pre-polymers are C3'–C5' hydrogen-bonded nucleotides that have been suggested to be the precursors of phosphodiester-bonded RNA polymers. We simulated wet–dry cycles by successively removing water molecules from the simulations, from ~60 to 3 water molecules per nucleotide. The nine substrates in this study include three clay minerals, one mica, one phosphate mineral, one silica, and two metal oxides. The substrates differ in their surface charge and ability to form hydrogen bonds with the nucleotides. From the MD simulations, we quantify the interactions between different nucleotides, and between nucleotides and substrates. For comparison, we included graphite as an inert substrate, which is not charged and cannot form hydrogen bonds. We also simulated the dehydration of a nucleotide-only system, which mimics the drying of small droplets. The number of hydrogen bonds between nucleotides and nucleotides and substrates was found to increase significantly when water molecules were removed from the systems. The largest number of C3'–C5' hydrogen bonds between nucleotides occurred in the graphite and nucleotide-only systems. While the surface of the substrates led to an organization and periodic arrangement of the nucleotides, none of the substrates was found to be a catalyst for pre-polymer formation, neither at full hydration, nor when dehydrated. While confinement and dehydration seem to be the main drivers for hydrogen bond formation, substrate interactions reduced the interactions between nucleotides in all cases. Our findings suggest that small supersaturated water droplets that could have been produced by geysers or springs on the primitive Earth may play an important role in non-enzymatic RNA polymerization.

**Keywords:** origins of life; non-enzymatic RNA polymerization; prebiotic mineral surfaces; molecular dynamics simulations; hydrogen-bonded RNA pre-polymers



**Citation:** Dujardin, A.; Himbert, S.; Pudritz, R.; Rheinstädter, M.C. The Formation of RNA Pre-Polymers in the Presence of Different Prebiotic Mineral Surfaces Studied by Molecular Dynamics Simulations. *Life* **2023**, *13*, 112. <https://doi.org/10.3390/life13010112>

Academic Editors: Michele Fiore and Emiliano Altamura

Received: 25 November 2022

Revised: 21 December 2022

Accepted: 24 December 2022

Published: 30 December 2022



**Copyright:** © 2022 by the authors. Licensee MDPI, Basel, Switzerland. This article is an open access article distributed under the terms and conditions of the Creative Commons Attribution (CC BY) license (<https://creativecommons.org/licenses/by/4.0/>).

## 1. Introduction

One of the most challenging questions about the origin of life is in what environment primitive life may have started. It has been suggested that life can form near hydrothermal vents [1–7], in warm little ponds [8–21], or in ice [22–25]. In all these scenarios, biomolecules are in contact with substrates. Minerals are known to be catalysts for many reactions, such as molecular synthesis, selection, protection, concentration, templating or even organization of biomolecules [26]. During the Hadean period (about 4 Gy ago), more than 420 different types of minerals were estimated to be distributed on Earth [26]. The question is what mineral potentially helped the formation of life, and what kind of interactions between biomolecules and minerals are important for the emergence of life? To answer those questions, numerous experiments included minerals, whether to understand how chirality of molecules started [27–31], to understand the synthesis of the first building blocks

of life [2,32–42], the first metabolism [1,43–56], the formation of primitive cells [57–60], to synthesize peptides [60–65], or to synthesize ribonucleic acids (RNA) [17,60,64,66–77].

RNA synthesis becomes particularly relevant since primitive life is thought to have started with RNA because RNA can store genetic information and it is also a catalyst [78–82]. RNA is also capable of evolution in vitro [83–89]. Modern RNA is mainly synthesized via RNA-polymerases by using DNA as a matrix. However, it is not clear how such molecules could have been synthesized 3.5 billion years ago. Since the discovery of the catalytic activities of RNA, many scientists have addressed the question of RNA synthesis in the prebiotic world [90]. Finding a catalyst/template to promote RNA synthesis is essential since it is thermodynamically not possible for polymerization to happen in water only.

Minerals are likely important for the origin of life research for multiple reasons. One of the main benefits of the minerals is to concentrate biomolecules in solution. It has been shown in many studies that charged surface minerals adsorb charged biomolecules. For example, Ferris and Ertem [72,91] highlighted that the protonated base and the negative charges of montmorillonite surface interact via electrostatic interactions. Franchi et al. [92] have shown the importance of the type of cation used for binding to the surface. They exposed that divalent cations were better at mediating the adsorption compared with the monovalent cations. Other substrates have been used to concentrate nucleotides [93]. It is, however, possible to concentrate biomolecules in water without surfaces. Mast et al. [94] conducted experiments on thermal gradients that led to the formation of polymers due to a thermal trap. They explained that the thermal trap increases the sequence space availability and induces active catalytic polymer formation.

As RNA synthesis from monomers is thermodynamically unfavorable in the presence of water, many of these studies in aqueous environments used activated nucleotides. In this study, we investigated the interaction between non-activated nucleotides and nine substrates that have been suggested to be present on primitive Earth [26] using all-atom Molecular Dynamics (MD) simulations. Water molecules were successively removed during the simulations to mimic dehydration. Three clays were investigated (montmorillonite, kaolinite, and pyrophosphate), one mica (muscovite), one phosphate mineral (hydroxyapatite), one silica (quartz), two metal oxides (corundum, and periclase), and one carbonaceous material (graphite).

These nine substrates were chosen because of their interest in origin of life research. Clays are known to have reactive surfaces, high cations exchange, and catalytic activities in aqueous environments [95] and clays are often used in origin of life research because of these properties [45,46,57,66–72,93,96–98]. Montmorillonite and kaolinite are abundant clays on Earth [99,100]. We also included pyrophyllite, which has aluminum atoms sandwiched between two silica sheets, and kaolinite, which consists of a single sheet of silica, only. All three clays can be found where hydrothermal alteration occurred, such as in warm little ponds or in epipelagic environments, as sketched in Figure 1. Montmorillonite and pyrophyllite are found at low-temperature metamorphism, and montmorillonite can also be present in meteorites [26]. Muscovite is a common mineral on Earth, which can be compared to clays because it has a similar structure to montmorillonite. It is authigenic (formed where it is found), but it can also be found in granitic igneous, and where hydrothermal alteration and regional metamorphism occurred. Some traces are found in Hadean zircons (the oldest mineral that survived Earth's transformation) [26,101]. Some scientists used muscovite as a “primitive cell” because it has common points with our modern cells [102–105].

Hydroxyapatite is the main constituent of dental enamel, dentin, and bones. It is found where hydrothermal alteration and serpentinization happened [26,74]. Hydroxyapatite was included in this study because it was used in several experiments for phosphate and nucleotide synthesis linked to the origin of life [38,39,74]. Silicate minerals (quartz) represent more than two-thirds of the Earth's crust. As a result of their abundance on Earth, silica was one of our minerals selected. They can be found in granitic igneous, where hydrothermal alteration occurred, in meteorites and clastic sedimentary environment,

M.A.Sc. Thesis – A. Dujardin; McMaster University – Chemistry and Chemical Biology

as well as in Hadean zircons inclusion [26,95]. Quartz is used in origin of life research related to the chirality of molecules [27–30].

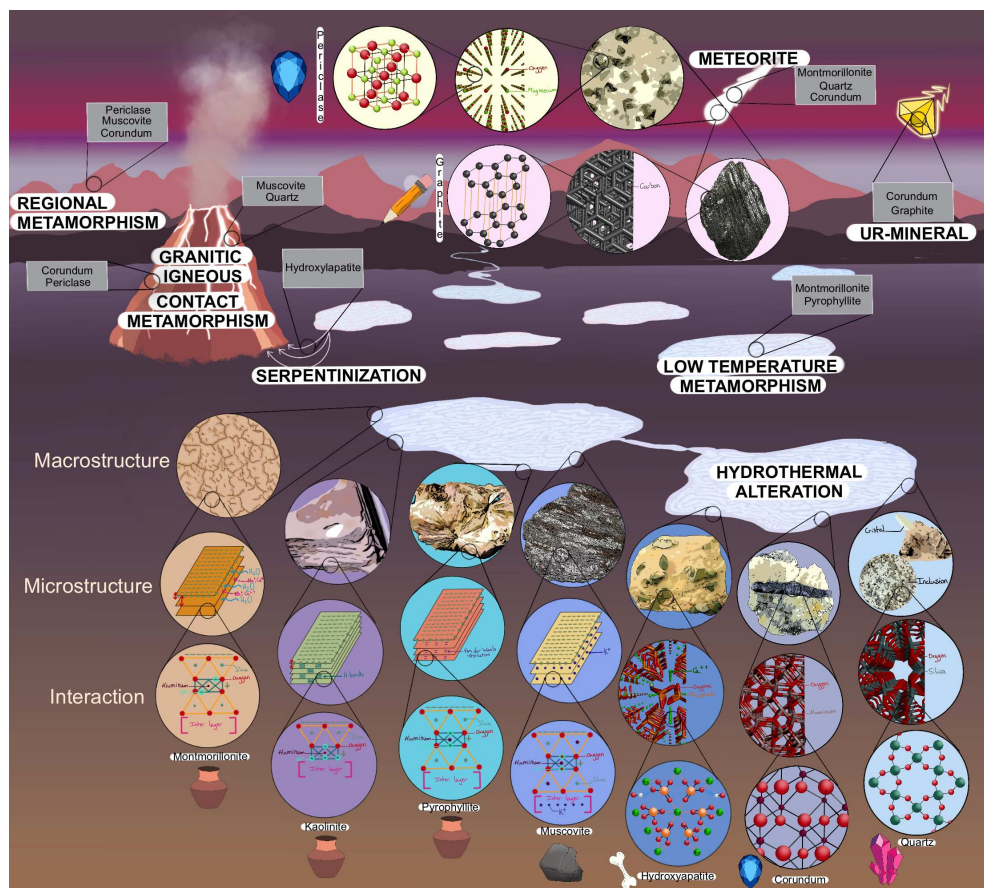


**Figure 1.** Sketch of primitive Earth including the nine substrates investigated in this study. Each substrate differs in its macrostructure, microstructure, and interaction between the atoms. They occur in different environments, such as hydrothermal alteration, low-temperature metamorphism (where pressure is higher), regional metamorphism (large-scale action of heat and pressure), contact metamorphism (contact with or proximity to a magmatic rock), serpentinization (contact between seawater and magmatic rock with a low silica rate), meteorite, in granitic igneous rocks (specific magmatic rocks), and in Ur-mineral (minerals formed from presolar grains) [26]. Clay substrates are represented by a jar (montmorillonite, kaolinite, pyrophyllite), mica is represented by a rock (muscovite), the phosphate mineral by bone (hydroxyapatite), metal oxides by sapphire (corundum, and periclase), the crystal represents the silicate mineral (quartz), and the pencil represents the carbonaceous material (graphite). Representations are used throughout the manuscript.

Corundum has, among others, two gem varieties: ruby and sapphire. It is commonly found in meteorites but it can also be found in alkali igneous (in the basic and volcanic environments), where contact and regional metamorphism happened, in hydrothermal alteration, in a clastic sedimentary environment, and Ur-minerals from pre-solar grains. This mineral was used to understand the formation and the stability of the first cells [106,107]. Periclase is usually found in marble produced by contact, and regional metamorphism in the form of inclusion, as well as in meteorites [26]. Periclase and corundum were chosen because these minerals can be found in small inclusions in bigger rocks. Their atoms' organization provides them a hardness that is not present in the other minerals studied. Graphite is one of the presolar dust grains [108], but it can also be found in metamor-

phic rocks. Some researchers used it to understand the first metabolism [109] and the concentration of nucleic bases [110,111].

In the wet–dry cycles hypothesis for the origin of life [15,16], nucleotides are mixed in an aqueous phase and then dried on a surface. At the same time, the available thermal energy for sufficiently warm conditions drives the formation of a phosphodiester bond between the C3' and C5' of neighboring nucleotides. This assumption implies that nucleotides align in a way that brings these two atoms in close proximity when they dry out on a surface. The question that we address is to what extent various mineral substrates are able to promote polymerization by either securing favorable proximity or securing favorable molecular arrangements of the nucleotides. We address this question by conducting a comprehensive series of MD simulations in which we carefully follow the dynamics of nucleotides in their interaction with one another and as well as the nine surfaces of minerals noted in Figure 1 as dehydration takes place. In particular, we track the appearance of hydrogen bonds between the C3' and C5' atoms that are probably precursors of covalent bond formation. These nucleotides, which are aligned, however, have not yet formed phosphodiester bonds have been named 'pre-polymers' [9]. These pre-polymers are thus in the right conformation and ready to bond; however, ester bond formation is a rate-limiting process, unlike hydrogen bonds. Even though the formation of phosphodiester bonds using wet–dry cycles is a thermodynamically favorable process [15], the formation rate of these bonds must be as fast as possible due to numerous exterior factors that can damage RNA polymers, such as hydrolysis, pH, or temperature. Our simulations suggest that surfaces may play a secondary role in this pre-polymerization phase. It is most likely that the stage leading to polymerization in such dehydration conditions occurs in the volume of drastically dehydrated ponds and, in particular, in small droplets that are nearly completely dehydrated.

## 2. Results

### 2.1. Substrate Properties: Charge and Hydrogen Bond Potential

In the following, we classify the substrates used in this study based on two physical properties, which we believe are important for their interaction with nucleotides: (1) their charge and (2) their potential to form hydrogen bonds (Hbonds) with the nucleotides.

#### 2.1.1. Charges

The type of atoms and their arrangement determine the surface charge of a substrate. This property determines what types of molecules or molecular groups would be attracted through electrostatic interactions. To better understand the surface charge of each substrate, an interpolated charge surface map was created and is shown in Figure 2. This map was generated using the software BIOVIA Discovery Studio 2021 [112]. A partial charge is assigned to each atom on the surface. If there is no partial charge available, the system calculates the Gasteiger charge which is determined on the basis of electronegativity equilibration [113]. The limits used are  $-0.1$  to  $+0.1$  C. The map is then created using a numerically mapped color spectrum. In Figure 2, the light blue represents a positive surface, the dark-purple blue is associated with a neutral surface, and the red color shows a negative surface.

From these calculations, three of the substrates are strictly positively charged: muscovite's surface is positive due to the potassium ions on the surface. Corundum is positively charged throughout its entire surface due to the aluminum present. Periclase's overall charge is positive due to the presence of magnesium.

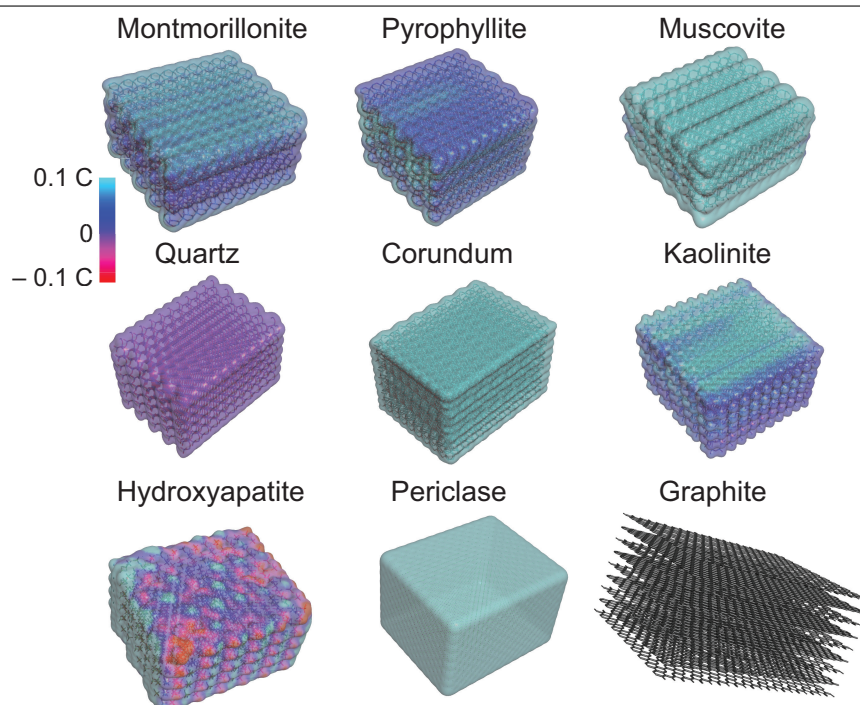


**Figure 2.** Surface map of interpolated charges for the different substrates. Light blue represents a positive charge, while red shows a negative charge. Charges vary between  $-0.1$  and  $+0.1$  C. Dark blue/purple illustrates a neutral charge. Montmorillonite, muscovite, corundum, kaolinite, and periclase are positively charged. Pyrophyllite and quartz are neutral. Hydroxyapatite is both positive and negative. Graphite has an inert surface. Maps were created using BIOVIA Discovery Studio 2021 [112].

The montmorillonite surface tends to be positively charged but less than  $+0.1$  C. The extremity of the folia is, however, neutral. Kaolinite tends to have similar charges as montmorillonite; however, its surface tends to be more positive due to the presence of hydrogen atoms. Hydroxyapatite's surface is both positively and negatively charged. The oxygen attached to the phosphate gives a negative charge, while the calcium provides a positive charge. Pyrophyllite's surface tends to be neutral due to the position of the hydroxide ions in the substrate. Quartz is also neutral because each oxygen is linked to a silica atom. Graphite is included here as a reference for a non-interacting substrate because it has no charges. The role of this substrate will be discussed further below.

### 2.1.2. Hydrogen Bond Potential

A substrate's capacity to form Hbonds with external molecules, such as the nucleotides, is an important physical property. The surface map in Figure 3 gives information on the area of the surface where nucleotides can bond. To do so, a map was created to extrapolate the potential donor or acceptor of each surface using BIOVIA discovery Studio 2021 [112]. Hydrogen atoms were added if needed to ensure a consistent surface. If an atom is considered as a donor, a fictitious charge  $q$  is given of  $+1$  C. A fictitious charge  $q$  of  $-1$  C is assigned for atoms considered acceptors. Other atoms are not taken into consideration. The charges are used to calculate a single-valued "potential" function at the location of each surface vertex. The potential is obtained as the weighted average  $\sum_q w(q) \cdot q$  of all charges  $q$ , with the weight  $w(q)$  for an individual charge  $q$  set to the ratio  $s(q)/s$ , where  $s(q)$  is the inverse of the square distance between the position of the surface vertex and the position of the atom carrying charge, and  $s = \sum_q s(q)$  is the sum of the contributions  $s(q)$  from all charges. This potential is then mapped using a numerically mapped color spectrum as well.

In this figure, green represents an acceptor surface, the magenta color represents a donor surface, and white is neutral.

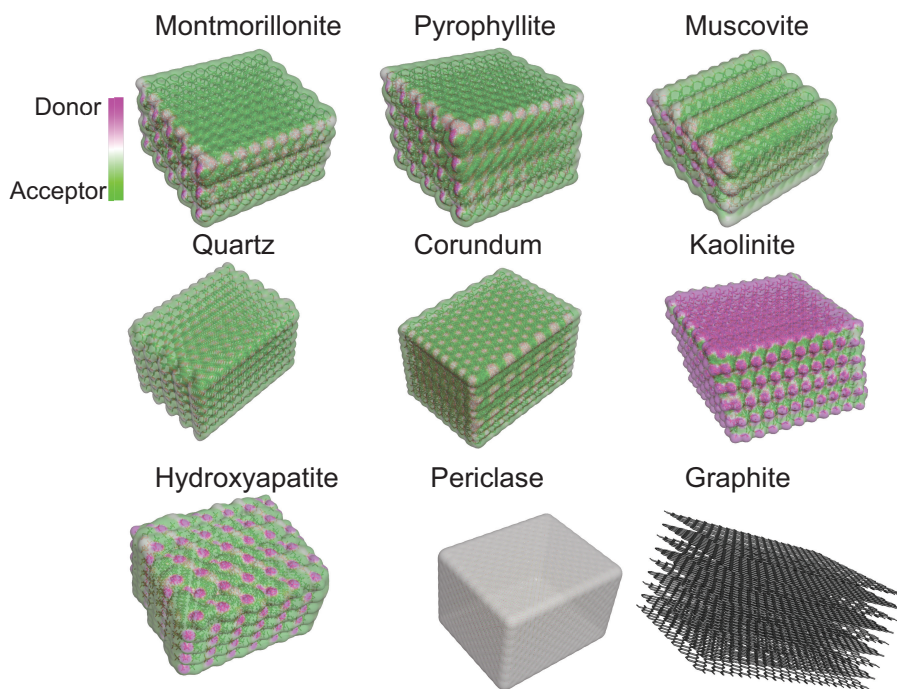


**Figure 3.** Surface map representing the substrates' capacity to form hydrogen bonding with other molecules. In green, the substrates tend to function as hydrogen bond acceptors, while the magenta color shows the surface which functions as hydrogen bond donors. White illustrates a neutral surface. Montmorillonite, pyrophyllite, muscovite, quartz, and corundum are acceptors. Kaolinite is a donor. Hydroxyapatite is both donor and acceptor. Periclase is neutral, and graphite is inert. Maps were created using BIOVIA Discovery Studio 2021 [112].

Following this analysis, five substrates have the potential to form Hbonds. Montmorillonite clay surface has the potential to accept hydrogen bonds due to oxygen on the surface. However, due to the hydrogen present at the aluminum layer's extremity, the folia's edge functions as a donor. Thus, magenta is seen in between each repeating unit. As montmorillonite, pyrophyllite will tend to form a hydrogen bond by accepting an electron on its surface. Muscovite's surface has the potential to accept electrons to make hydrogen bonds due to the presence of oxygen. Quartz's overall surface functions as a hydrogen bond acceptor due to the oxygen present in the mineral. Corundum will tend to receive electrons because not all oxygens are fully connected with aluminum.

Kaolinite's surface is the only one to work as a potential hydrogen bond donor. This is due to the presence of hydrogen linked to oxygen which made the bond between the silica atoms. At the extremity of the folia, oxygen is exposed; thus, this part of the surface is a hydrogen bond donor. The hydroxyapatite surface has both donor and acceptor properties. The oxygen ions are acceptor, while the hydrogen linked to the oxygen serve as donors. Periclase does not accept or give hydrogen because all oxygen is linked with a magnesium ion.

Charge distribution and the potential to form Hbonds were also created for the nucleotide molecules. In Figure 4a, adenosine monophosphate (AMP) is shown as an example. Figure 4b shows the potential Hbonds surface map. The nucleotide's atoms do not have the same capacity to form Hbonds throughout the molecule. The phosphate of the nucleotide is a hydrogen bond acceptor, while the hydroxyl on the C2' and C3' are donors as well as the amine group on the base. The other atoms of the molecules are neutral. Figure 4c

shows the surface charge of the AMP molecule. Nucleotides have heterogeneous charges throughout the molecule. The phosphate of the nucleotide is negatively charged, while the other parts of the nucleotides tend to be more neutral. This figure gives information on which part of the nucleotide can potentially form electrostatic interactions and hydrogen bonds with the different substrates.

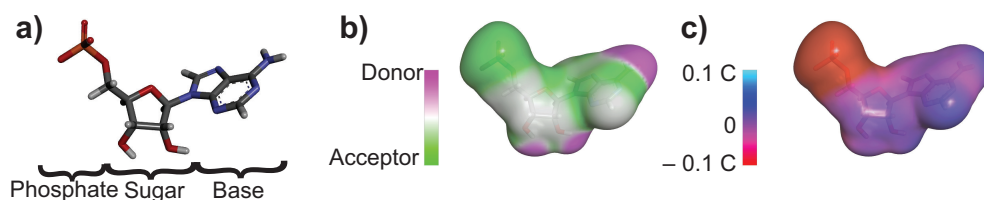


**Figure 4.** Example of a nucleotide used in the simulations. (a) Adenosine monophosphate (AMP) molecule. (b) Map of the hydrogen bond potential of AMP. (c) Map of the charge distribution of AMP.

## 2.2. Molecular Dynamics Simulations

All-atom MD simulations were performed using GROMACS 2016.3 on MacSim, a GPU-accelerated computer workstation [114]. Each simulation was set up using CHARMM-GUI [115–117]. The size of the simulation box was  $85 \text{ \AA}^3$ . All systems contained 200 nucleotides (50 nucleotides of AMP, UMP, CMP, and GMP, respectively), the substrate, and water molecules. The system was first energy minimized and then equilibrated. Hydration was reduced in 10 steps from  $\sim 12,500$  water molecules to  $\sim 600$  water molecules in total, equivalent to a dehydration from  $\sim 62$  to  $\sim 3$  water molecules per nucleotide. Each simulation's total production simulation time using this dehydration script was  $\sim 200$  ns, resulting in a total production simulation time of about  $2 \mu\text{s}$  of all-atom MD simulations for this study. More details can be found in Section 5.

Figure 5a shows snapshots of the MD simulation run in the presence of hydroxyapatite. Hydroxyapatite is represented in pink, nucleotides in purple, and water in gray. Snapshots were taken at four different hydration levels:  $\sim 100\%$ ,  $\sim 70\%$ ,  $\sim 40\%$ , and  $\sim 5\%$ . These frames were taken at 10 ns at  $\sim 100\%$  and 15 ns for the last three. The figure shows that every time water molecules are removed from the system, nucleotides move closer to the substrate until they saturate the substrate surface at  $\sim 5\%$  hydration.

We used this MD simulation also to calculate the number of Hbonds during dehydration. Hydrogen bond analysis was performed using Visual Molecular Dynamics algorithms [118]. Three different interactions are plotted in Figure 5b: the Hbonds between C3' and C5' of the nucleotides in blue, the Hbonds between C3' and C5' of the nucleotides within a  $7 \text{ \AA}$  distance from the substrate are represented in orange, and the Hbonds between the nucleotides (non-specific atoms) and the substrate in yellow. All substrates resulted in similar profiles, with the number of Hbonds significantly increasing when water molecules were removed from the system, resulting in denser packing and increased substrate interaction. When fully hydrated, all types combined the number of Hbonds was found to be low ( $\sim 5$  on average). When decreasing the number of water molecules, the number of Hbonds started to increase in all cases. A number of hydrogen bonds of  $\sim 50$  at the lowest hydration of  $5\%$  then means that  $25\%$  of the nucleotides have formed hydrogen bonds (out of 200 nucleotides in total). We will focus on the results at  $\sim 5\%$  hydration in the following, representing the fully dehydrated state.

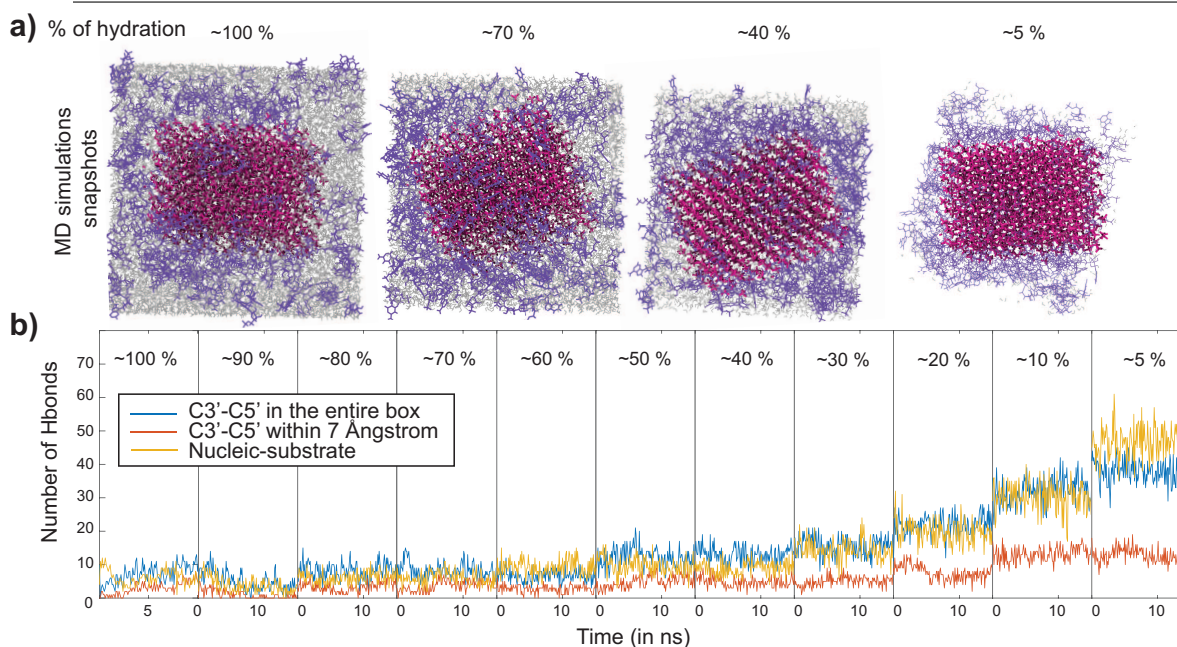


**Figure 5.** MD simulation results for hydroxyapatite as an example. (a) Snapshot of MD simulations at ~100%, ~70%, ~40%, and ~5% hydration. The simulation contained 200 nucleotides. Hydroxyapatite is shown in pink, nucleotides in purple, and water in gray. (b) Number of hydrogen bonds (Hbonds) between the C3' and the C5' of the nucleotides in the entire simulation box (blue); between the nucleotides' C3' and the C5' within a distance of 7 Å to the substrate (orange), and between the nucleotides and the substrate (yellow), as a function of hydration. While the number of hydrogen bonds nucleotides is small (~5) when fully hydrated (at 100% hydration), bonding significantly increases during dehydration.

### 2.3. Substrates with Positive Charges Attract the Nucleotides' Phosphate Group

The surface charge of the substrates determines the orientation and the attraction of the nucleotides to the surface. Different parts of the nucleotides will be attracted by electrostatic interactions and will interact with the substrate. In our study, five substrates have a positively charged surface, pyrophyllite and quartz are neutral, and hydroxyapatite has both positive and negative charges. A representation of the nucleotide orientation on the different surfaces is pictured in Figure 6. A positive surface will attract the negatively charged phosphate group of the nucleotides due to their opposite attraction (Figure 6a). Then, depending on the Hbonds potential of the surface, the nucleotides would be able to form hydrogen bonds with different parts of the molecule (Figure 6b). The donor surface will form Hbonds with the phosphate of the nucleotides because of the oxygen present. The hydroxyl on the sugar and the hydrogen on the base will form Hbonds with an acceptor surface because of their donor property. Figure 6c shows a snapshot of the hydroxyapatite MD simulation at ~5% showing the nucleotide conformations equivalent to the cartoons in parts a and b. In this figure, only AMP molecules are shown for clarity.

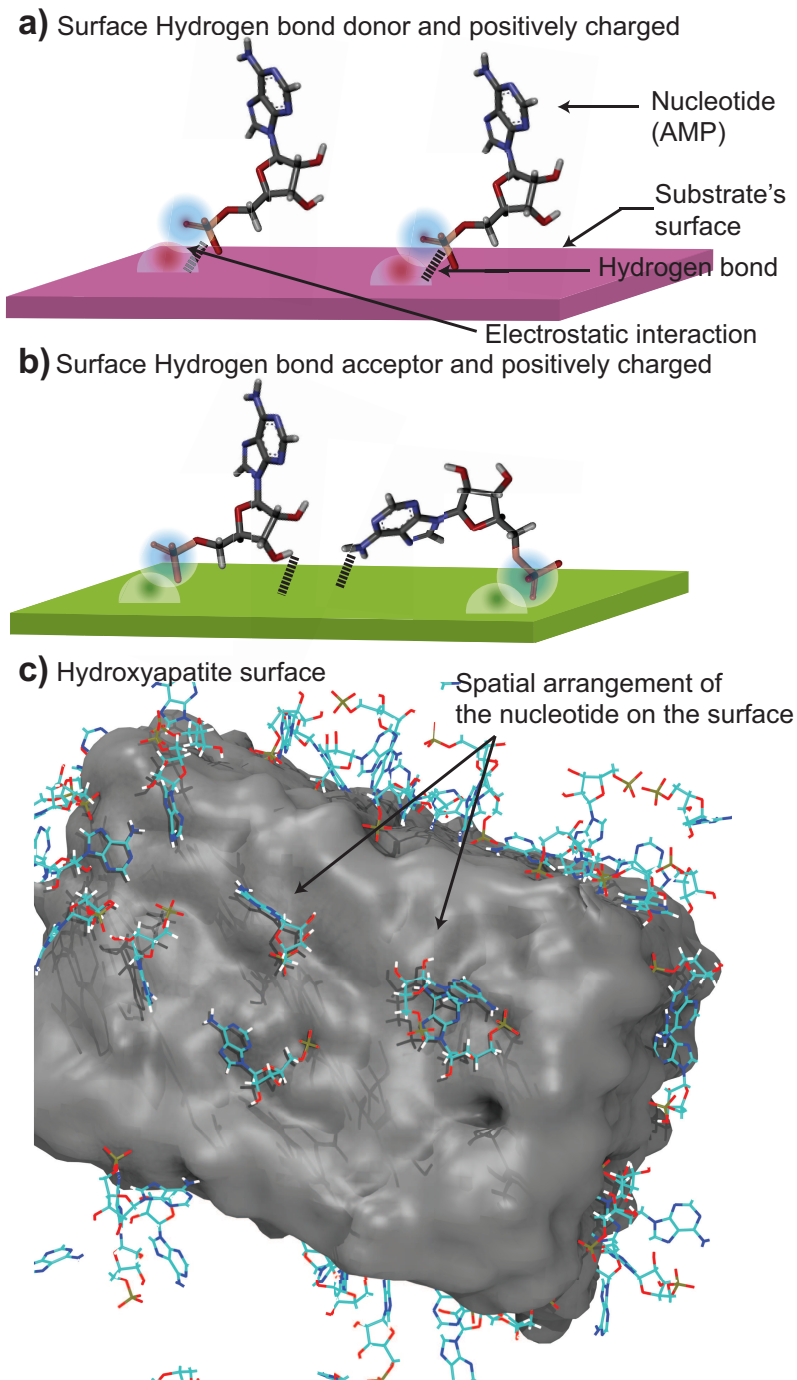


**Figure 6.** Sketch of the organization of nucleotides on the different substrates. (a) When the surface is a hydrogen donor and positively charged, the negatively charged phosphate is attracted through electrostatic interactions and will form Hbonds with the surface. (b) If the surface is an acceptor and positively charged, the phosphate will be attracted; however, the hydroxyl part of the sugar and the base will form Hbonds with the surface. (c) Screenshot of the hydroxyapatite MD simulation at ~5% at 15 ns showing the nucleotide conformations, sketched in (a,b). Only AMP molecules are shown for clarity.

#### 2.4. Substrates form Hydrogen Bonds with Different Parts of the Nucleotides

We calculated the number of Hbonds between the nucleotides (all atoms combined) and the different substrates. Figure 7 shows the average number of Hbonds formed at ~5% hydration. Error bars represent one standard deviation. It is evident that the different substrates bond very differently with the nucleotides. Three of the four acceptor substrates do not form a significant amount of Hbonds with the substrates, as seen in Figure 7 (montmorillonite: ~10; pyrophyllite: ~12; muscovite: ~8). Corundum is an exception and it formed ~37 Hbonds with the nucleotides. Kaolinite, which is a hydrogen donor, formed ~24 Hbonds with the nucleotides. Hydroxyapatite was the most efficient for forming Hbonds with the nucleotides by having both hydrogen donor and acceptor atoms. It formed Hbonds up to ~47 bonds. The neutral surface periclase formed ~9 Hbonds with the nucleotides.

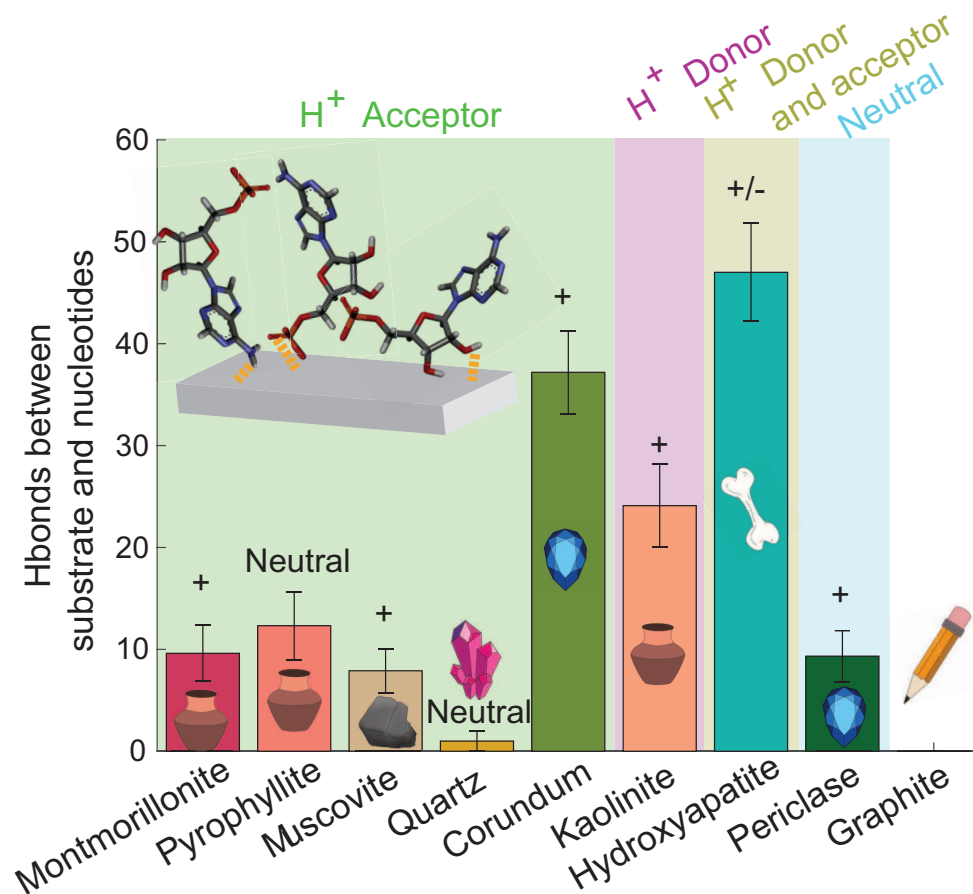


**Figure 7.** The average number of Hbonds formed between the substrates and the nucleotides at ~5% hydration. The error bars represent one standard deviation. The color blocks represent the substrates' potential as donors or acceptors. The "+" and "-" represent the positive and negative surface charges, respectively. The largest number of Hbonds are observed for corundum, kaolinite, and hydroxyapatite.

We then calculated the number of Hbonds between the phosphate, the base, and the hydroxyl of the nucleotides and the substrates. Figure 8 shows the number of Hbonds between the nucleotide base and the substrate (purple), between the nucleotide sugar and the substrate (to be more specific, between C2' and C3' of the sugar) in yellow, and the nucleotide phosphate group and the substrate (blue) for all substrates in this study.

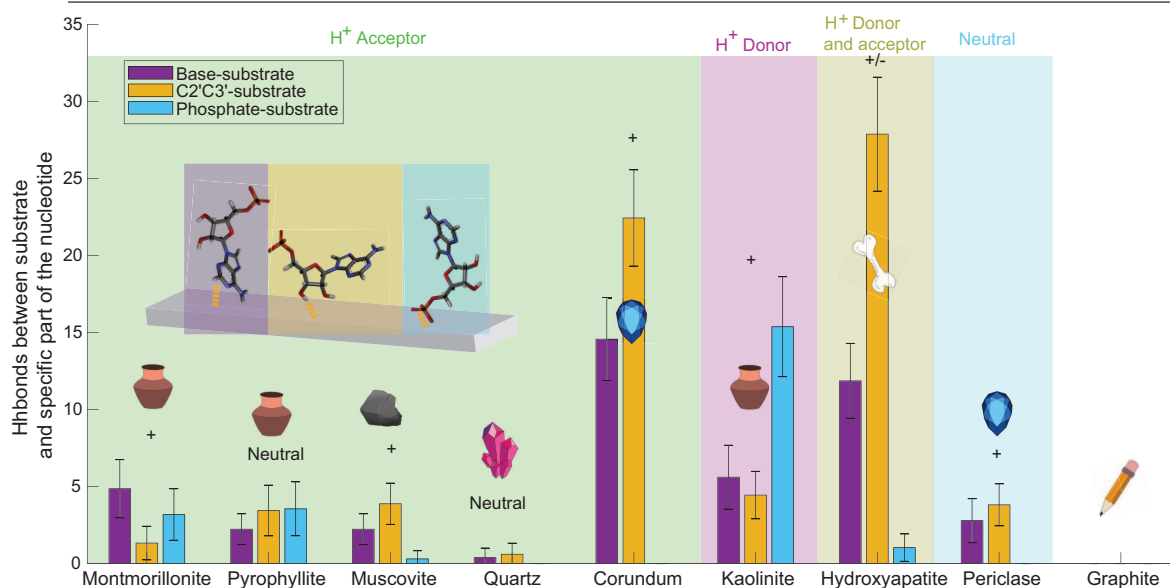


**Figure 8.** The average number of Hbonds formed between the different substrates and the different parts of the nucleotides at ~5% hydration. Three nucleotide parts were considered: the nucleotides' base (purple), the hydroxyl C2' and/or C3' (yellow), and the phosphate (blue). Error bars represent one standard deviation. The color blocks visualize the substrates' potential to serve as Hbond donors or acceptors. The "+" and "-" represent the positive and negative surface's charge, respectively. The largest number of bonds was observed for corundum, kaolinite, and hydroxyapatite, between C2' and/or C3' and the substrate.

Figure 8 shows that not all parts of the nucleotides interact in the same way with the different substrates. Except for montmorillonite, three of the four acceptor surfaces were found to form bonds mainly with the nucleotides' C2' and/or the C3'. They also created Hbonds with the base of the nucleotides, however, with a lower rate, and they formed a few Hbonds with the phosphate of the nucleotides. Montmorillonite mainly formed Hbonds with the base of the nucleotides. Kaolinite formed 62% of its Hbonds with the phosphate of the nucleotides. Hydroxyapatite mainly formed Hbonds with the C2' and/or C3' and the base of the nucleotide. It formed only one Hbond with the phosphate of a nucleotide. Periclase formed around the same number of Hbonds with the C2'/C3' and the base of the nucleotides (four and three, respectively), and none with the phosphate.

### 2.5. No Substrate Is a Good Catalyst for the Formation of Pre-Polymers

The C3' link to the C5' is the most critical linkage for the origin of life as it is the bond that links the nucleotides in modern RNA and DNA. We thus calculated the number of Hbonds between those two atoms in the presence of the different substrates. Figure 9a shows the number of Hbonds between C3' and C5' in the entire simulation box at ~5% hydration. Figure 9b shows the same type of Hbonds, however, only including nucleotides at a distance closer than 7 Å to the surface to check whether the direct proximity of the substrate has an influence on the formation of these pre-polymers. Figure 9c plots the number of nucleotides closer than 7 Å to the surface.

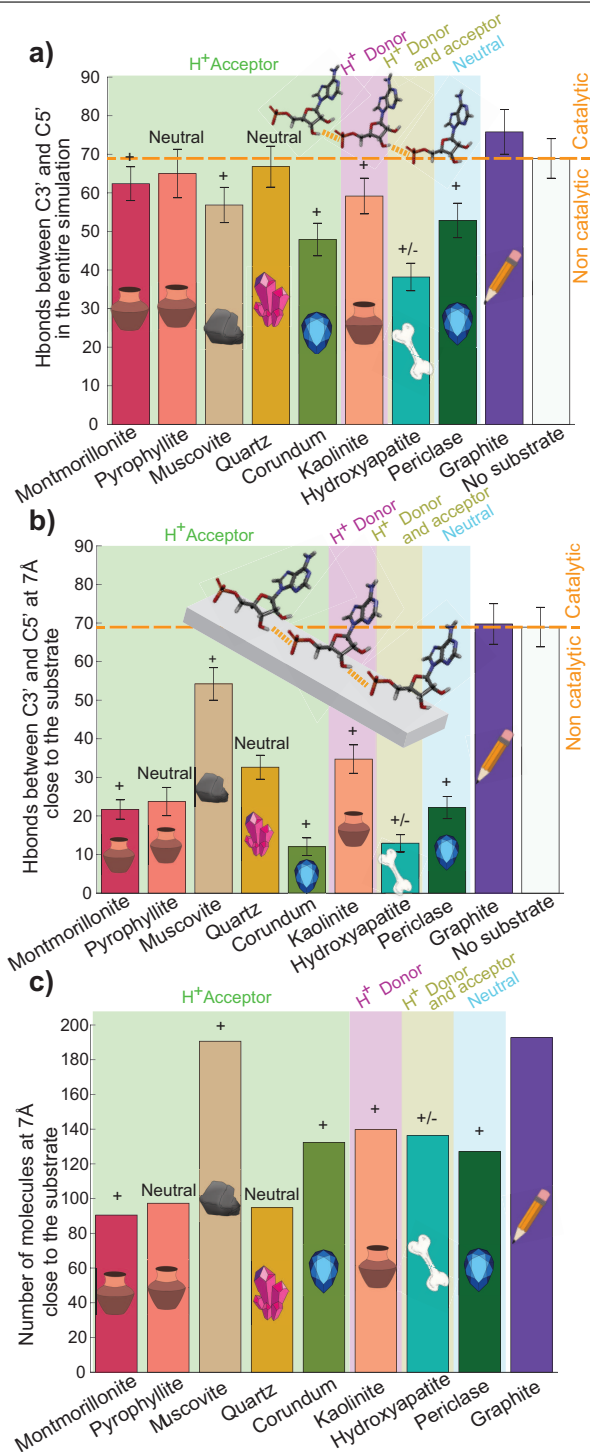


**Figure 9.** (a) The average number of Hbonds formed in the entire box between C3' and the phosphate of the nucleotides (C5') in the presence of the different substrates. (b) The average number of C3'–C5' Hbonds between molecules within a 7 Å distance to each substrate. (c) The average number of nucleotides close to the substrate. All results at ~5% hydration, error bars represent one standard deviation. The color blocks visualize the substrates' potential to serve as Hbond donors or acceptors. The "+" and "-" represent the positive and negative surface's charge respectively. See text for explanations.

In Figure 9, we also included values for two additional systems. We included graphite in the simulations as an inert substrate, which is not charged nor capable of forming hydrogen bonds with the nucleotides. Graphite thus allowed us to study the effect of a non-interacting surface on pre-polymer formation. We also simulated a nucleotide-only system, i.e., 200 nucleotides, that were dehydrated using the same protocol as in the substrate simulations. By comparing to this simulation, one should be able to determine the efficiency of the different substrates, and if they actually work as catalysts for pre-polymer formation.

As a first finding, the largest number of C3'–C5' Hbonds is found in the presence of the neutral graphite, or in the absence of a substrate, as shown in Figure 9a. Within the given statistics, only montmorillonite, pyrophyllite, and quartz lead to a similar number of Hbonds; the number of Hbonds for the other substrates falls below the standard deviation of the nucleotide-only and graphite systems. All of the other substrates thus seem to inhibit the formation of pre-polymers, which include muscovite, corundum, kaolinite, hydroxyapatite, and periclase.

From the data in Figure 9b, the role of the substrate for pre-polymer formation can be determined, as only nucleotides closer than 7 Å to the surface were selected. The largest number of Hbonds was again observed for the neutral graphite and the nucleotide-only system. Except for muscovite, the number of all bonds was significantly lower than the number of total bonds in part a. This is indicative that the presence of a substrate does not drive bond formation as C3'–C5' Hbonds are primarily formed further away than 7 Å from the substrate. To support this hypothesis, Figure 9c displays the number of nucleotides closer than 7 Å to the substrate. For three substrates (montmorillonite, pyrophyllite, and quartz), more than half the nucleotides are further than 7 Å from the surface. Those substrates do not seem to attract the nucleotides efficiently. The other substrates, corundum, kaolinite, hydroxyapatite, and periclase, seem to be attractive to the nucleotides, however, the substrates do not seem to strongly support the formation of pre-polymers.

#### 2.6. Substrate Surfaces Can Align Nucleotide through Interactions

It is important to notice that even though substrates do not seem to support the formation of pre-polymers, they serve to organize the nucleotides. The radial pair distribution function  $g(r)$  between the C3' of the nucleotides has been calculated for all systems, and is presented in Figure 10. No defined peaks are visible in Figure 10a for  $g(r)$  of the nucleotide-only system at ~5%. In the presence of graphite, however, in Figure 10b, three peaks can be distinguished at 4.3 Å, 6 Å, and 6.8 Å.  $g(r)$  of muscovite, quartz, and periclase are exemplary shown in Figure 10c (the other substrates provided similar results). Distinct peaks were observed here as well, at positions of 4.5 Å, 5.7 Å, and 7.3 Å, slightly shifted in comparison to graphite.

These graphs reveal an organization of the nucleotides in the presence of substrates, as sketched in Figure 11. Without a substrate in Figure 11a, the nucleotides are completely disordered in the water phase. This can also be seen in the MD simulations, in the snapshot in Figure 12a. In the presence of graphite (at ~5% hydration) in Figure 11b, the nucleotides align flat on the substrates, forming a hexagonal unit cell with side lengths  $a = 6.8$  Å, and  $b = 4.3$  Å, and angle  $\alpha = 120^\circ$ . Evidence for this type of organization is found in the simulations, as shown in Figure 12b, where nucleotides have a tendency to form flat layers on the graphite sheets.

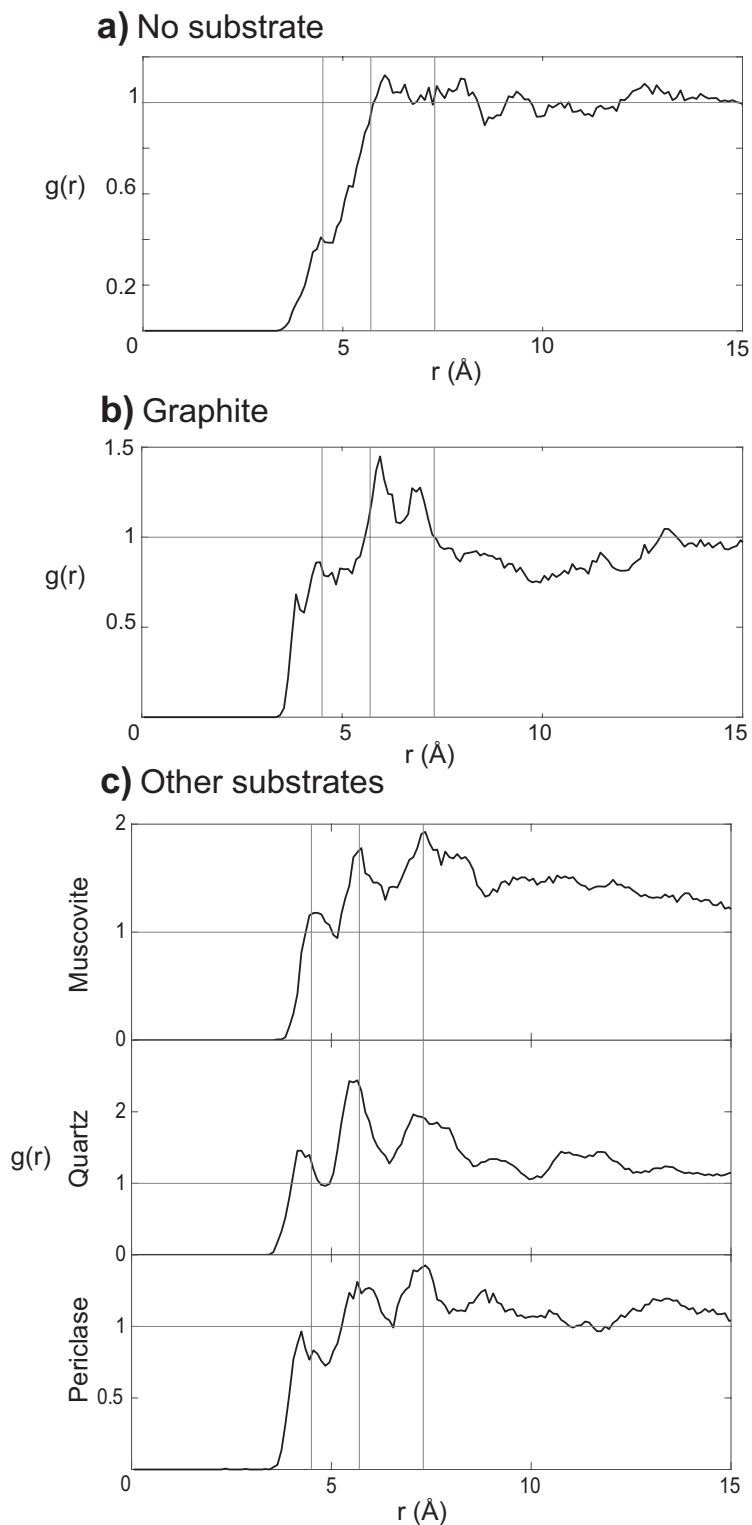


**Figure 10.** Radial pair distribution function  $g(r)$ . (a) The  $g(r)$  of the simulation without substrate at  $\sim 5\%$  hydration. (b) The  $g(r)$  of the nucleotides with graphite at  $\sim 5\%$  hydration. Three peaks are distinguished at 4.3 Å, 6 Å and 6.8 Å. (c) The  $g(r)$  of muscovite, quartz, and periclase as examples. Three peaks can be seen at 4.5 Å, 5.7 Å and 7.3 Å.

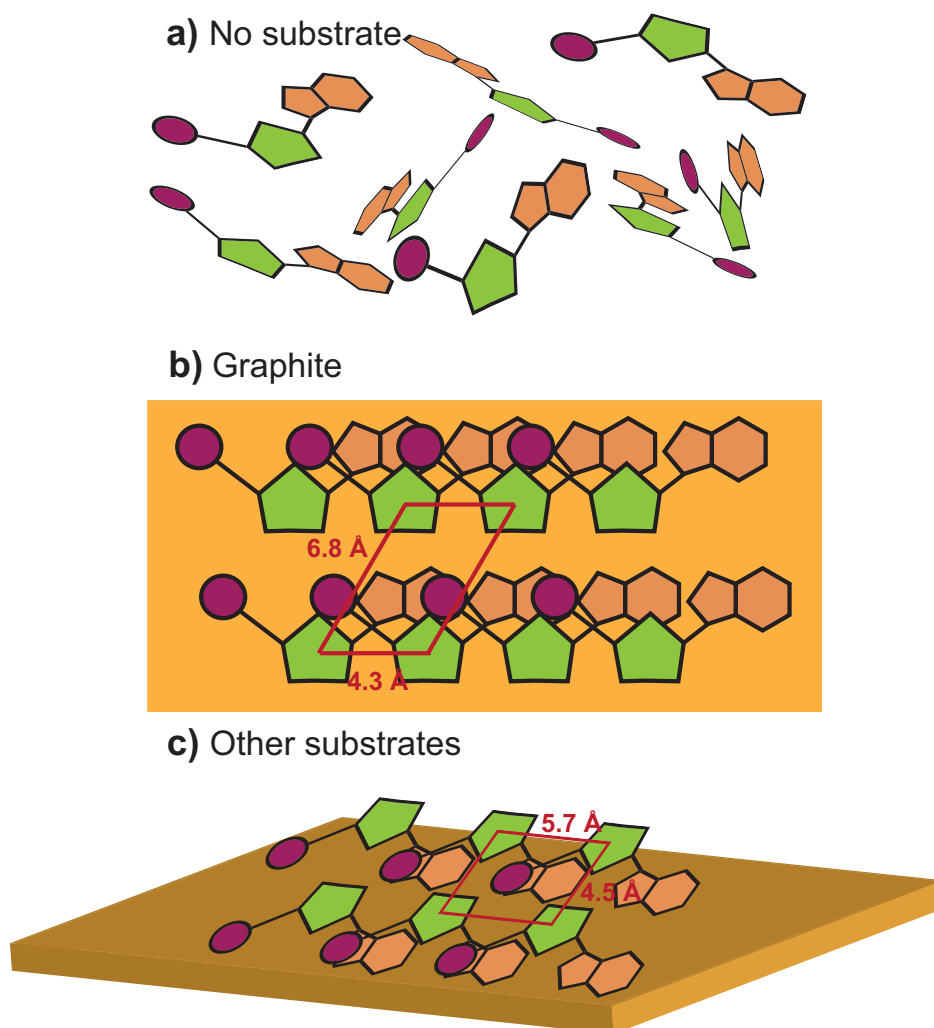


**Figure 11.** Organization of the nucleotides in the simulations. (a) The non-organization of the simulation without substrate at  $\sim 5\%$  hydration. (b) The nucleotide organization with graphite at  $\sim 5\%$  hydration. The nucleotides are laying down on the substrates. The unit cell is a parallelogram with  $a = 6.8 \text{ \AA}$  and  $b = 4.3 \text{ \AA}$ . (c) The nucleotide organization in presence of the other substrates studied at  $\sim 5\%$  hydration. The unit cell is rectangular with  $a = 5.7 \text{ \AA}$  and  $b = 4.5 \text{ \AA}$ .

In the presence of charges, there is an attraction between certain molecular groups in the nucleotides and the substrate, and in order to minimize this electrostatic energy, the nucleotides are no longer aligning flat on those substrates. The electrostatic interactions between the phosphate and the base, for instance, would lead to an arrangement as in Figure 11c, where the nucleotides are slightly tilted, and the different layers can move more closely and become more densely packed. This type of organization can be observed in the MD snapshots in Figure 12c. When the nucleotides are slightly tilted, a second layer of nucleotides can slide under the first layer. The corresponding unit cell is rectangular with  $a = 5.7 \text{ \AA}$ , and  $b = 4.5 \text{ \AA}$ .

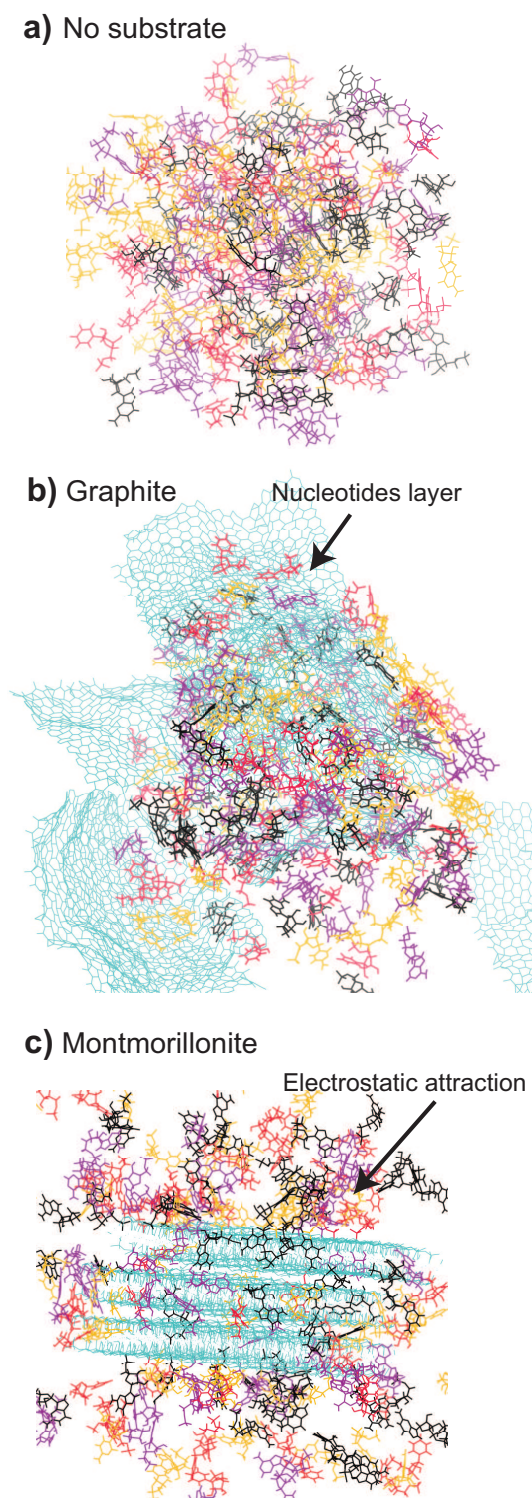


**Figure 12.** Snapshot of the different simulations at ~5% hydration. In purple is AMP, in red—UMP, in black—GMP, and in orange—CMP. The substrates are shown in cyan. (a) Snapshot of the simulation without substrate. (b) The graphite simulation. Nucleotides formed a flat layer on the sheets of graphite. (c) Montmorillonite simulation as an example. Nucleotide phosphates are attracted to the substrate due to the different charges.

### 3. Discussion

Our goal was to find the physical properties of the substrates that support the formation of RNA polymers in a prebiotic environment in the context of the wet–dry cycling theory. To do so, we used Molecular Dynamics simulations using nine different substrates with different charges and hydrogen bonding potential. Some researcher used MD simulations to study wettability of clay [119]. They found that kaolinite is overall hydrophilic and that the *OH*-groups on the *O* surface can form unstable hydrogen bonds with water. MD simulations were also studied for the polymerization of peptides. Quartz and clays were used in this research [120–130]. Other groups studied the formation of nucleotides using MD simulations [131–133], but to our knowledge, these are the first simulations to study the interaction between nucleotides and substrates. Our initial hypothesis was that the presence of substrates has a catalytic effect on the formation of pre-polymers that show C3′–C5′ hydrogen bonds between nucleotides.

Ferris, Ferris et al. [66–68,134], and Huang and Ferris [77] used montmorillonite clay as a catalyst to promote RNA polymerization. Using activated nucleotides, they were able to form RNA polymers up to 40 mers. More recently, rock glasses have been used to convert ribonucleosides 5′-triphosphates into RNA long of 9–150 mers on average [135].

Substrates are also used for template-directed synthesis. Holm et al. [73] used iron oxide hydroxide polymorph to concentrate and form a longer chain of polymers. They again explain the adsorption of the nucleotides onto the surface by electrostatic interaction between the negative charge of the phosphate and the positive surface, as underlined in the introduction. Using hydroxyapatite, Acevedo et al. [74] were able to form polymers of up to 20–25 nucleotides after only one cycle of reactivation and ligation using a template. The length of the polymers increased when increasing the number of reactivation–ligation cycling.

The implicit effect of the concentration is the stabilization of biomolecules by the surfaces. Biondi et al. [136,137] emphasized that opal, alkaline carbonate, and sulfate minerals also stabilized polymers, in addition to concentrating RNA. Along with stabilization, it has been shown that minerals protect biomolecules from environmental damage. Huang and Ferris [77] have established that montmorillonite protected nucleotides from hydrolysis. Other research has shown that polymers could have been protected from UV radiation by diver minerals on primitive Earth [75,96,138].

We found that the charge of the substrates impacts the attraction and the binding of the nucleotides onto the substrate. Positively charged substrates showed a tendency to attract the negatively charged phosphate group. The substrates that work as hydrogen bond donors can form hydrogen bonds with the phosphates. This number increases when water is removed from the system. Overall, the nucleotides behaved as expected while in contact with the different substrates.

The next step was to calculate the number of pre-polymers in different environments. The surprising result is that none of the charged and hydrogen bond potential substrates has been found to be a catalyst when compared to the nucleotide-only system. The three substrates that give the best results had very different properties. Muscovite is a positively charged hydrogen acceptor, kaolinite is a positively charged hydrogen donor, and quartz is neutral and a hydrogen acceptor. Hydroxyapatite, which is a donor and a hydrogen acceptor substrate, with positive and negative charges, formed an important number of Hbonds with the nucleotides, but the nucleotides did not form a significant number of C3′–C5′ Hbonds in the presence of this substrate.

Our simulations of graphite provide the deepest insight into the role of mineral surfaces for pre-polymerization. Unlike the other minerals we simulated, graphite does not have any charges, or the ability to form Hbonds with the nucleotides, but it was found to strongly promote the formation of C3′–C5′ Hbonds. In fact, graphite was as efficient as the nucleotide-only system without a substrate to promote pre-polymers' formation. Graphite was already studied in the origin of life context by Sowerby et al. [110,139]. They showed that xanthine formed monolayers on graphite at a solid–liquid interface. They also

observed a periodic lattice structure. Other papers highlight the position of different bases on graphite. By measuring the adsorption isotherm, they also found that some bases are adsorbed on the surface better than others. Therefore, we conclude that inert substrates, such as graphite, or the complete absence of a substrate are likely preferred for forming pre-polymers on primitive Earth. While it has been speculated that a substrate can help to organize and confine nucleotides, the presence of a substrate at the same time was found to reduce the number of interactions between nucleotides.

While it is straightforward to set up a system that contains nucleotides and water, and successively reduces the number of water molecules to mimic dehydration, the question remains how relevant such a system is. Such a system mimics supersaturated water, maybe droplets, but it is a system that is almost dried out. We suggest that those systems could have been present on primitive Earth via the presence of geysers for example. Indeed, springs or geysers can produce very fine water droplets that dry quickly when exposed to air, heat, and the Sun, depending on the size of the droplets. During this drying process, pre-polymers can form in the first step, and phosphodiester bonds between the nucleotides to form RNA polymers can be formed in a second step when additional energy in the form of heat is provided. The dried pellet can potentially become part of a pond where the RNA can later be encapsulated. In case amphiphilic molecules are present in the droplet simultaneously as nucleotides, the RNA polymers could be encapsulated in liposomes in the same process [16].

What is the possibility of having such droplets that linger in the air for long enough (several seconds) for those reactions to occur? Several forces affect the length of time of a droplet in the air: gravity ( $F_g = \rho_{water} V_{droplet} g$ ), the force of buoyancy ( $F_B = \rho_{air} V_{droplet} g$ ), and the viscous resistance of air ( $F_{Stokes} = 6\pi r \eta v$ ), see, for instance, [140]. The terminal sedimentation velocity of droplets is then calculated to  $v_t = 2r^2 g (\rho_{water} - \rho_{air}) / (9\eta)$ , where  $r$  is the droplet's radius,  $g$  is the gravity constant,  $\eta$  is the viscosity of the air,  $\rho_{water}$  is the density of water and  $\rho_{air}$  is the density of air. Assuming that such a droplet would fall from a certain height, the time of the fall is calculated as  $t_{fall} = H/v_t$ . At the same time, evaporation limits the lifetime of a water drop by  $t_{life} = 2r^2 / (q_0 \Delta T)$ , where  $r$  corresponds to the radius of the droplet,  $\Delta T$  is the difference between 'dry-bulb' and 'wet-bulb' temperature (the 'wet-bulb' temperature corresponds to the temperature where the drop is cooling down due to evaporation), and  $q_0$  (in  $\mu\text{m}^2\text{s}^{-1}\text{K}^{-1}$ ) depends on the ambient conditions and the liquid properties [140]. At 20 °C and 50% RH,  $\Delta T$  is equal to 6.1 °C and  $q_0$  is equal to  $89.84 \mu\text{m}^2\text{s}^{-1}\text{K}^{-1}$  [140].

In Figure 13,  $t_{fall}$  is plotted (for a height of 5 m, yellow) together with the lifetime of a droplet (at 20 °C and 50% relative humidity, purple). Smaller droplets would stay in the air long enough for pre-polymerization and polymerization to happen; however, they will evaporate too quickly. Larger droplets on the other hand would live longer but they would not stay in the air long enough but quickly fall to the ground. The intersection of the two lines provides an estimate of an optimal droplet size of about  $\sim 200 \mu\text{m}$  in diameter, which corresponds to a volume of  $0.0042 \mu\text{L}$ . Such droplets would live for  $\sim 100$  s, which would likely leave enough time for pre-polymerization and polymerization to occur [15].

It is important to note that the literature emphasizes the importance of substrates and their catalytic properties when reactions are carried out in aqueous environments. However, as the synthesis of RNA from monomers is thermodynamically impossible in the presence of water [141], these studies typically involve activated nucleotides, and RNA polymerization is observed in the presence of substrates. We found that non-activated nucleotides first start to interact in aqueous environments via hydrogen bonds, however, hydrogen bond formation becomes significant only when water is removed, and the system is dehydrated. In the absence of water, we then found that substrates may have played a secondary role in the formation of pre-polymers and potentially also in the origin of life. Substrates do play a role in the organization of nucleotides; however, because of their interaction with the surface, nucleotides are limited in their availability to interact with each

other. Our results suggest that non-interactive surfaces, or even the absence of substrates, are likely best for bond formation while drying the system in an origin of life context.

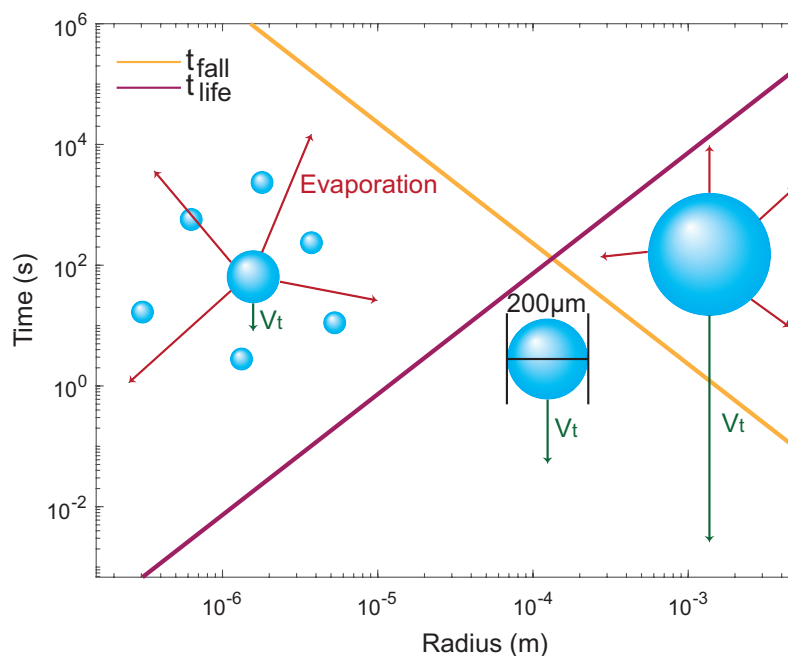


**Figure 13.** Graph of the time of a droplet in the air (to sediment from a height of 5 m, yellow), and the lifetime of a droplet limited by evaporation (purple) as a function of the droplet radius. Droplets around  $r = 100 \mu\text{m}$  can live for  $\sim 100$  s, which would provide enough time for pre-polymers and polymers to form.

#### 4. Conclusions

We used all-atom Molecular Dynamics computer simulations to investigate the effect of substrates on the formation of C3'–C5' hydrogen bonds between the four nucleotides in RNA (AMP, UMP, CMP, GMP). These hydrogen-bonded pre-polymers have been suggested to be the precursors of phosphodiester bonded RNA-polymers. The nine substrates in this study included three clay minerals, one mica, one phosphate mineral, one silica, and two metal oxides. We also included graphite, a non-charged and non-hydrogen bonding substrate. Wet–dry cycles were simulated by slowly removing water molecules from the simulations. No substrate was found to be a good catalyst for the formation of hydrogen-bonded pre-polymers. The highest number of C3'–C5' hydrogen bonds between nucleotides was found in the presence of graphite or in the absence of a substrate, in a nucleotide-only system. While confinement and dehydration seem to be mainly responsible for hydrogen bond formation, substrate interactions were found to reduce the interactions between nucleotides in all cases, independent of their charge and ability to form hydrogen bonds with the nucleotides. The findings suggest that small supersaturated droplets may be an efficient way to produce pre-polymers. Geysers and springs could have produced these droplets in an early-Earth environment.

#### 5. Materials and Methods

##### 5.1. Substrates

Nine different substrates were prepared using the CHARMM-GUI nanomaterial modeler [115–117] and are listed in Table 1. All substrates had a size of  $40 \text{ \AA} \times 50 \text{ \AA} \times 30 \text{ \AA}$ .

Some of the substrates can be found in granitic igneous rocks (specific magmatic rocks), in meteorites, and in Ur-minerals (mineral form from presolar grain) [105]. Clay surfaces have a grain size of  $< 2 \mu\text{m}$ . When wet, clays tend to be more ductile and they harden when dry. Montmorillonite is composed of layers that include one sheet of alumina between two

## M.A.Sc. Thesis – A. Dujardin; McMaster University – Chemistry and Chemical Biology

sheets of silica linked through oxygen atoms. Each layer has a thickness of  $\sim 1$  nm, while the interlayer has a thickness from 0 to 4 nm. Sodium or calcium ions can be present in between the layers, as well as water. Montmorillonite can swell when water is incorporated between the layers. The overall charge of the montmorillonite surface is negative but it is compensated with the absorption of cation around the edges to maintain balance [95]. Montmorillonite used in the simulations has a three repeating unit, each having a thickness of  $\sim 7$  Å, with an interlayer spacing of  $\sim 4$  Å. Kaolinite is another type of clay. One kaolinite layer comprises one sheet of silica and one sheet of alumina, linked together via oxygen atoms [95]. Its interlayer size is typically 0.7 nm. No ions are found between the layers, so kaolinite has a low exchange capacity. Layers are linked together via hydrogen bonding. Kaolinite used in the simulation is composed of five repeating units. Each layer has a thickness of  $\sim 4.5$  Å and an interlayer spacing of  $\sim 2$  Å. Pyrophyllite's layers have the same thickness and the same organization as montmorillonite (Silica-Alumina-Silica); however, cations are not present between the layers. Layers are neutral and held together with weak van der Waals bonds [95,142]. This clay is flexible but not elastic. Pyrophyllite presented in this study is composed of four repeated units, with a thickness of  $\sim 6$  Å and an interlayer distance of  $\sim 2.5$  Å.

**Table 1.** List of all substrates in this study and their composition.

Material	Mineral	Formula
Clay	Montmorillonite	$(K,Na)_n[Si_4O_8][Al_{2n}Mg_nO_2(OH)_2]$
	Kaolinite	$Al_2Si_2O_5(OH)_4$
	Pyrophyllite	$Al_2Si_4O_{10}(OH)_2$
Mica	Muscovite	$(KAl_2(AlSi_3)O_{10}(OH)_2)$
Phosphate minerals	Hydroxyapatite	$Ca_5(PO_4)_3(OH)$
Silica	$\alpha$ -quartz	$SiO_2$
Metal oxides	Corundum	$Al_2O_3$
	Periclase	$MgO$
Carbonaceous material	Graphite	C

Muscovite is also composed of repeating units. Each unit is composed of three sheets, two silica sheets, and one alumina sheet in between. Potassium is the cation present in between the layers, but mica minerals have little or no exchangeable water. Muscovite's layers are flexible and elastic. The silica layer has a net negative charge [95]. In our study, muscovite is composed of three layers, with a thickness of  $\sim 6.5$  Å and an interlayer of  $\sim 5$  Å with potassium ions in between the layers.

Hydroxyapatite is a phosphate mineral composed of  $PO_4^{3-}$  groups bonded laterally through  $Ca^{2+}$  [95]. Hydroxyapatite does not have a uniform hydrogen property throughout its surface because of the atoms' organization in the minerals. In the quartz mineral ( $SiO_2$ ), each silica is held together via four oxygen atoms. Quartz structure is open so it can be incorporated large cations such as  $Ca^{2+}$ ,  $Na^{2+}$ ,  $K^+$  [95]. Quartz was also used as a substrate in the origin of life research [27–30]. Quartz is formed of just one block of material. An oxide is a group of minerals that include natural compounds in which oxygen anions ( $O^{2-}$ ) are combined with one or more metals. Strong ionic bonds maintain the atoms together in oxide minerals [95]. All of these minerals do not contain anionic groups. In the corundum case ( $Al_2O_3$ ),  $Al^{3+}$  is surrounded by six oxygens, and four bonds can radiate from an oxygen [95]. For periclase ( $MgO$ ), each oxygen is shared between six Mg-O (and not just four Al-O); therefore,  $MgO$  does not show cation vacancies [95]. Corundum and periclase are also just composed of just one block of material.

Graphitic carbon is a general term given to solid carbonaceous compounds whose structure is based on 6-fold rings of carbon atoms [101]. Graphite sheets are bonded to each other with van der Waals interaction [95]. Six sheets of graphite were used in our simulations.

### 5.2. Molecular Dynamics Simulations

Substrates were then run in presence of 50 molecules of adenosine monophosphate (AMP), uridine monophosphate (UMP), cytidine monophosphate (CMP), and guanosine monophosphate (GMP) each. Molecules were taken from the CHARMM-GUI archive-small molecules library using CHARMM-GUI multi component assembler [115–117]. The size of the simulation box was  $85 \text{ \AA}^3$ . Simulations were run with GROMACS 2016.3 on MacSim, a GPU-accelerated computer workstation [114]. This computer was equipped with a 40 Core central processing unit (CPU, Intel(R) Xeon(R) CPU E5-2630 v4 @ 2.20GHz), 130 GB random-access memory (RAM), and three graphic processing units (GPU, 2 NVIDIA 1080 TDI + 1 GeForce GT 730).

The systems were first energy minimized and then equilibrated for 100 ps using an NVT ensemble before being simulated for 10 ns at 100% hydration. All simulations used a 2 fs time step, a periodic boundary cutoff of 1.2 nm, the particle-mesh Ewald method using a real-space cutoff of 1.2 nm, fourth-order interpolation, and 0.16 nm grid spacing to solve for long-range electrostatics. The parallel LINCS (P-LINCS) algorithm was used to determine bond constraints [143]. Temperature and pressure were maintained at 303 K and 1.0 bar using a Nosé–Hoover thermostat [144–146] at 30 °C ( $\tau = 1.0$  ps) and Parrinello–Rahman isotropic weak coupling ( $\tau = 1$  ps) [147]. All analyses were performed on the entire simulations.

Water was removed successively during the simulations to mimic dehydration and a wet–dry cycle. For each step of the dehydration protocol, the next simulation, a new index file was created by selecting all the molecules except the water molecules. The last frame from the previous simulation was extracted using the GROMACS command *gmx trjconv*. The last frame was solvated and a new system was created using the GROMACS command *gmx solvate*. The new system was then energy minimized, equilibrated, and run in the same condition than 100% hydration. The systems were run for 15 ns. The number of water molecules per simulation is listed in Table S1 (in the Supplementary Material) for the system with substrates and in Table S2 (Supplementary Material) for the nucleotides-only system. Hydrogen bond analysis was performed using VMD built-in algorithms.

**Supplementary Materials:** The following supporting information can be downloaded at: <https://www.mdpi.com/article/10.3390/life13010112/s1>, Table S1: Percentage of hydration and number of water molecules for all simulations containing a substrate; Table S2: Percentage of hydration and water molecules for the nucleotides-only system.

**Author Contributions:** Conceptualization, R.P. and M.C.R.; Methodology, A.D., S.H. and M.C.R.; Software, A.D. and S.H.; Validation, A.D.; Formal analysis, A.D.; Investigation, A.D.; Resources, R.P. and M.C.R.; Data curation, A.D.; Writing—original draft, A.D. and M.C.R.; Writing—review & editing, A.D., S.H., R.P. and M.C.R.; Supervision, R.P. and M.C.R.; Project administration, R.P. and M.C.R.; Funding acquisition, R.P. and M.C.R. All authors have read and agreed to the published version of the manuscript.

**Funding:** This research was funded by the Natural Sciences and Engineering Research Council of Canada (NSERC) RGPIN-2021-03926. The Origins of Life Laboratory was created using funds provided by the Canada Foundation for Innovation (CFI), the Ontario Ministry of Economic Development and Innovation, and McMaster University. M.C.R. is the recipient of a University Scholar Award from McMaster University. The funders had no role in study design, data collection and analysis, decision to publish, or preparation of the manuscript.

**Data Availability Statement:** All data including MD files and trajectories are available upon request.

**Acknowledgments:** We are indebted to David Deamer for fruitful discussions and input on the work and manuscript.

**Conflicts of Interest:** The authors declare no conflict of interest.

## References

1. Martin, W.; Baross, J.; Kelley, D.; Russell, M.J. Hydrothermal vents and the origin of life. *Nat. Rev. Microbiol.* **2008**, *6*, 805–814. [[CrossRef](#)] [[PubMed](#)]
2. Wächtershäuser, G. Evolution of the first metabolic cycles. *Proc. Natl. Acad. Sci. USA* **1990**, *87*, 200–204. [[CrossRef](#)] [[PubMed](#)]
3. Sojo, V.; Herschy, B.; Whicher, A.; Camprubi, E.; Lane, N. The origin of life in alkaline hydrothermal vents. *Astrobiology* **2016**, *16*, 181–197. [[CrossRef](#)] [[PubMed](#)]
4. Powner, M.W.; Gerland, B.; Sutherland, J.D. Synthesis of activated pyrimidine ribonucleotides in prebiotically plausible conditions. *Nature* **2009**, *459*, 239–242. [[CrossRef](#)] [[PubMed](#)]
5. Baross, J.A.; Hoffman, S.E. Submarine hydrothermal vents and associated gradient environments as sites for the origin and evolution of life. *Orig. Life Evol. Biosph.* **1985**, *15*, 327–345. [[CrossRef](#)]
6. Ooka, H.; McGlynn, S.E.; Nakamura, R. Electrochemistry at deep-sea hydrothermal vents: Utilization of the thermodynamic driving force towards the autotrophic origin of life. *ChemElectroChem* **2019**, *6*, 1316–1323. [[CrossRef](#)]
7. Macleod, G.; McKeown, C.; Hall, A.J.; Russell, M.J. Hydrothermal and oceanic pH conditions of possible relevance to the origin of life. *Orig. Life Evol. Biosph.* **1994**, *24*, 19–41. [[CrossRef](#)]
8. Topozini, L.; Dies, H.; Deamer, D.W.; Rheinstädter, M.C. Adenosine monophosphate forms ordered arrays in multilamellar lipid matrices: Insights into assembly of nucleic acid for primitive life. *PLoS ONE* **2013**, *8*, e62810. [[CrossRef](#)]
9. Himbert, S.; Chapman, M.; Deamer, D.W.; Rheinstädter, M.C. Organization of nucleotides in different environments and the formation of pre-polymers. *Sci. Rep.* **2016**, *6*, 1–12. [[CrossRef](#)]
10. Deamer, D. Where Did Life Begin? Testing Ideas in Prebiotic Analogue Conditions. *Life* **2021**, *11*, 134. [[CrossRef](#)]
11. Deamer, D.; Damer, B.; Kompanichenko, V. Hydrothermal chemistry and the origin of cellular life. *Astrobiology* **2019**, *19*, 1523–1537. [[CrossRef](#)]
12. Deamer, D.W.; Georgiou, C.D. Hydrothermal Conditions and the Origin of Cellular Life. *Astrobiology* **2015**, *15*, 1091–1095. [[CrossRef](#)] [[PubMed](#)]
13. Deamer, D. Liquid-crystalline nano structures: Organizing matrices for non-enzymatic nucleic acid polymerization. *Chem. Soc. Rev.* **2012**, *41*, 5375–5379. [[CrossRef](#)] [[PubMed](#)]
14. Hassenkam, T.; Damer, B.; Mednick, G.; Deamer, D. Viroid-sized rings self-assemble from mononucleotides through wet-dry cycling: Implications for the origin of life. *bioRxiv* **2020**, *10*, 321. [[CrossRef](#)] [[PubMed](#)]
15. Ross, D.S.; Deamer, D. Dry/wet cycling and the thermodynamics and kinetics of prebiotic polymer synthesis. *Life* **2016**, *6*, 28. [[CrossRef](#)]
16. Damer, B.; Deamer, D. The hot spring hypothesis for an origin of life. *Astrobiology* **2020**, *20*, 429–452. [[CrossRef](#)]
17. Da Silva, L.; Maurel, M.C.; Deamer, D. Salt-promoted synthesis of RNA-like molecules in simulated hydrothermal conditions. *J. Mol. Evol.* **2015**, *80*, 86–97. [[CrossRef](#)]
18. Hargrave, M.; Thompson, S.K.; Deamer, D. Computational models of polymer synthesis driven by dehydration/rehydration cycles: Repurination in simulated hydrothermal fields. *J. Mol. Evol.* **2018**, *86*, 501–510. [[CrossRef](#)]
19. Deamer, D.W. *First Life: Discovering the Connections between Stars, Cells, and How Life Began*; University of California Press: Berkeley, CA, USA, 2011.
20. Damer, B.; Deamer, D. Coupled phases and combinatorial selection in fluctuating hydrothermal pools: A scenario to guide experimental approaches to the origin of cellular life. *Life* **2015**, *5*, 872–887. [[CrossRef](#)]
21. DeGuzman, V.; Vercoutere, W.; Shenasa, H.; Deamer, D. Generation of Oligonucleotides Under Hydrothermal Conditions by Non-enzymatic Polymerization. *J. Mol. Evol.* **2014**, *78*, 251–262. [[CrossRef](#)]
22. Trinks, H.; Schröder, W.; Biebricher, C.K. Ice and the origin of life. *Orig. Life Evol. Biosph.* **2005**, *35*, 429–445. [[CrossRef](#)] [[PubMed](#)]
23. Menor-Salván, C.; Marín-Yaseli, M.R. Prebiotic chemistry in eutectic solutions at the water–ice matrix. *Chem. Soc. Rev.* **2012**, *41*, 5404–5415. [[CrossRef](#)] [[PubMed](#)]
24. Attwater, J.; Wochner, A.; Pinheiro, V.B.; Coulson, A.; Holliger, P. Ice as a protocellular medium for RNA replication. *Nat. Commun.* **2010**, *1*, 1–9. [[CrossRef](#)] [[PubMed](#)]
25. Monnard, P.A.; Kanavarioti, A.; Deamer, D.W. Eutectic phase polymerization of activated ribonucleotide mixtures yields quasi-equimolar incorporation of purine and pyrimidine nucleobases. *J. Am. Chem. Soc.* **2003**, *125*, 13734–13740. [[CrossRef](#)]
26. Hazen, R.M. Paleomineralogy of the Hadean Eon: A preliminary species list. *Am. J. Sci.* **2013**, *313*, 807–843. [[CrossRef](#)]
27. Bonner, W.A.; Kavasmaneck, P.R.; Martin, F.S.; Flores, J.J. Asymmetric adsorption of alanine by quartz. *Science* **1974**, *186*, 143–144. [[CrossRef](#)]
28. Bonner, W.A.; Kavasmaneck, P.R.; Martin, F.S.; Flores, J.J. Asymmetric adsorption by quartz: A model for the prebiotic origin of optical activity. *Orig. Life* **1975**, *6*, 367–376. [[CrossRef](#)]
29. Soai, K.; Osanai, S.; Kadowaki, K.; Yonekubo, S.; Shibata, T.; Sato, I. D- and L-quartz-promoted highly enantioselective synthesis of a chiral organic compound. *J. Am. Chem. Soc.* **1999**, *121*, 11235–11236. [[CrossRef](#)]
30. Evgenii, K.; Wolfram, T. The role of quartz in the origin of optical activity on Earth. *Orig. Life Evol. Biosph.* **2000**, *30*, 431–434. [[CrossRef](#)]
31. Hazen, R.M.; Filley, T.R.; Goodfriend, G.A. Selective adsorption of L- and D-amino acids on calcite: Implications for biochemical homochirality. *Proc. Natl. Acad. Sci. USA* **2001**, *98*, 5487–5490. [[CrossRef](#)]
32. Ricardo, A.; Carrigan, M.; Olcott, A.; Benner, S. Borate minerals stabilize ribose. *Science* **2004**, *303*, 196. [[CrossRef](#)] [[PubMed](#)]

## M.A.Sc. Thesis – A. Dujardin; McMaster University – Chemistry and Chemical Biology

33. Wächtershäuser, G. The case for the chemoautotrophic origin of life in an iron-sulfur world. *Orig. Life Evol. Biosph.* **1990**, *20*, 173–176. [[CrossRef](#)]
34. Wächtershäuser, G. The cradle chemistry of life: On the origin of natural products in a pyrite-pulled chemoautotrophic origin of life. *Pure Appl. Chem.* **1993**, *65*, 1343–1348. [[CrossRef](#)]
35. Blöchl, E.; Keller, M.; Wächtershäuser, G.; Stetter, K.O. Reactions depending on iron sulfide and linking geochemistry with biochemistry. *Proc. Natl. Acad. Sci. USA* **1992**, *89*, 8117–8120. [[CrossRef](#)] [[PubMed](#)]
36. Cody, G.D.; Boctor, N.Z.; Filley, T.R.; Hazen, R.M.; Scott, J.H.; Sharma, A.; Yoder, H.S., Jr. Primordial carbonylated iron-sulfur compounds and the synthesis of pyruvate. *Science* **2000**, *289*, 1337–1340. [[CrossRef](#)]
37. Summers, D.P.; Chang, S. Prebiotic ammonia from reduction of nitrite by iron (II) on the early Earth. *Nature* **1993**, *365*, 630–633. [[CrossRef](#)] [[PubMed](#)]
38. Pitsch, S.; Eschenmoser, A.; Gedulin, B.; Hui, S.; Arrhenius, G. Mineral induced formation of sugar phosphates. *Orig. Life Evol. Biosph.* **1995**, *25*, 297–334. [[CrossRef](#)]
39. Weber, A.L. Formation of pyrophosphate on hydroxyapatite with thioesters as condensing agents. *Biosystems* **1982**, *15*, 183–189. [[CrossRef](#)]
40. Smirnov, A.; Hausner, D.; Laffers, R.; Strongin, D.R.; Schoonen, M.A. Abiotic ammonium formation in the presence of Ni-Fe metals and alloys and its implications for the Hadean nitrogen cycle. *Geochem. Trans.* **2008**, *9*, 1–20. [[CrossRef](#)]
41. Pasek, M.A.; Dworkin, J.P.; Lauretta, D.S. A radical pathway for organic phosphorylation during schreibersite corrosion with implications for the origin of life. *Geochim. Cosmochim. Acta* **2007**, *71*, 1721–1736. [[CrossRef](#)]
42. Grew, E.S.; Bada, J.L.; Hazen, R.M. Borate minerals and origin of the RNA world. *Orig. Life Evol. Biosph.* **2011**, *41*, 307–316. [[CrossRef](#)] [[PubMed](#)]
43. Wächtershäuser, G. Pyrite formation, the first energy source for life: A hypothesis. *Syst. Appl. Microbiol.* **1988**, *10*, 207–210. [[CrossRef](#)]
44. Wächtershäuser, G. Before enzymes and templates: Theory of surface metabolism. *Microbiol. Rev.* **1988**, *52*, 452–484. [[CrossRef](#)] [[PubMed](#)]
45. Cairns-Smith, A. Takeover mechanisms and early biochemical evolution. *Biosystems* **1977**, *9*, 105–109. [[CrossRef](#)]
46. Cairns-Smith, A.G. Sketches for a mineral genetic material. *Elements* **2005**, *1*, 157–161. [[CrossRef](#)]
47. Huber, C.; Wächtershäuser, G. Activated acetic acid by carbon fixation on (Fe, Ni) S under primordial conditions. *Science* **1997**, *276*, 245–247. [[CrossRef](#)]
48. Brandes, J.A.; Boctor, N.Z.; Cody, G.D.; Cooper, B.A.; Hazen, R.M.; Yoder, H.S. Abiotic nitrogen reduction on the early Earth. *Nature* **1998**, *395*, 365–367. [[CrossRef](#)]
49. Cody, G.; Boctor, N.; Hazen, R.; Brandes, J.; Morowitz, H.J.; Yoder, H., Jr. Geochemical roots of autotrophic carbon fixation: hydrothermal experiments in the system citric acid, H<sub>2</sub>O-(±FeS)-(±NiS). *Geochim. Cosmochim. Acta* **2001**, *65*, 3557–3576. [[CrossRef](#)]
50. Cody, G.; Boctor, N.; Brandes, J.; Filley, T.; Hazen, R.; Yoder, H., Jr. Assaying the catalytic potential of transition metal sulfides for abiotic carbon fixation. *Geochim. Cosmochim. Acta* **2004**, *68*, 2185–2196. [[CrossRef](#)]
51. Huber, C.; Kraus, F.; Hanzlik, M.; Eisenreich, W.; Wächtershäuser, G. Elements of metabolic evolution. *Chem. Eur. J.* **2012**, *18*, 2063–2080. [[CrossRef](#)]
52. Cody, G.D. Transition metal sulfides and the origins of metabolism. *Annu. Rev. Earth Planet. Sci.* **2004**, *32*, 569. [[CrossRef](#)]
53. Cody, G.D. Geochemical connections to primitive metabolism. *Elements* **2005**, *1*, 139–143. [[CrossRef](#)]
54. Berndt, M.E.; Allen, D.E.; Seyfried, W.E., Jr. Reduction of CO<sub>2</sub> during serpentinization of olivine at 300 C and 500 bar. *Geology* **1996**, *24*, 351–354. [[CrossRef](#)]
55. McCollom, T.M.; Seewald, J.S. A reassessment of the potential for reduction of dissolved CO<sub>2</sub> to hydrocarbons during serpentinization of olivine. *Geochim. Cosmochim. Acta* **2001**, *65*, 3769–3778. [[CrossRef](#)]
56. Weber, A.L. Prebiotic polymerization: Oxidative polymerization of 2,3-dimercapto-1-propanol on the surface of iron (III) hydroxide oxide. *Orig. Life Evol. Biosph.* **1995**, *25*, 53–60. [[CrossRef](#)]
57. Hanczyc, M.M.; Fujikawa, S.M.; Szostak, J.W. Experimental models of primitive cellular compartments: Encapsulation, growth, and division. *Science* **2003**, *302*, 618–622. [[CrossRef](#)]
58. Russell, M.J.; Daniel, R.M.; Hall, A.J.; Sherrington, J.A. A hydrothermally precipitated catalytic iron sulphide membrane as a first step toward life. *J. Mol. Evol.* **1994**, *39*, 231–243. [[CrossRef](#)]
59. Parsons, I.; Lee, M.R.; Smith, J.V. Biochemical evolution II: Origin of life in tubular microstructures on weathered feldspar surfaces. *Proc. Natl. Acad. Sci. USA* **1998**, *95*, 15173–15176. [[CrossRef](#)]
60. Smith, J.V.; Arnold, F.P., Jr.; Parsons, I.; Lee, M.R. Biochemical evolution III: Polymerization on organophilic silica-rich surfaces, crystal-chemical modeling, formation of first cells, and geological clues. *Proc. Natl. Acad. Sci. USA* **1999**, *96*, 3479–3485. [[CrossRef](#)]
61. Lahav, N.; White, D.; Chang, S. Peptide formation in the prebiotic era: Thermal condensation of glycine in fluctuating clay environments. *Science* **1978**, *201*, 67–69. [[CrossRef](#)]
62. Huber, C.; Wächtershäuser, G. Peptides by activation of amino acids with CO on (Ni, Fe) S surfaces: Implications for the origin of life. *Science* **1998**, *281*, 670–672. [[CrossRef](#)] [[PubMed](#)]
63. Huber, C.; Eisenreich, W.; Hecht, S.; Wächtershäuser, G. A possible primordial peptide cycle. *Science* **2003**, *301*, 938–940. [[CrossRef](#)] [[PubMed](#)]

## M.A.Sc. Thesis – A. Dujardin; McMaster University – Chemistry and Chemical Biology

64. Smith, J.V. Biochemical evolution I: Polymerization on internal, organophilic silica surfaces of dealuminated zeolites and feldspars. *Proc. Natl. Acad. Sci. USA* **1998**, *95*, 3370–3375. [[CrossRef](#)] [[PubMed](#)]
65. Jonsson, C.M.; Jonsson, C.L.; Sverjensky, D.A.; Cleaves, H.J.; Hazen, R.M. Attachment of l-glutamate to rutile ( $\alpha$ -TiO<sub>2</sub>): A potentiometric, adsorption, and surface complexation study. *Langmuir* **2009**, *25*, 12127–12135. [[CrossRef](#)] [[PubMed](#)]
66. Ferris, J.P. Mineral catalysis and prebiotic synthesis: Montmorillonite-catalyzed formation of RNA. *Elements* **2005**, *1*, 145–149. [[CrossRef](#)]
67. Ferris, J.P. Montmorillonite-catalysed formation of RNA oligomers: The possible role of catalysis in the origins of life. *Philos. Trans. R. Soc. Biol. Sci.* **2006**, *361*, 1777–1786. [[CrossRef](#)]
68. Ferris, J.P.; Ertem, G. Oligomerization of ribonucleotides on montmorillonite: Reaction of the 5'-phosphorimidazolide of adenosine. *Science* **1992**, *257*, 1387–1389. [[CrossRef](#)]
69. Ferris, J.P. Catalysis and prebiotic RNA synthesis. *Orig. Life Evol. Biosph.* **1993**, *23*, 307–315. [[CrossRef](#)]
70. Ferris, J.P.; Ertem, G. Montmorillonite catalysis of RNA oligomer formation in aqueous solution. A model for the prebiotic formation of RNA. *J. Am. Chem. Soc.* **1993**, *115*, 12270–12275. [[CrossRef](#)]
71. Ertem, G.; Ferris, J.P. Synthesis of RNA oligomers on heterogeneous templates. *Nature* **1996**, *379*, 238–240. [[CrossRef](#)]
72. Ertem, G.; Ferris, J.P. Template-directed synthesis using the heterogeneous templates produced by montmorillonite catalysis. A possible bridge between the prebiotic and RNA worlds. *J. Am. Chem. Soc.* **1997**, *119*, 7197–7201. [[CrossRef](#)] [[PubMed](#)]
73. Holm, N.G.; Ertem, G.; Ferris, J.P. The binding and reactions of nucleotides and polynucleotides on iron oxide hydroxide polymorphs. *Orig. Life Evol. Biosph.* **1993**, *23*, 195–215. [[CrossRef](#)] [[PubMed](#)]
74. Acevedo, O.L.; Orgel, L.E. Template-directed oligonucleotide ligation on hydroxylapatite. *Nature* **1986**, *321*, 790–792. [[CrossRef](#)]
75. Ciciriello, F.; Costanzo, G.; Crestini, C.; Saladino, R.; Di Mauro, E. Origin of informational polymers and the search for non-terran life: protection of the polymeric state of DNA by phosphate minerals. *Astrobiology* **2007**, *7*, 616–630. [[CrossRef](#)]
76. Benner, S.A.; Hutter, D. Phosphates, DNA, and the search for nonterrestrial life: A second generation model for genetic molecules. *Bioorg. Chem.* **2002**, *30*, 62–80. [[CrossRef](#)] [[PubMed](#)]
77. Huang, W.; Ferris, J.P. One-step, regioselective synthesis of up to 50-mers of RNA oligomers by montmorillonite catalysis. *J. Am. Chem. Soc.* **2006**, *128*, 8914–8919. [[CrossRef](#)]
78. Gilbert, W. Origin of life: The RNA world. *Nature* **1986**, *319*, 618. [[CrossRef](#)]
79. Rich, A. On the problems of evolution and biochemical information transfer. *Horizons Biochem.* **1962**, 103–126.
80. Cech, T.R. A model for the RNA-catalyzed replication of RNA. *Proc. Natl. Acad. Sci. USA* **1986**, *83*, 4360–4363. [[CrossRef](#)]
81. Cech, T.R. The RNA worlds in context. *Cold Spring Harb. Perspect. Biol.* **2012**, *4*, a006742. [[CrossRef](#)]
82. Hud, N.V.; Cafferty, B.J.; Krishnamurthy, R.; Williams, L.D. The origin of RNA and “my grandfather’s axe”. *Chem. Biol.* **2013**, *20*, 466–474. [[CrossRef](#)] [[PubMed](#)]
83. Joyce, G.F. Forty years of in vitro evolution. *Angew. Chem. Int. Ed.* **2007**, *46*, 6420–6436. [[CrossRef](#)]
84. Biebricher, C.K.; Orgel, L.E. An RNA that multiplies indefinitely with DNA-dependent RNA polymerase: Selection from a random copolymer. *Proc. Natl. Acad. Sci. USA* **1973**, *70*, 934–938. [[CrossRef](#)] [[PubMed](#)]
85. Biebricher, C.K.; Eigen, M.; Gardiner, W.C., Jr. Kinetics of RNA replication: Competition and selection among self-replicating RNA species. *Biochemistry* **1985**, *24*, 6550–6560. [[CrossRef](#)] [[PubMed](#)]
86. Robertson, D.L.; Joyce, G.F. Selection in vitro of an RNA enzyme that specifically cleaves single-stranded DNA. *Nature* **1990**, *344*, 467–468. [[CrossRef](#)]
87. Beaudry, A.A.; Joyce, G.F. Directed evolution of an RNA enzyme. *Science* **1992**, *257*, 635–641. [[CrossRef](#)] [[PubMed](#)]
88. Tuerk, C.; Gold, L. Systematic evolution of ligands by exponential enrichment: RNA ligands to bacteriophage T4 DNA polymerase. *Science* **1990**, *249*, 505–510. [[CrossRef](#)]
89. Ellington, A.D.; Szostak, J.W. In vitro selection of RNA molecules that bind specific ligands. *Nature* **1990**, *346*, 818–822. [[CrossRef](#)]
90. Neveu, M.; Kim, H.J.; Benner, S.A. The “strong” RNA world hypothesis: Fifty years old. *Astrobiology* **2013**, *13*, 391–403. [[CrossRef](#)]
91. Ferris, J.P.; Ertem, G.; Agarwal, V.K. The adsorption of nucleotides and polynucleotides on montmorillonite clay. *Orig. Life Evol. Biosph.* **1989**, *19*, 153–164. [[CrossRef](#)]
92. Franchi, M.; Ferris, J.P.; Gallori, E. Cations as mediators of the adsorption of nucleic acids on clay surfaces in prebiotic environments. *Orig. Life Evol. Biosph.* **2003**, *33*, 1–16. [[CrossRef](#)] [[PubMed](#)]
93. Pedreira-Segade, U.; Feuillie, C.; Pelletier, M.; Michot, L.J.; Daniel, I. Adsorption of nucleotides onto ferromagnesian phyllosilicates: Significance for the origin of life. *Geochim. Cosmochim. Acta* **2016**, *176*, 81–95. [[CrossRef](#)]
94. Mast, C.B.; Schink, S.; Gerland, U.; Braun, D. Escalation of polymerization in a thermal gradient. *Proc. Natl. Acad. Sci. USA* **2013**, *110*, 8030–8035. [[CrossRef](#)]
95. Klein, C.; Dutrow, B.; Dana, J.D. *The 23rd Edition of the Manual of Mineral Science: (After James D. Dana)*; Number 549 KLE; John Wiley: Hoboken, NJ, USA, 2007.
96. Scappini, F.; Casadei, F.; Zamboni, R.; Franchi, M.; Gallori, E.; Monti, S. Protective effect of clay minerals on adsorbed nucleic acid against UV radiation: Possible role in the origin of life. *Int. J. Astrobiol.* **2004**, *3*, 17–19. [[CrossRef](#)]
97. Kasprzhitskii, A.; Lazorenko, G.; Kharytonau, D.S.; Osipenko, M.A.; Kasach, A.A.; Kurilo, I.I. Adsorption mechanism of aliphatic amino acids on kaolinite surfaces. *Appl. Clay Sci.* **2022**, *226*, 106566. [[CrossRef](#)]
98. Strigunkova, T.; Lavrentiev, G.; Otroshchenko, V. Abiogenic synthesis of oligonucleotides on kaolinite under the action of ultraviolet radiation. *J. Mol. Evol.* **1986**, *23*, 290–293. [[CrossRef](#)]

## M.A.Sc. Thesis – A. Dujardin; McMaster University – Chemistry and Chemical Biology

99. Zhang, C.; Yu, Z.G.; Zeng, G.M.; Jiang, M.; Yang, Z.Z.; Cui, F.; Zhu, M.Y.; Shen, L.Q.; Hu, L. Effects of sediment geochemical properties on heavy metal bioavailability. *Environ. Int.* **2014**, *73*, 270–281. [[CrossRef](#)]
100. Murray, H.H. Overview—Clay mineral applications. *Appl. Clay Sci.* **1991**, *5*, 379–395. [[CrossRef](#)]
101. Nesse, W.D. *Introduction to Mineralogy*; Oxford University Press: Oxford, UK, 2012.
102. Hansma, H.G. The power of crowding for the origins of life. *Orig. Life Evol. Biosph.* **2014**, *44*, 307–311. [[CrossRef](#)]
103. Hansma, H.G. Possible origin of life between mica sheets: Does life imitate mica? *J. Biomol. Struct. Dyn.* **2013**, *31*, 888–895. [[CrossRef](#)]
104. Hansma, H.G. Possible origin of life between mica sheets. *J. Theor. Biol.* **2010**, *266*, 175–188. [[CrossRef](#)] [[PubMed](#)]
105. Hazen, R.M.; Papineau, D.; Bleeker, W.; Downs, R.T.; Ferry, J.M.; McCoy, T.J.; Sverjensky, D.A.; Yang, H. Mineral evolution. *Am. Mineral.* **2008**, *93*, 1693–1720. [[CrossRef](#)]
106. Cleaves, H.J., II; Scott, A.M.; Hill, F.C.; Leszczynski, J.; Sahai, N.; Hazen, R. Mineral–organic interfacial processes: Potential roles in the origins of life. *Chem. Soc. Rev.* **2012**, *41*, 5502–5525. [[CrossRef](#)]
107. Dalai, P.; Sahai, N. Mineral–lipid interactions in the origins of life. *Trends Biochem. Sci.* **2019**, *44*, 331–341. [[CrossRef](#)]
108. Nittler, L.R. Presolar stardust in meteorites: Recent advances and scientific frontiers. *Earth Planet. Sci. Lett.* **2003**, *209*, 259–273. [[CrossRef](#)]
109. Cuéllar-Cruz, M.; Moreno, A. Synthesis of Crystalline Silica–Carbonate Biomorphs of Ba (II) under the Presence of RNA and Positively and Negatively Charged ITO Electrodes: Obtainment of Graphite via Bioreduction of CO<sub>2</sub> and Its Implications to the Chemical Origin of Life on Primitive Earth. *ACS Omega* **2020**, *5*, 5460–5469. [[PubMed](#)]
110. Sowerby, S.J.; Cohn, C.A.; Heckl, W.M.; Holm, N.G. Differential adsorption of nucleic acid bases: Relevance to the origin of life. *Proc. Natl. Acad. Sci. USA* **2001**, *98*, 820–822. [[CrossRef](#)]
111. Ortmann, F.; Schmidt, W.G.; Bechstedt, F. Attracted by long-range electron correlation: Adenine on graphite. *Phys. Rev. Lett.* **2005**, *95*, 186101. [[CrossRef](#)]
112. BIOVIA, Dassault Systemes. *BIOVIA Discovery Studio Visualizer*; Dassault Systemes: San Diego, CA, USA, 2021.
113. Gasteiger, J.; Marsili, M. Iterative partial equalization of orbital electronegativity—A rapid access to atomic charges. *Tetrahedron* **1980**, *36*, 3219–3228. [[CrossRef](#)]
114. Abraham, M.J.; Murtola, T.; Schulz, R.; Páll, S.; Smith, J.C.; Hess, B.; Lindahl, E. GROMACS: High performance molecular simulations through multi-level parallelism from laptops to supercomputers. *SoftwareX* **2015**, *1*, 19–25. [[CrossRef](#)]
115. Jo, S.; Kim, T.; Iyer, V.G.; Im, W. CHARMM-GUI: A web-based graphical user interface for CHARMM. *J. Comput. Chem.* **2008**, *29*, 1859–1865. [[CrossRef](#)] [[PubMed](#)]
116. Lee, J.; Cheng, X.; Swails, J.M.; Yeom, M.S.; Eastman, P.K.; Lemkul, J.A.; Wei, S.; Buckner, J.; Jeong, J.C.; Qi, Y.; et al. CHARMM-GUI input generator for NAMD, GROMACS, AMBER, OpenMM, and CHARMM/OpenMM simulations using the CHARMM36 additive force field. *J. Chem. Theory Comput.* **2016**, *12*, 405–413. [[CrossRef](#)] [[PubMed](#)]
117. Brooks, B.R.; Brooks, C.L., III; Mackerell, A.D., Jr.; Nilsson, L.; Petrella, R.J.; Roux, B.; Won, Y.; Archontis, G.; Bartels, C.; Boresch, S.; et al. CHARMM: The biomolecular simulation program. *J. Comput. Chem.* **2009**, *30*, 1545–1614. [[CrossRef](#)] [[PubMed](#)]
118. Humphrey, W.; Dalke, A.; Schulten, K. VMD: Visual molecular dynamics. *J. Mol. Graph.* **1996**, *14*, 33–38. [[CrossRef](#)] [[PubMed](#)]
119. Šolc, R.; Gerzabek, M.H.; Lischka, H.; Tunega, D. Wettability of kaolinite (001) surfaces—Molecular dynamic study. *Geoderma* **2011**, *169*, 47–54. [[CrossRef](#)]
120. Hench, L.L.; West, J.K. Inorganic pathways for biosynthesis: A molecular orbital modeling approach. *J. Vac. Sci. Technol.* **1994**, *12*, 2962–2965. [[CrossRef](#)]
121. Gambino, G.L.; Lombardo, G.M.; Grassi, A.; Marletta, G. Molecular modeling of interactions between L-lysine and a hydroxylated quartz surface. *J. Phys. Chem. B* **2004**, *108*, 2600–2607. [[CrossRef](#)]
122. Gambino, G.L.; Grassi, A.; Marletta, G. Molecular modeling of interactions between L-lysine and functionalized quartz surfaces. *J. Phys. Chem. B* **2006**, *110*, 4836–4845. [[CrossRef](#)]
123. Lomenech, C.; Bery, G.; Costa, D.; Stievano, L.; Lambert, J.F. Theoretical and experimental study of the adsorption of neutral glycine on silica from the gas phase. *ChemPhysChem* **2005**, *6*, 1061–1070. [[CrossRef](#)]
124. Rimola, A.; Tosoni, S.; Sodupe, M.; Ugliengo, P. Peptide bond formation activated by the interplay of Lewis and Brønsted catalysts. *Chem. Phys. Lett.* **2005**, *408*, 295–301. [[CrossRef](#)]
125. Rimola, A.; Tosoni, S.; Sodupe, M.; Ugliengo, P. Does Silica Surface Catalyse Peptide Bond Formation? New Insights from First-Principles Calculations. *ChemPhysChem* **2006**, *7*, 157–163. [[CrossRef](#)] [[PubMed](#)]
126. Rimola, A.; Sodupe, M.; Ugliengo, P. Aluminosilicate surfaces as promoters for peptide bond formation: An assessment of Bernal’s hypothesis by ab Initio methods. *J. Am. Chem. Soc.* **2007**, *129*, 8333–8344. [[CrossRef](#)] [[PubMed](#)]
127. Costa, D.; Lomenech, C.; Meng, M.; Stievano, L.; Lambert, J.F. Microsolvation of glycine by silanol ligands: A DFT study. *J. Mol. Struct. Theochem* **2007**, *806*, 253–259. [[CrossRef](#)]
128. Stievano, L.; Piao, L.Y.; Lopes, I.; Meng, M.; Costa, D.; Lambert, J.F. Glycine and lysine adsorption and reactivity on the surface of amorphous silica. *Eur. J. Mineral.* **2007**, *19*, 321–331. [[CrossRef](#)]
129. Collins, J.R.; Loew, G.H.; Luke, B.T.; White, D.H. Theoretical investigation of the role of clay edges in prebiotic peptide bond formation. *Orig. Life Evol. Biosph.* **1988**, *18*, 107–119. [[CrossRef](#)]
130. Yu, C.H.; Newton, S.Q.; Miller, D.M.; Teppen, B.J.; Schäfer, L. Ab initio study of the nonequivalence of adsorption of D- and L-peptides on clay mineral surfaces. *Struct. Chem.* **2001**, *12*, 393–398. [[CrossRef](#)]

## M.A.Sc. Thesis – A. Dujardin; McMaster University – Chemistry and Chemical Biology

131. Pérez-Villa, A.; Saitta, A.M.; Georgelin, T.; Lambert, J.F.; Guyot, F.; Maurel, M.C.; Pietrucci, F. Synthesis of RNA nucleotides in plausible prebiotic conditions from ab initio computer simulations. *J. Phys. Chem. Lett.* **2018**, *9*, 4981–4987. [[CrossRef](#)]
132. Bertram, L.; Roberts, S.J.; Powner, M.W.; Szabla, R. Photochemistry of 2-thiooxazole: A plausible prebiotic precursor to RNA nucleotides. *Phys. Chem. Chem. Phys.* **2022**, *24*, 21406–21416. [[CrossRef](#)]
133. Niether, D.; Afanasenkau, D.; Dhont, J.K.; Wiegand, S. Accumulation of formamide in hydrothermal pores to form prebiotic nucleobases. *Proc. Natl. Acad. Sci. USA* **2016**, *113*, 4272–4277. [[CrossRef](#)]
134. Ferris, J.P.; Hill, A.R.; Liu, R.; Orgel, L.E. Synthesis of long prebiotic oligomers on mineral surfaces. *Nature* **1996**, *381*, 59–61. [[CrossRef](#)]
135. Jerome, C.A.; Kim, H.J.; Mojzsis, S.J.; Benner, S.A.; Biondi, E. Catalytic Synthesis of Polyribonucleic Acid on Prebiotic Rock Glasses. *Astrobiology* **2022**, *22*. [[CrossRef](#)] [[PubMed](#)]
136. Biondi, E.; Furukawa, Y.; Kawai, J.; Benner, S.A. Adsorption of RNA on mineral surfaces and mineral precipitates. *Beilstein J. Org. Chem.* **2017**, *13*, 393–404. [[CrossRef](#)] [[PubMed](#)]
137. Biondi, E.; Howell, L.; Benner, S.A. Opal adsorbs and stabilizes RNA—a hierarchy of prebiotic silica minerals. *Synlett* **2017**, *28*, 84–88. [[CrossRef](#)]
138. Biondi, E.; Branciamore, S.; Maurel, M.C.; Gallori, E. Montmorillonite protection of an UV-irradiated hairpin ribozyme: Evolution of the RNA world in a mineral environment. *BMC Evol. Biol.* **2007**, *7*, 1–7. [[CrossRef](#)]
139. Sowerby, S.J.; Petersen, G.B. Scanning tunnelling microscopy and molecular modelling of xanthine monolayers self-assembled at the solid-liquid interface: Relevance to the origin of life. *Orig. Life Evol. Biosph.* **1999**, *29*, 597–614. [[CrossRef](#)]
140. Holterman, H. *Kinetics and Evaporation of Water Drops in Air*; Number 2003-12; IMAG: Wageningen, The Netherlands, 2003.
141. Ferris, J.; Joshi, P.; Wang, K.J.; Miyakawa, S.; Huang, W. Catalysis in prebiotic chemistry: Application to the synthesis of RNA oligomers. *Adv. Space Res.* **2004**, *33*, 100–105. [[CrossRef](#)]
142. Klopogge, J. Raman spectroscopy of clay minerals. In *Developments in Clay Science*; Elsevier: Amsterdam, The Netherlands, 2017; Volume 8, pp. 150–199.
143. Hess, B. P-LINCS: A parallel linear constraint solver for molecular simulation. *J. Chem. Theory Comput.* **2008**, *4*, 116–122. [[CrossRef](#)]
144. Nosé, S. A molecular dynamics method for simulations in the canonical ensemble. *Mol. Phys.* **1984**, *52*, 255–268. [[CrossRef](#)]
145. Nosé, S. A unified formulation of the constant temperature molecular dynamics methods. *J. Chem. Phys.* **1984**, *81*, 511–519. [[CrossRef](#)]
146. Hoover, W.G. Canonical dynamics: Equilibrium phase-space distributions. *Phys. Rev. A* **1985**, *31*, 1695. [[CrossRef](#)]
147. Parrinello, M.; Rahman, A. Polymorphic transitions in single crystals: A new molecular dynamics method. *J. Appl. Phys.* **1981**, *52*, 7182–7190. [[CrossRef](#)]

**Disclaimer/Publisher’s Note:** The statements, opinions and data contained in all publications are solely those of the individual author(s) and contributor(s) and not of MDPI and/or the editor(s). MDPI and/or the editor(s) disclaim responsibility for any injury to people or property resulting from any ideas, methods, instructions or products referred to in the content.

M.A.Sc. Thesis - A. Dujardin, McMaster University - Chemistry and Chemical Biology

**SUPPLEMENTARY MATERIAL TO:  
THE FORMATION OF RNA PRE-POLYMERS IN THE PRESENCE  
OF DIFFERENT PREBIOTIC MINERAL SURFACES STUDIED BY  
MOLECULAR DYNAMICS SIMULATIONS**

Percentage of hydration (%)	Total number of water molecules	Approximate number of water molecules per nucleotide
100	12263-12878	61-64
85.4-89.7	10170-11000	51-55
75.3-78.9	8949-9680	45-48
61.3-69.7	7175-8470	36-42
53.5-59.2	6258-7260	31-36
40.8-51.6	5217-6050	26-30
31.4-41.3	4019-4840	20-24
24.2-31.1	3094-3630	15-18
18.8-20.7	2399-2420	12
9.0-10.3	1210	6
4.6-5.2	605	3

Supplementary Material, Table S1. Percentage of hydration and number of water molecules for all simulations containing a substrate.

Percentage of hydration (%)	Total number of water molecules	Approximate number of water molecules per nucleotide
100	15436	77
71.3	11014	55
61.9	9549	48
54.8	8462	42
47.6	7344	37
34.6	5340	27
28.8	4452	22
23.2	3579	18
16.2	2500	12
6.5	1000	5
3.2	500	3

Supplementary Material, Table S2. Percentage of hydration and water molecules for the nucleotides-only system.

# Chapter 4

## The formation of RNA oligomers in supersaturated levitated droplets

*Alix Dujardin<sup>1,2</sup>, Rachel Hambly<sup>1,2</sup>, Jake Brill<sup>1,3</sup>, Yingfu Li<sup>1,3</sup>, Ralph E. Pudritz<sup>1,2</sup>,  
Maikel C. Rheinstädter<sup>1,2</sup>*

<sup>1</sup>Origins Institute, McMaster University, Hamilton, ON, Canada

<sup>2</sup>Department of Physics and Astronomy, McMaster University, Hamilton, ON, Canada

<sup>3</sup>Department of Biochemistry and Biomedical Sciences, McMaster University, Hamilton, ON, Canada

## 4.1 Preface for The formation of RNA oligomers in supersaturated levitated droplets

The results from paper I showed that minerals interacted with nucleotides, and thus, nucleotides interacted less with each other. Our best results were found with graphite which is a non-interactive mineral and in the absence of a surface. Without a surface, simulations showed that nucleotides were freer to interact with each other. The absence of any surface could be and has been related to water droplets.

Therefore we wanted to understand if the formation of RNA using non-activated nucleotides would have been possible in droplets. We used a levitator using sound waves to suspend a droplet and observe it while it dried. The dehydration of the droplets and the confinement of the nucleotides could have formed RNA polymers in a prebiotic world. Furthermore, in a bulk solution, the surface effect becomes too dominant.

The construction and the set-up of the levitator were realized principally by Rachel Hambly. The sample preparation and data analysis were principally run by myself. Jake Brill, working in Yingfu Li laboratory, ran the radio-labeling gel electrophoresis.

Only preliminary results are shown here. Only one trial has been done with an experimental setup that needs to be improved. Indeed, the current setup does not allow the control of the environmental temperature and humidity. Once that is done, experiments can be used for publication.

This research will be carried on later by Rachel Hambly, Jake Brill, Ralph Pudritz, and Maikel Rheinstädter.

**Status:** Only preliminary results have been taken.

**Author Contributions:**

Set-up construction: Rachel Hambly, Alix Dujardin, Maikel C. Rheinstädter

Sample preparation: Alix Dujardin

Radio-labeling gel electrophoresis: Jake Brill, Yingfu Li

Data Analysis: Alix Dujardin, Jake Brill, Maikel C. Rheinstädter

## 4.2 Introduction

The formation of ribonucleic acids (RNA) without enzymes is still a prime question regarding the origin of life on Earth.

Different pathways could have led to the formation of non-activated nucleotides as explained in the first chapter of this thesis (*1.2.1 Non-activated nucleotides*) where minerals surfaces containing iron, aluminum, and silica were involved [105, 104, 84, 86, 107, 108, 106, 52, 58, 110]. But one of them not exposed earlier is via micro-droplets. Nam *et al.* showed that sugar phosphates and ribonucleoside could form spontaneously in micro-droplets, that were formed using electrospray ionization and analyzed with mass spectrometry, without enzymes or external energy sources [95]. They could also form nucleotide bases in the presence of a small quantity of  $Mg^{2+}$  [96]. Droplets were also used to create peptides formed at the air-water interface [56, 51, 76].

In our previous paper [41], we argued that tiny supersaturated water droplets that could have been produced by geysers or springs on the primitive Earth might have played an essential role in non-enzymatic RNA polymerization (have seen in Fig .4.1) based on the numerical simulations of high interaction between nucleotides and formation of pre-polymers in the absence of surface. Using droplets as three-dimensional confinement for forming complex molecules such as RNA is particularly relevant since organic components were found in marine aerosol particles [121, 88], as well as aerosols at 5 to 19 kilometers [94]. Moreover, it has been shown that molecules can be organized at the air-water interface [20, 83, 53]. Other research focused on the formation of protocells by using droplets and their role in protection for encapsulated molecules [121, 44, 39, 127, 40].

In this research, we are investigating the formation of RNA polymers using non-activated nucleotides in droplets using sound waves techniques to levitate and dry droplets in suspension in the air to mimic the formation of droplets formed by geysers in small ponds (4.1). We also examined the role of pre-polymer formation [41] by increasing the pH of the droplet containing nucleotides. Pre-polymers are *C3'C5'* hydrogen-bonded nucleotides that have been suggested to be the precursors of phosphodiester-bonded RNA polymers. After 45 min in the levitator, once the droplet was dried, we analyzed the pellet obtained using  $\gamma$ -<sup>32</sup>P ATP Radio labeling and gel electrophoresis techniques.

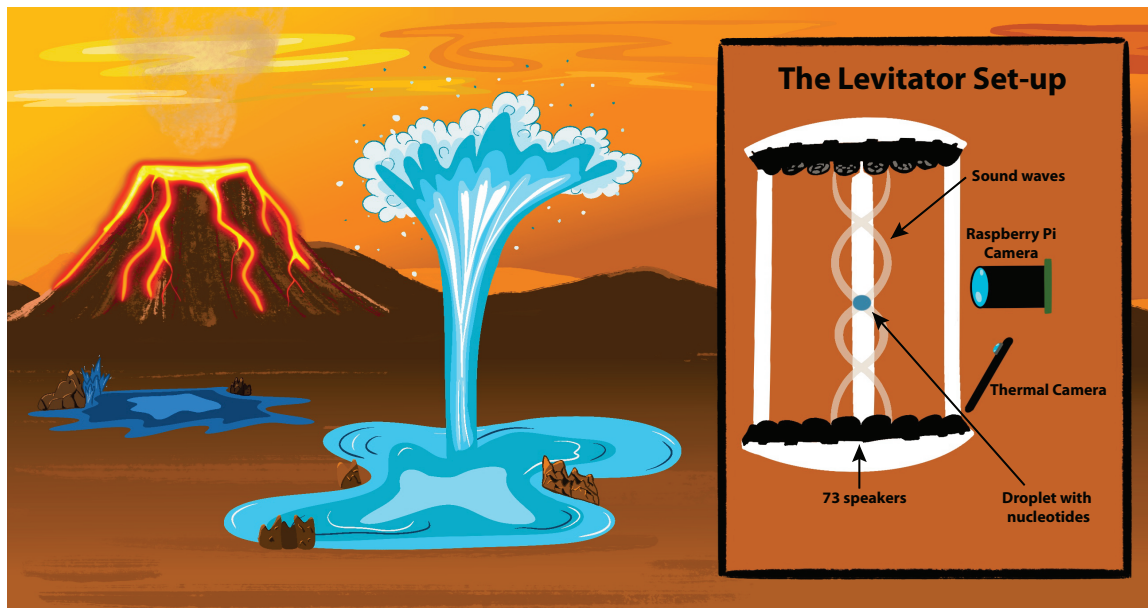


Figure 4.1: Sketch of primitive Earth including warm little ponds. Geysers of water, or water ricocheting off rocks, could have formed tiny droplets containing nucleotides. The dehydration and confinement could have led to RNA formation. The experiment set-up using an acoustic levitator containing a droplet with nucleotides can be seen on the right. Videos were taken using a Raspberry Pi camera, and temperatures were recorded using a thermal camera.

Our results suggested that water-droplet could have been a favorable environment

to form RNA polymers in the context of the origin of life both at acidic pH and basic pH.

## 4.3 Materials and Methods

### 4.3.1 Sample preparation

A  $\sim 24.3$  g/L stock solution of AMP (Sigma-Aldrich), initially in powder form, was made with ultrapure ( $18.2 \text{ M}\Omega\cdot\text{cm}$ ) water. Subsequently, solutions were sonicated for approximately 15 min using a tip sonicator (10 s pulse, 15 s off). A  $\sim 22.6$  g/L stock solution of UMP (Sigma-Aldrich), initially in crystal form, was prepared. The solution was vortexed for 10 s until crystals were completely dissolved, and the solution appeared homogeneous when observed through a flashlight. AMP and UMP solutions were mixed in a 1:1 molar and volumetric ratio and vortexed for 10 s to form a homogeneous solution. The pH of the initial solution is  $\sim 2$  because nucleotides are naturally acidic. The pH was adjusted using 1 M KOH solution to increase the pH and study the reaction at different pHs. The pH-meter used was *Orion Star A211* with the Thermo Scientific Orion Micro pH electrode. The concentration of nucleotides was then adjusted using ultrapure water to 20 g/L of nucleotides.

AMP:UMP solution was the main source of nucleotides in these experiments. AMP and UMP were selected as they are complimentary, which facilitates bonding.

### 4.3.2 Acoustic levitator

The acoustic levitator was built using a kit that can be found online [22], made accessible by *UpnaLab*, as seen in Fig 4.2. The kit comprises seventy-two 10 mm

40kHz transducers, one 3D-printed TinyLev support, one Arduino Nano, an L298N Dual Motor Drive Board, a power switch, a DC adaptor variable between 7V and 12V, and a DC female connector. The kit was assembled following the instruction on <https://www.instructables.com/Acoustic-Levigator/>. The levitator creates standing waves, and thus nodes are formed. At the node, a water droplet containing non-activated nucleotides is levitated. The drop is dried for  $\sim 45$  min until all the water evaporates. The pellet is then retrieved with a quartz slide (nucleotides do not form a lot of bond with quartz, see [41]), cleaned beforehand with dichloromethane, rinsed using methanol and water, and dried. The pellet is then retrieved from the slide using 100  $\mu\text{L}$  of water. The pellet is finally ethanol precipitated.

### 4.3.3 Cameras

Videos of the droplet were taken using a Raspberry Pi camera module with a 3 Mega Pixel lens, 8-50 mm IR F1.4C (Fig. 4.2).

A HIKMICRO Pocket1 192 x 144 IR Resolution Thermal Imaging Camera with 8MP Visual Camera, 25 Hz, was used to record the temperature of the droplet through time (Fig. 4.2).

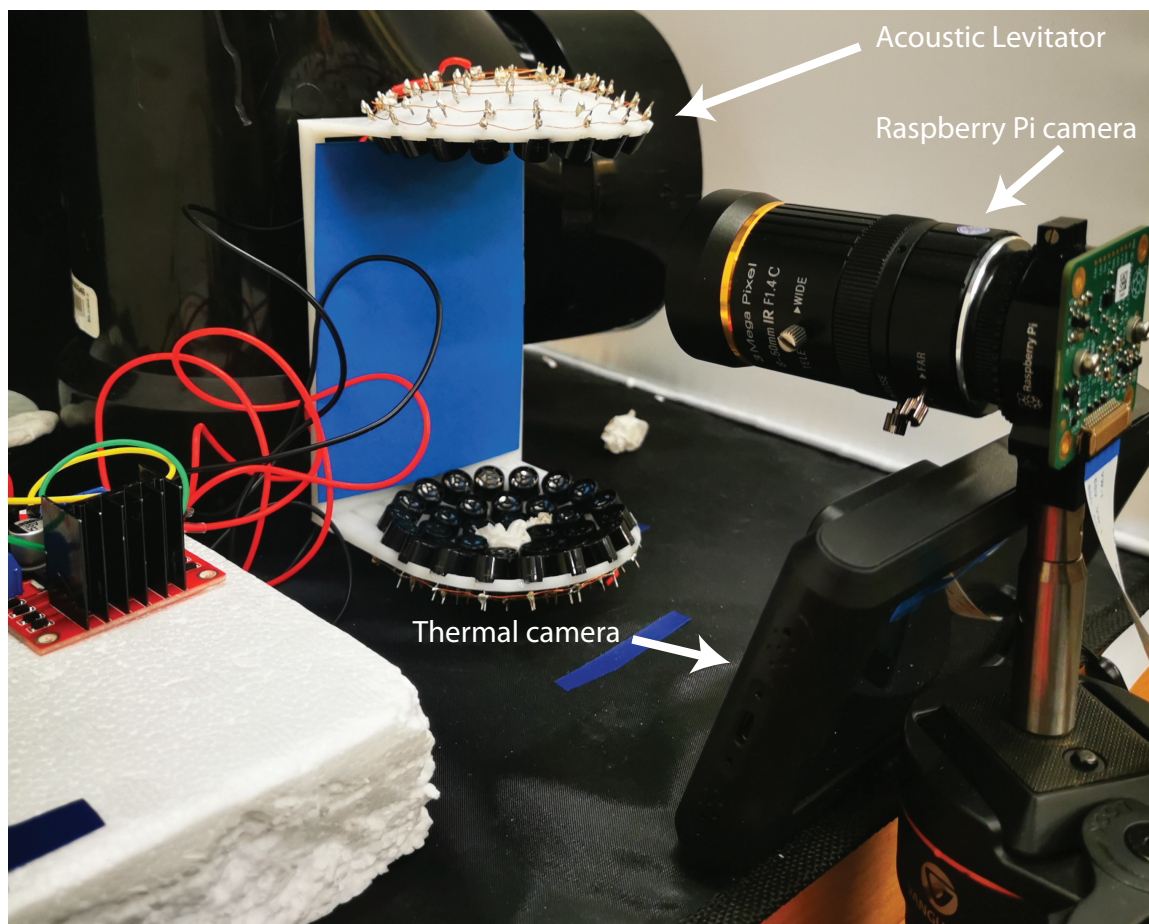


Figure 4.2: Picture of the experiment set-up. The acoustic levitator was placed in front of the Raspberry Pi camera module as well as the thermal camera.

#### 4.3.4 $\gamma$ - $^{32}\text{P}$ ATP Radio-labeling and gel electrophoresis

The radio-labeling technique allows a quick but still efficient and more resolution than standard fluorescence stains (such as SYBR Gold). This radio-labeling technique involves the phosphates of the polymers. In the first step, the 5'-phosphate of the polymer is removed to be replaced by a radioactive phosphate  $^{32}\text{P}$ . Like a standard gel, the RNA polymers, now radio-labeled, are going to migrate through the gel depending on their size. After the migration, the  $^{32}$ -phosphate is excited, and the polymers can

be revealed on the gel. The advantage of radio-labeling thus relates to imaging. Indeed, it gives a much higher resolution and basically eliminates background noise [109].

After ethanol precipitation of the sample, the 5'-phosphate termini of RNA was dephosphorylated by alkaline phosphatase (FastAP, ThermoFisher Scientific™), purified, then phosphorylated with  $^{32}\text{P}$  by T4 polynucleotide kinase (PNK, Thermo Scientific™). 80-100 ng of each sample was added to 1 U FastAP, 1× FastAP buffer (10 mM Tris-HCl pH 8.0, 5 mM  $\text{MgCl}_2$ , 500 mM KCl, 0.02% Triton X-100 and 0.1 mg/ml BSA, ThermoFisher Scientific™) and incubated for 30 minutes at 37°C. The dephosphorylated RNA was purified by the addition of equal volume phenol-chloroform-isoamyl alcohol 25:24:1 pH 6.7/8.0, which was then centrifuged for 2 minutes to separate out the aqueous layer. This was repeated with 99% chloroform to remove any residual phenol from the RNA-containing aqueous layer. The aqueous layer was removed, EtOH precipitated and dried by SpeedVac. The dried RNA was resuspended in a solution containing 10  $\mu\text{M}$  Ci  $\gamma$ - $^{32}\text{P}$  radio-labeled ATP, 10 U PNK, 1× PNK buffer A (50 mM imidazole-HCl pH 6.4, 18 mM  $\text{MgCl}_2$ , 5 mM DTT, 0.1 mM spermidine and 0.1 mM ADP, Thermo Scientific™) and incubated for 20 minutes at 37°C. 1× quenching buffer was added to the solution and separated on a 10% PAGE gel with 8 M Urea. The gel was exposed on an Amersham™ Biosciences storage phosphor screen and imaged on an Amersham™ Typhoon 9200 scanner with a photo-multiplier tube sensitivity of 4000 V and pixel size of 200  $\mu\text{m}$ . The radio-labeled transcripts were excised, crushed, soaked in 1× elution buffer, EtOH precipitated and dried by SpeedVac.

## 4.4 Preliminary Results

The formation of RNA from non-activated nucleotides was tested at acidic, neutral, and basic pH in droplets maintained in the air by acoustic waves in levitation.

Firstly, the size of the droplets was determined over time. They were obtained by taking the difference in the grey value of the background and the grey value of the droplet for each frame was recorded with the Raspberry Pi module. In other terms, the background color was subtracted by the droplet color to obtain the size of the droplet. At the beginning of the experiment, the droplet size was usually around 2.2 mm, as seen in Fig. 4.3A) (example taken with a pH 10 droplet). After  $\sim 25$  min, the water completely evaporated, and only the pellet on nucleotides remained, as seen by the flat signal. The size of the pellet was about 0.75 mm, losing  $\sim 34\%$  of its initial volume.

The temperature of the droplet is another parameter that was carefully followed over time using a thermal camera. At the beginning of the experiment, the temperature of the droplet was colder than in the outside environment, as seen in Fig. 4.3B) (example taken with a pH 10 droplet). The droplet was  $20.1^{\circ}\text{C}$ , and the outside environment was about  $29^{\circ}\text{C}$ . However, after 40 min, the droplet had reached the outside temperature of about  $30^{\circ}\text{C}$ .

A gel electrophoresis was performed with samples at different pHs, as seen in Fig. 4.3C). Two experiments were performed at pH 2. The first one, labeled pH 2,  $25^{\circ}\text{C}$  was dried using the same protocol as described in *3.3 Materials and Methods, Acoustic levitator*, and directly ethanol precipitated. The second acidic sample, labeled pH 2,  $85^{\circ}\text{C}$ , was dried at room temperature in suspension, retrieved from the levitator using a slide, and heated at  $85^{\circ}\text{C}$  on a hot plate for 5 min before ethanol

precipitation. The goal was to see if heating up would increase the polymerization rate. Our results suggested otherwise. The same signal is seen at  $\sim 18$  nt for both experiments at acidic pH.

From these preliminary results, neutral pH did not give any signal on the electrophoresis gel. Basic pH, pH 9, however, gives the highest rate of polymerization with RNA formed of about 50 nt.

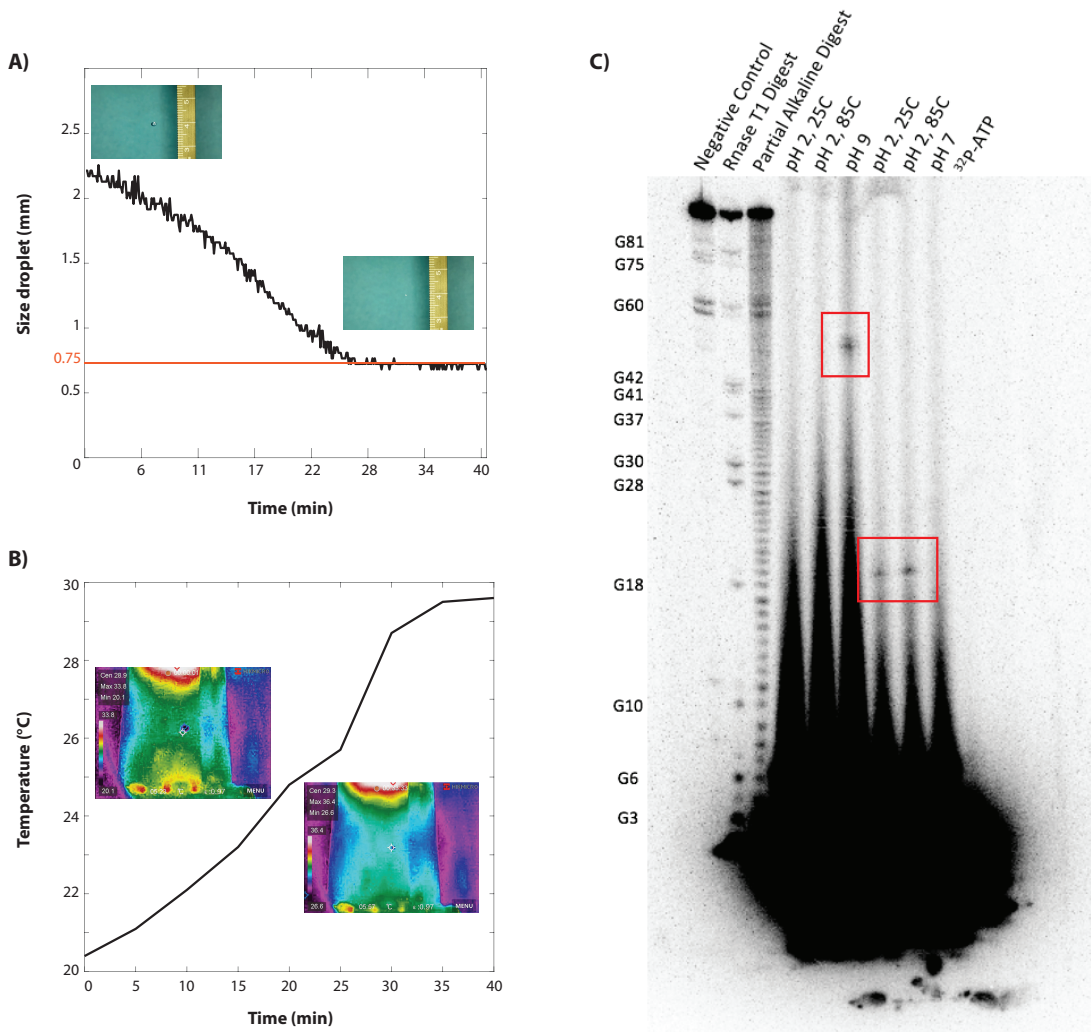


Figure 4.3: Preliminary results. A) shows the size of the droplet over time. At the beginning of the experiment, the size of the droplet is about  $\sim 2.3$  mm. Once all the water evaporates, the pellet is about  $\sim 0.75$  mm. B) display the temperature of the droplet over time. At the beginning of the experiment, the droplet is  $20.4^{\circ}\text{C}$ . After 40 min, the droplet warms up until  $29.6^{\circ}\text{C}$  which is the environment temperature inside the levitator. C) is a radio-labeling electrophoresis gel. At pH 9, a signal can be seen at 50 nt. At pH 2 dry at  $25^{\circ}\text{C}$  and at pH 2 dry at  $25^{\circ}\text{C}$  and once on the slide, heat-up at  $85^{\circ}\text{C}$ , signals around 18 nt are observed.

It is also noticed that at the bottom of the gel in Fig.4.3C), a large band can be observed under the polymer signals. This can be due to a large number of polymers.

Other experiments can be done to confirm these results and explain these large bands, which are explained further below in the discussion.

## 4.5 Discussion

The formation of RNA using non-activated nucleotides using parameters that mimic primitive Earth is not an easy task. Our goal was to experiment with our previous results obtained by computer modeling [41], which were that substrate inhibits the formation of RNA. Based on these results, a new model of RNA synthesized of primitive Earth emerged: the RNA formation in micro-droplets. To our knowledge, it is the first time that such experiments have been done regarding the origin of RNA on Earth.

The acoustic levitator allowed us to study in a controlled environment the formation of RNA in a water droplet. The average size of the droplets pipped in the levitator is  $\sim 2$  mm. Only  $\sim 25$  min is needed for the water to evaporate completely. It has been calculated by Dujardin *et al.* (2022) that the optimal droplet would have been around 0.2 mm in diameter to not evaporates too quickly or drops too fast. The evaporation rate of these droplets is about 100 s. Such droplets are, however, too small to study the polymerization rate in them. Nevertheless, our model can be compared to these micro-supersaturated droplets that could be formed by geysers or hot springs.

Thanks to the study by  $\gamma$ - $^{32}\text{P}$  ATP radio-labeling and gel electrophoresis, it has been shown that at acidic and basic pHs, RNA polymers can be synthesized from non-activated nucleotides. At basic pH, the bases and the hydroxyl are protonated while the phosphates are deprotonated [125]. These results also revealed that the 2-D

confinement in the droplets is enough activated energy to carry the polymerization and that no extreme heat would have been needed to activate the nucleotides. On the other hand, it has been shown that alkaline and warm environment accelerate RNA decomposition [72].

Another point to underline is that we thought pre-polymers would have been necessary for forming polymers. However, our best result yet was with a basic pH.

Our results suggest that supersaturated droplets containing non-activated nucleotides would have been an efficient way to form RNA on a prebiotic Earth. Back in the ponds, these RNA strands formed in the droplets could have been either protected by a protocell membrane [121, 44, 39, 127, 40] or minerals could have stabilized the RNA formed to avoid hydrolyze [12, 13, 66, 11, 116, 21].

It is important to highlight that these results are a first trial, and they need to be repeated and reproducible. The appearance of the gel, with a large band at the bottom and clear bands at the top, have already been published in the literature [70]. To prove the formation of polymers, the percentage of the PAGE gel could be increased. Thus, if the signal observed on the gel is indeed polymers, they would have difficulties moving through the gel, and the signal will be seen at the same place relative to the ladder. The opposite experiment can be done in a smaller percentage. These experiments have been done by Jerome *et al.* [70] to prove their results using radio-labeling gel electrophoresis. These experiments could be done in correlation with other techniques, such as mass spectrometry, to ensure the polymer formation and the integrity of the polymers (*e.g.* no bases lost) and also see if the large band at the bottom is polymers or not. Finally, the band in the gel could be extracted and run again through a gel and through a mass spectrometer to verify the size of the

band observed.

It is however important to note that, even though precautions have been taken to avoid contamination, being more careful working with RNA-free material would be necessary for the next steps of the experiments.

## 4.6 Conclusion

We used an acoustic levitator to study the RNA polymerization in water droplets using non-activated nucleotides. The water droplet was first dried for  $\sim 45$  min at room temperature. Our preliminary results suggested that RNA polymerization from non-activated nucleotides is possible, even without the addition of external heat. The 3-D confinement of the droplet would have been enough to carry the polymerization further, due to the internal heat in the droplet and the water-air interaction. pHs would have played an important role in the formation of RNA; basic pH would have been the optimal environment for RNA formation with non-activated nucleotides.

We acknowledge, however, that this setup is not perfect and can be improved. For example, a hermetic box can be placed around the levitator to control the environmental temperature. Other experiments that repeated this first one need to be done to see if the same bands are seen. The percentage of the PAGE gel can be changed to see if the signal observed on the gel is the same relative to the ladder. The results can also be correlated with other techniques such as mass spectrometry.

# Chapter 5

## Conclusions

The main question of this thesis is the emergence of life on primitive Earth, with a focus on RNA formation with non-activated nucleotides using the warm little ponds model and hydration-dehydration cycles. This research is split into three chapters, chapters 2, 3, and 4.

In Chapter 2, we presented a new simulator able to control five physical parameters (temperature, humidity, pressure, radiation, and gas environment) to mimic the wet-dry cycles. Using this new technology, we set up an experiment using non-activated nucleotides to reproduce warm little ponds in the presence of ammonium salts at pH 2. Gel electrophoresis and mass spectrometry, unfortunately, did not lead to a positive result regarding the formation of RNA.

Acidic conditions correlate with a warm environment leading to the degradation of the nucleotides. It is, however, important to keep in mind that shipping overseas could also have degraded the eventual polymers formed during the experiment. We are trying to have Mass Spectrometry running at McMaster to avoid the shipment, but setting up a Mass spectrometer for short RNA polymers is complex. Indeed,

Mass spectrometry is usually set up for proteins and not nucleic molecules. Molecular Dynamics simulations ran at pH 7, have shown that tight clusters of nucleotides were formed in the presence of ammonium ions due to the formation of hydrogen bonds between the ions and the nucleotides. This clusterization led to the formation of pre-polymers (hydrogen bonds between the *C3'* and the *C5'* of the nucleotides) when the system was dehydrated.

These conclusions led us to continue running MD computer simulations to have a better understanding of the role of the different substrates in RNA polymerization in the context of the origin of life research. Our research is exposed in Chapter 3 of this thesis. Indeed, substrates are almost systematically used for RNA polymerization research. Substrates are used as a catalyst for chemical reactions, protection of biomolecules, understanding the chirality of molecules, the first metabolism, and the formation of proto-cells. It is important to note that other groups such as Ferris or Orgel used activated nucleotides in their experiments.

Our main findings were that all charged substrates interact with the nucleotides by forming hydrogen bonds, leaving few chances for the formation of pre-polymers between the nucleotides, and would have thus inhibited the polymerization of RNA. Our simulations revealed that our best result was in the total absence of substrates.

We thus concluded that the formation of RNA polymers would have been possible in supersaturated droplets formed by geysers or springs. This is a new environmental vision that was not studied before in the RNA synthesis context for the origin of life, to the best of our knowledge. It is essential to note that even though substrates would not help with the formation of RNA, substrates tend to organize the nucleotides due to their charges. We also wanted to report that, to our knowledge, no other research

groups have done such computer simulations to study nucleotide organization in the presence of different substrates.

We want to highlight that the substrates used in our simulation were run without any impurities on their surfaces, they were perfectly smooth. Other groups such as Campisi *et al.* [17] have shown that defects, like the presence of iron or nickel in the substrates as a point defect, could be beneficial to activate certain types of bonds and dissociating them such as  $C - H$  to form new bonds between other molecules like  $C - Si$  and  $O - H$  bonds with the surface. These points consider it might be interesting to run Molecular Dynamics simulations with nucleotides and substrates with defects included in them, because we acknowledge that the results obtain and presented in Paper I are still the first step to understanding the role of minerals in the formation of life.

Thus, Chapter 4 regroups the preliminary experimental results of this new theory: life could have emerged from supersaturated micro-droplet. We used an acoustic levitator to make levitate a droplet containing non-activated nucleotides. Again, to our knowledge, no other research groups have done such experimentation before. Our results suggested that the formation of RNA from non-activated nucleotides would have been possible in small droplets. Our best result was obtained at basic pH, but smaller RNA polymers also formed at acid pH. Furthermore, these results were obtained without increasing the heat of the environment; the 2-dimensional confinement was enough to form phosphodiester bonds between nucleotides. This favors our first results presented in Chapter 2, where we found that heat increased the degradation rate of the nucleotides. But, the longest polymerization chains have been formed at alkaline pH, which would mean that pre-polymers would not have

been a pre-requisite for the formation of RNA polymer.

This last research must be continued because only a few tries have been tested. The setup can also be improved by enclosing the levitator in a hermetic box avoiding contact with outside air, where the temperature and humidity can be controlled. The acoustic levitator can also be set up inside the *Planet Simulator* to have optimal control over the droplet. In addition to the gel electrophoresis, mass spectrometry should be performed on the samples.

But the first experiment that needs to be done is the phase diagram using Nuclear Magnetic Resonance (NMR) to understand the stability of the nucleotides at different pHs and temperatures.

Another experiment can be done to prove the results exposed in Chapter 3, obtained with Molecular Dynamics simulations. For example, *Synth-Med Biotechnology* [23] uses gold biosensors to understand the bindings of cells and bacteria to lipids membranes. This technology could be used to study the binding of nucleotides to different substrates.

Finally, experiments involving the Planet Simulator can be redone using activated nucleotides such as cyclic ones or nucleoside triphosphates. For example, Jerome *et al.* [70] have shown promising results using nucleoside triphosphates to form RNA polymers under prebiotic conditions.

When these new experiments are going to be done, it is important to be certain that the materials use and the environment is RNA-free.

# Appendix A

## Appendix

### A.1 Gel electrophoresis

Compound	Concentration stock (mg/ml)
Adenosine 5'-monophosphate monohydrate (AMP) ( $C_{10}H_{14}N_5O_7P$ )	10.2433
Uridine 5'-monophosphate (UMP) ( $C_9H_{13}N_2O_9P$ )	9.5636
Ammonium chloride ( $NH_4Cl$ )	1.5790
Ammonium sulfate ( $(NH_4)_2SO_4$ )	3.8981
Ammonium nitrate ( $NH_4NO_3$ )	2.3613
Ammonium acetate ( $NH_3COONH_4$ )	2.2739

Table A.1: List of all solutions prepared and their concentrations.

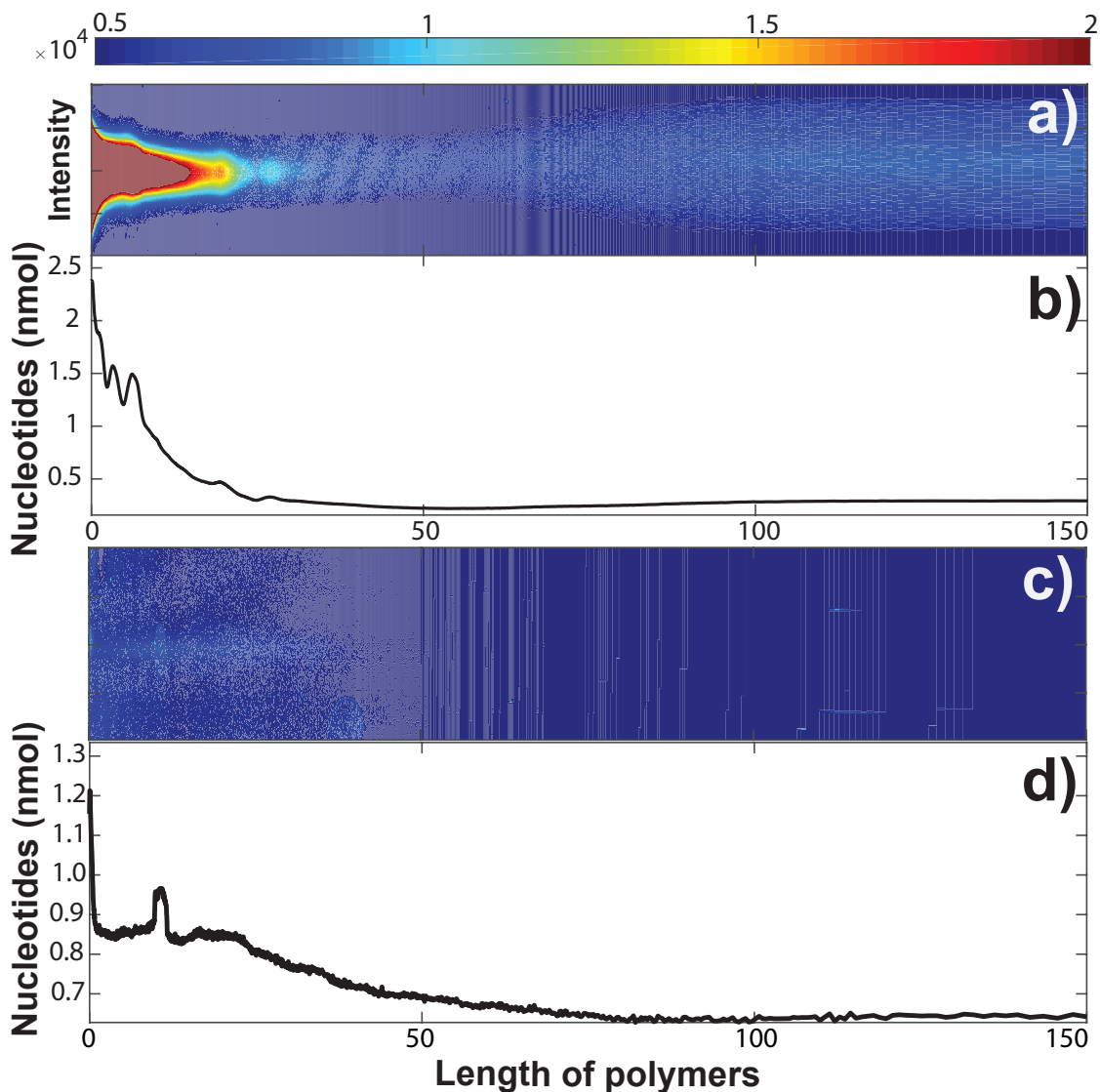


Figure A.1: AMP:UMP after 40 cycles a), b). AMP:UMP after 4 days without cycles, at 25°C c),d). The distribution of polymers length is shown in the gel line in a), and c). The quantitative analysis is shown in b) and d). With cycles, degradation of AMP:UMP can be seen. Without the cycles, no degradation nor polymers are revealed by the gel analysis. Only noise can be observed in the quantitative analysis.

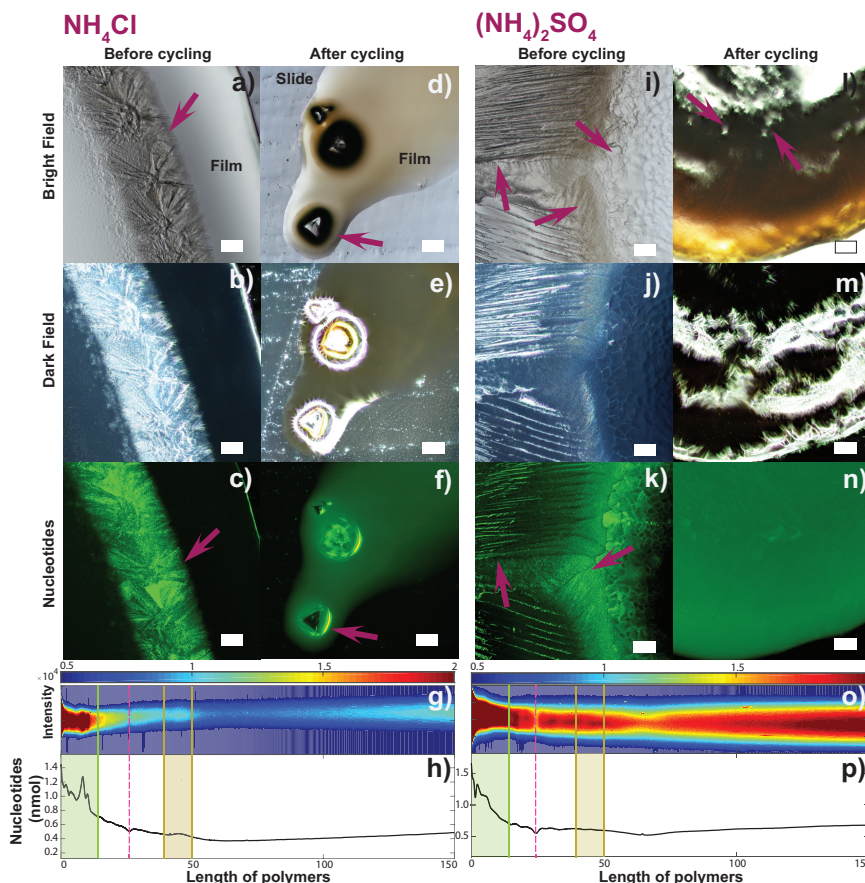


Figure A.2: Microscope images of an AMP:UMP: $\text{NH}_4\text{Cl}$  film before (a), b), c)) and after (d), e), f)) 40 hydration-dehydration cycles (scale:  $250\ \mu\text{m}$ ). Before cycling, a film and a crystalline structure are seen in a), b). Nucleotides are concentrated on the crystals' surfaces, in c). After cycling, triangular-shaped crystals are observed in d), e). Nucleotides are concentrated at the periphery of the crystals (f)). The intensity through the gel is shown on the band in g). The gel's quantitative analysis (h)) indicates a substantial amount of degradation. Microscope images of an AMP:UMP: $(\text{NH}_4)_2\text{SO}_4$  film before (i), j), k)) and after (l), m), n)) 40 hydration-dehydration cycles (scale:  $250\ \mu\text{m}$ ). Before cycling, a crystalline structure and an amorphous phase are seen (i), j)). Nucleotides are concentrated on the crystals and on the film (k)). After cycling, irregular structures are observed in the film (l)). Darkfield, in m) shows tiny crystals inside the film. Nucleotides are uniformly distributed in the film (n)). The overall intensity through the gel is strong which might indicate a higher degradation, as seen in o).

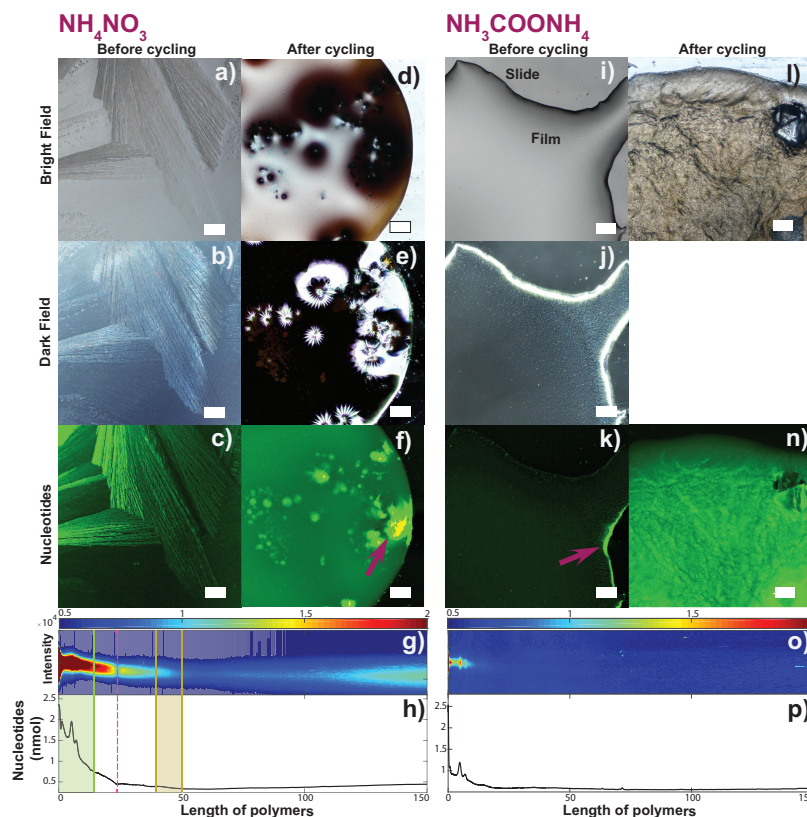


Figure A.3: Microscope images of an AMP:UMP: $\text{NH}_4\text{NO}_3$  film before (a), b), c)) and after (d), e), f)) 40 hydration-dehydration cycles (scale: 250  $\mu\text{m}$ ). Before cycling, crystalline structures are seen in the film (a), b)); nucleotides are concentrated on the crystals. After cycling, small crystals appear in (d). Nucleotides are concentrated on and around those crystals (f)). In the gel, a band is observed, indicating degradation (g). Microscope images of an AMP:UMP: $\text{NH}_3\text{COONH}_4$  film before (i), j), k)) and after (l), m), n)) 40 hydration-dehydration cycles (scale: 250  $\mu\text{m}$ ). Before cycling, a smooth film is observed on the slide (i), j)). Nucleotides are uniformly distributed inside the film even if the highest concentration is observed along the edge of the film (k)). After cycling, in l), the sample takes a rough clumpy structure. This mix does not form crystal (m)). Nucleotides are found to be everywhere throughout the sample (n)). The overall intensity on the gel line (o)) is minimal, and no large band can be seen.

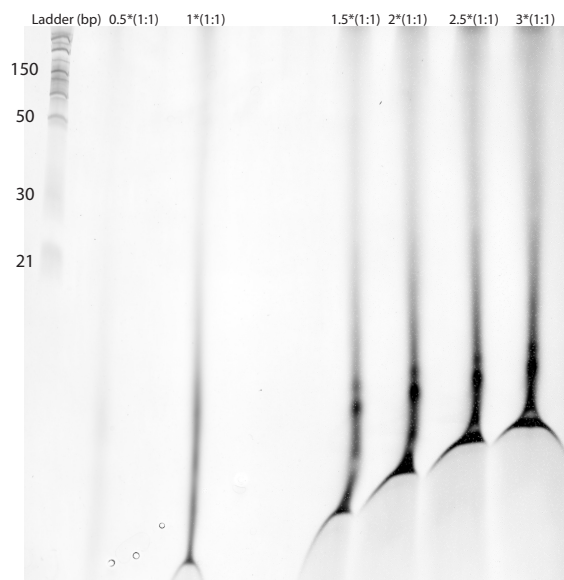


Figure A.4: Gel electrophoresis of AMP:UMP:(NH<sub>4</sub>)<sub>2</sub>SO<sub>4</sub> after 40 hydration-dehydration cycles. The coloration was inverted so that the results appeared black on the gel. The sample ran with 1:1 nucleotides:salt ratio, and mixed at the end of the experiment before precipitation (Materials and Methods, Electrophoresis gel preparation). The intensity is stronger when the ratio is higher. Nothing is detected with a ratio lower than 1:1.

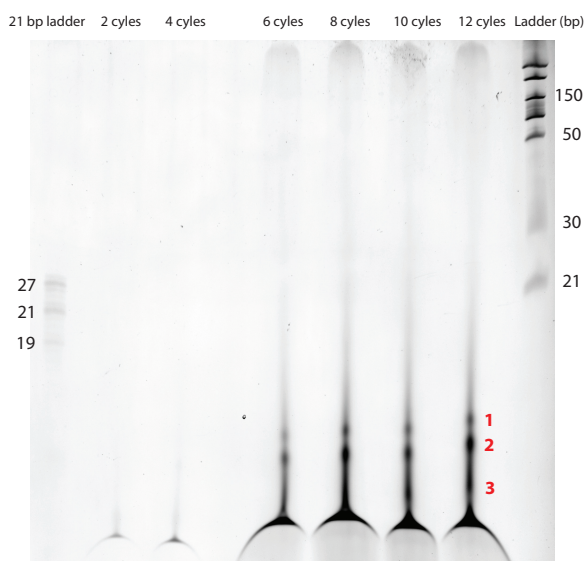


Figure A.5: Gel electrophoresis of AMP:UMP:(NH<sub>4</sub>)<sub>2</sub>SO<sub>4</sub> after 2, 4, 6, 8, 10, and 12 hydration-dehydration cycles. The coloration was inverted so that the results appeared black on the gel. After 2 and 4 cycles, the band is weak, and nothing appears on the gel. After 6 cycles, the bands' intensity is stronger. At 8 cycles, the migration shape is the same as after 6 cycles, but the overall intensity is stronger.

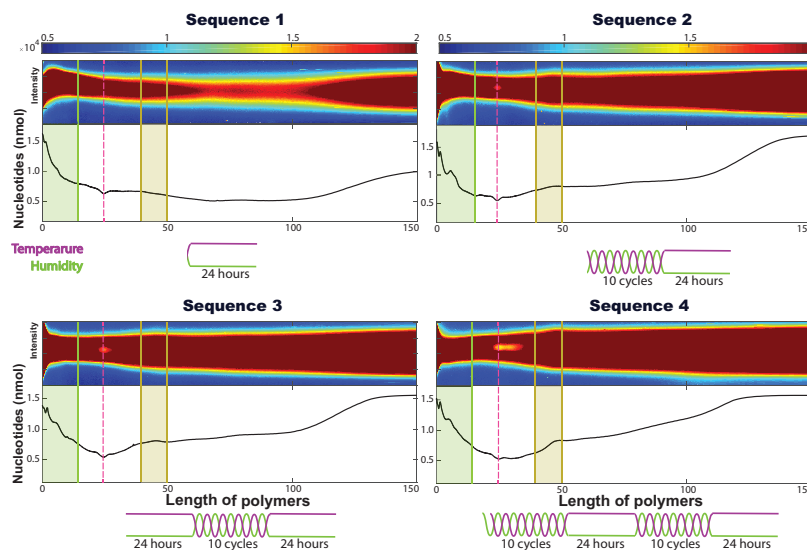


Figure A.6: Gel electrophoresis of AMP:UMP:NH<sub>4</sub>Cl. Sequence 1 underwent 24 hours of high temperature and low humidity. Sequence 2 went through 24 hours of cycling and 24 hours of high temperature and low humidity. Sequence 3 shows the sample result that ran during 24 hours of high temperature and low humidity, plus the same parameters as sequence 2. The last sequence underwent 24 more hours of cycles at the beginning of the experiment compared to sequence 3. The overall intensity on the gel is vigorous.

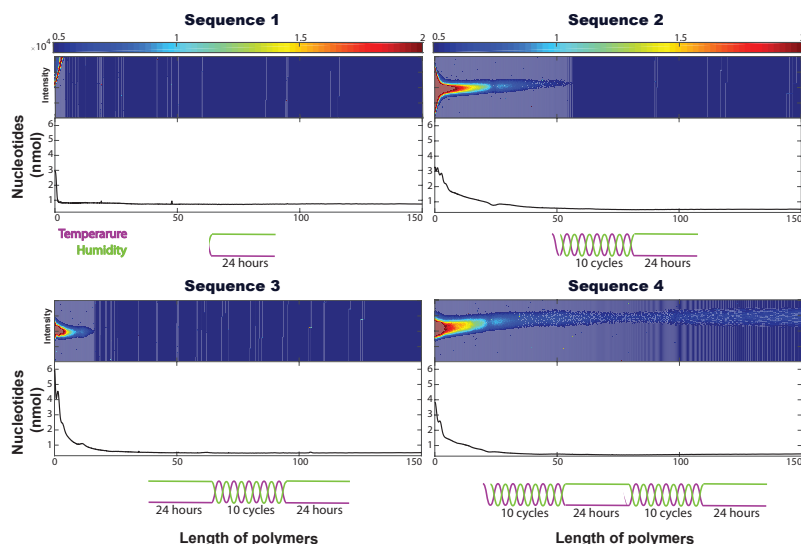


Figure A.7: Gel electrophoresis of AMP:UMP:NH<sub>4</sub>Cl. This experiment is the opposite of the one before. Instead of high temperature and low humidity, the effect of the humidity is tested, so the sample underwent high humidity and low temperature. Sequence 1 went through 24 hours of low temperature and high humidity. Sequence 2 had 24 hours of cycling and 24 hours of high temperature and low humidity. Sequence 3 underwent 24 hours of high temperature and low humidity, plus the same parameters as sequence 2. The last sequence ran 24 more hours of cycles at the beginning of the experiment compared to sequence 3. When samples underwent more cycling than the other samples, the degradation is more intense, like indicate by a longueur and larger band on the gel.

## A.2 MD Simulations

### MD simulations at 100% hydration

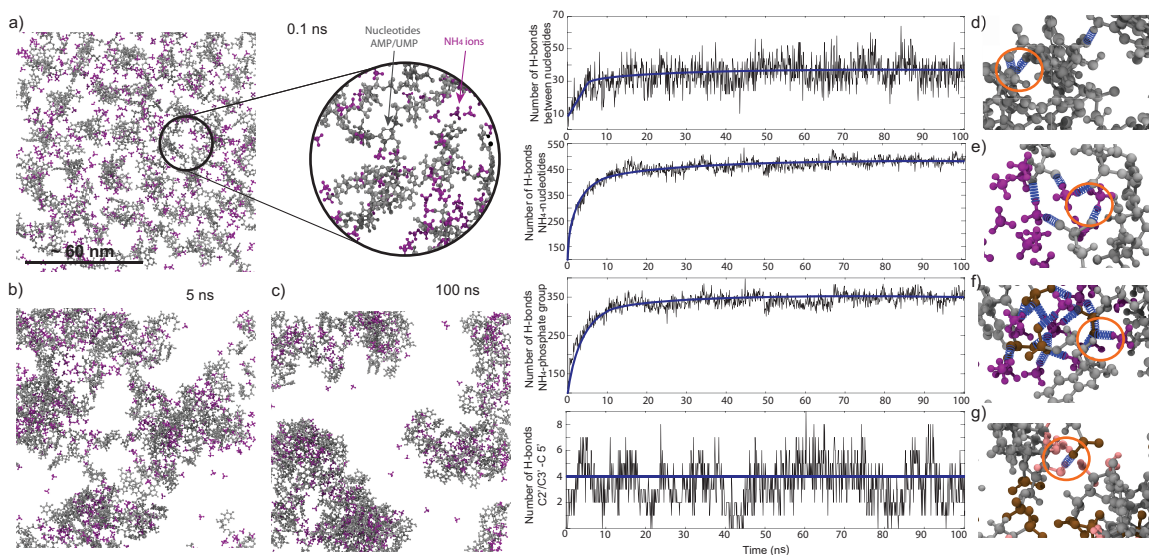


Figure A.8: Computer simulations of AMP:UMP (in gray) in the presence of  $(\text{NH}_4)_2\text{SO}_4$  in water. Only  $\text{NH}_4$  ions are represented (in purple). a), b), c) represent the position of the nucleotides in presence of  $\text{NH}_4$  ions at 0.1 ns, 5 ns, and 100 ns respectively. The graphic d) indicates the number of Hbonds between the nucleotides over time. The average was found to be 30. e) represents the number of Hbonds between  $\text{NH}_4$  ions and the nucleotides over time. During the first 5 ns, the number increases and stabilized at  $\sim 475$ . The graphic f) shows the evolution of the number of Hbonds between  $\text{NH}_4$  ions and  $C5'$  of nucleotides. As same as e), the number of Hbonds increases during the first 5 ns and then stabilized at  $\sim 350$ . The number of Hbonds between  $C2'/C3' - C5'$  is indicated in g). The average number was estimated at 4. The Hbonds are represented in blue, the phosphate group in brown, and the  $C2'$  and  $C3'$  groups in pink.

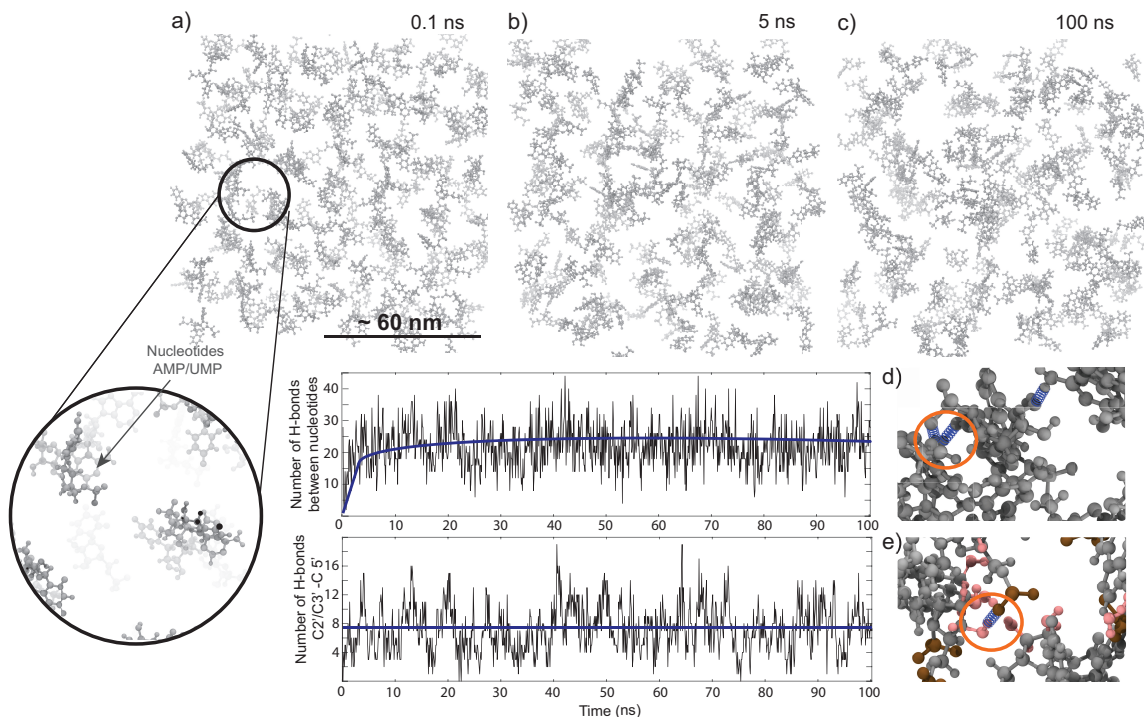


Figure A.9: Computer simulations of AMP:UMP (in gray) in water. a), b), c) show the nucleotide distribution at 0.1 ns, 5 ns, and 100 ns respectively. The nucleotides are homogeneously dispersed over time. The graphic d) represents the number of Hbonds between nucleotides over time. The average number of H-bonds is  $\sim 20$ .

The graphic e) indicates the number of  $C2'/C3' - C5'$  Hbonds over time. The average number is  $\sim 8$  Hbonds. The Hbonds are represented in blue, the phosphate group in brown, and the  $C2'$  and  $C3'$  groups in pink.

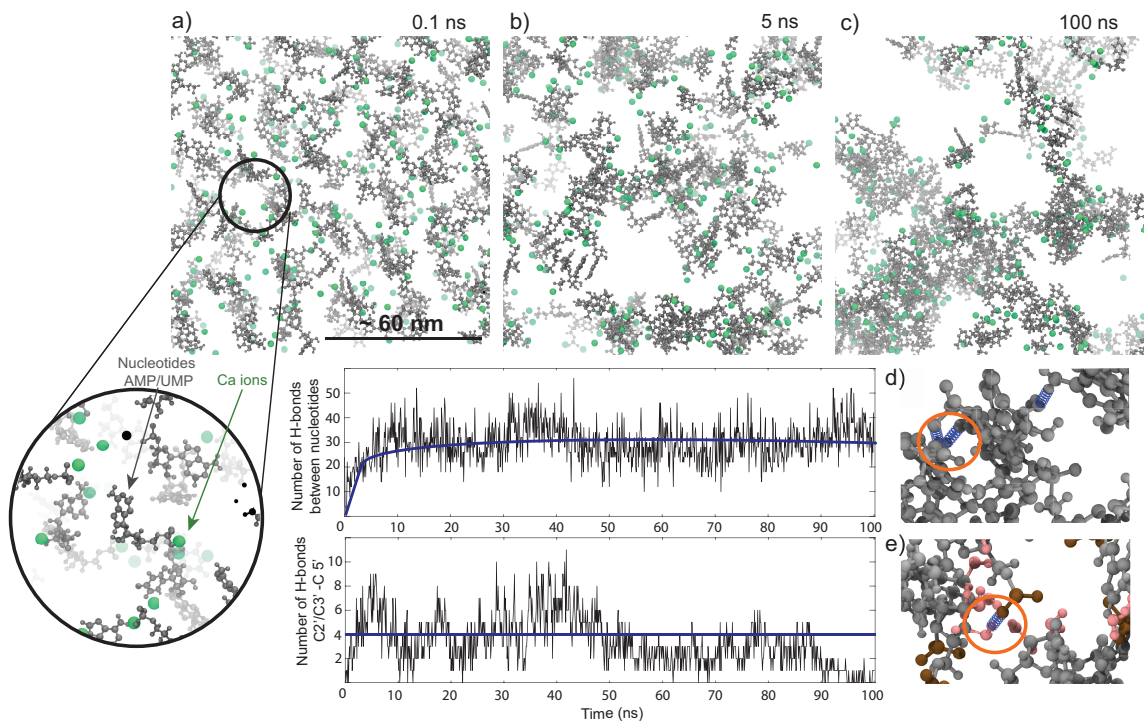


Figure A.10: Computer simulations of AMP:UMP (in gray) in the presence of CaCl<sub>2</sub> in water. Only Ca ions are represented (in green). a), b), c) show the evolution of the nucleotides in presence of Ca ions in solution at 0.1 ns, 5 ns, and 10 ns respectively. The graphic d) represents the number of Hbonds between nucleotides over time. The average number of Hbonds is  $\sim 30$ . The graphic e) indicates the number of C2'/C3' - C5' Hbonds over time. The average number has been found to be  $\sim 4$  Hbonds. The Hbonds are represented in blue, the phosphate group in brown, and the C2' and C3' groups in pink.

### Ammonium ions do not intercalate in existing RNA

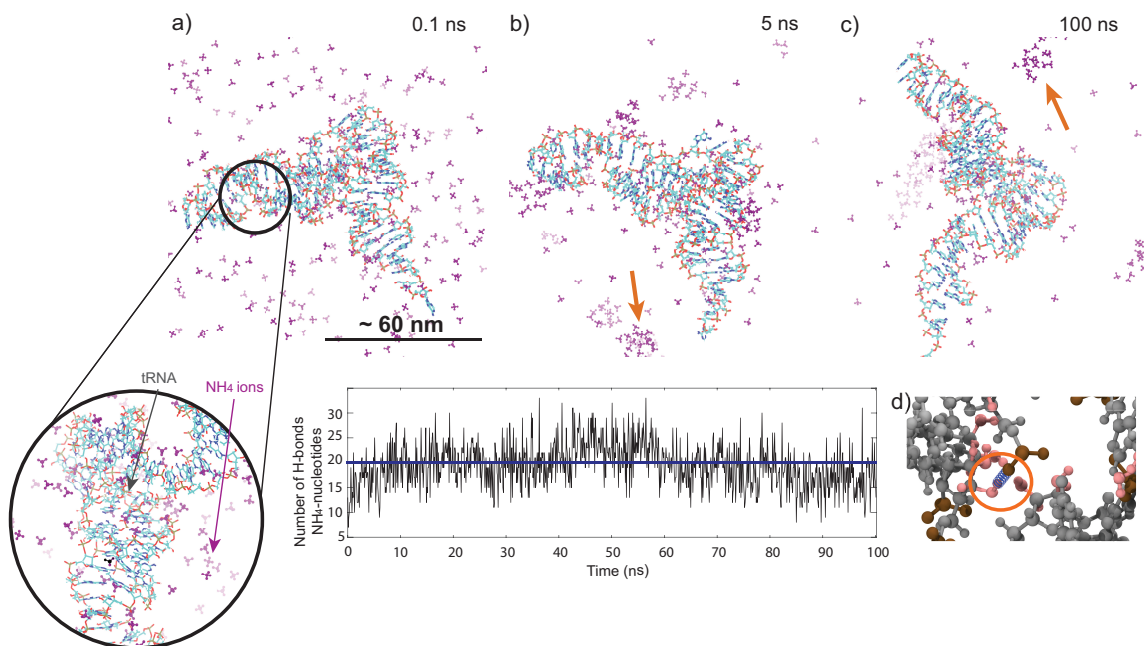


Figure A.11: Computer simulations of tRNA in the presence of  $(\text{NH}_4)_2\text{SO}_4$  in water.

Only  $\text{NH}_4$  is represented (in purple) in a), b), and c). The graphic shows the number of Hbonds between nucleotides and  $\text{NH}_4$  ions over time (ns) (f). a) shows a homogenous distribution of the ions in water, at 0.1 ns. After 5 ns, ions clusters start to form but not inside the tRNA. The same phenomenon is observed after 100 ns. The number of Hbond between tRNA and ions is stable over time ( $\sim 20$ ).

### Formation of pre-polymers is a bulk, not a surface effect

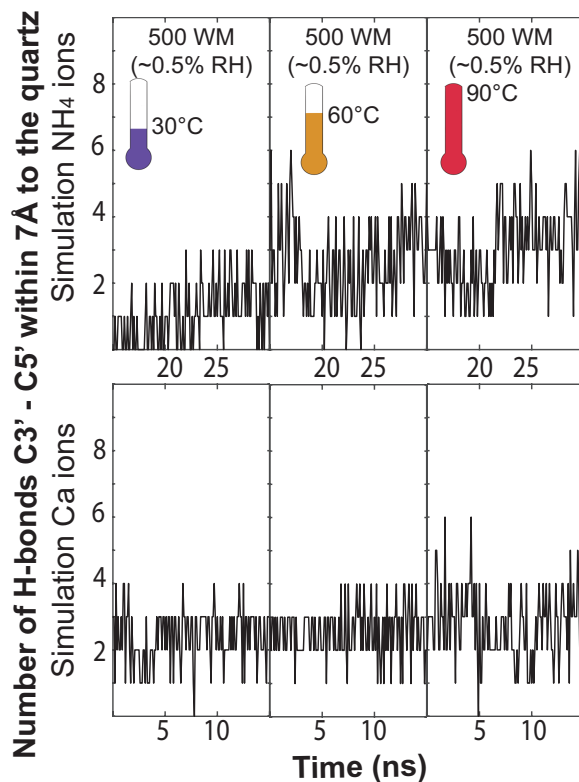


Figure A.12: Number of Hbonds between  $C3'$  and  $C5'$  within 7 Å close to the quartz. The overall number of Hbonds is lower than observed in the entire simulation box meaning that the quartz does not affect the formation of Hbonds between the nucleotides.

# Bibliography

- [1] M. J. Abraham, T. Murtola, R. Schulz, S. Páll, J. C. Smith, B. Hess, and E. Lindahl. Gromacs: High performance molecular simulations through multi-level parallelism from laptops to supercomputers. *SoftwareX*, 1:19–25, 2015.
- [2] K. Adamala, F. Anella, R. Wieczorek, P. Stano, C. Chiarabelli, and P. L. Luisi. Open questions in origin of life: Experimental studies on the origin of nucleic acids and proteins with specific and functional sequences by a chemical synthetic biology approach. *Computational and Structural Biotechnology Journal*, 9(14): e201402004, 2014.
- [3] J. Adkinss. James webb space telescope, 2022. URL [https://www.nasa.gov/mission\\_pages/webb/main/index.html](https://www.nasa.gov/mission_pages/webb/main/index.html).
- [4] J. Attwater, A. Wochner, V. B. Pinheiro, A. Coulson, and P. Holliger. Ice as a protocellular medium for RNA replication. *Nature Communications*, 1(1):1–9, 2010.
- [5] J. A. Baross and S. E. Hoffman. Submarine hydrothermal vents and associated gradient environments as sites for the origin and evolution of life. *Origins of Life and Evolution of the Biosphere*, 15(4):327–345, 1985.

- [6] A. A. Beaudry and G. F. Joyce. Directed evolution of an RNA enzyme. *Science*, 257(5070):635–641, 1992.
- [7] S. A. Benner. Understanding nucleic acids using synthetic chemistry. *Accounts of Chemical Research*, 37(10):784–797, 2004.
- [8] P. Berche. Louis pasteur, from crystals of life to vaccination. *Clinical microbiology and infection*, 18:1–6, 2012.
- [9] C. K. Biebricher and L. E. Orgel. An RNA that multiplies indefinitely with dna-dependent RNA polymerase: selection from a random copolymer. *Proceedings of the National Academy of Sciences*, 70(3):934–938, 1973.
- [10] C. K. Biebricher, M. Eigen, and W. C. Gardiner Jr. Kinetics of RNA replication: competition and selection among self-replicating RNA species. *Biochemistry*, 24(23):6550–6560, 1985.
- [11] E. Biondi, S. Branciamore, M.-C. Maurel, and E. Gallori. Montmorillonite protection of an uv-irradiated hairpin ribozyme: evolution of the RNA world in a mineral environment. *BMC Evolutionary Biology*, 7(2):1–7, 2007.
- [12] E. Biondi, Y. Furukawa, J. Kawai, and S. A. Benner. Adsorption of RNA on mineral surfaces and mineral precipitates. *Beilstein Journal of Organic Chemistry*, 13(1):393–404, 2017.
- [13] E. Biondi, L. Howell, and S. A. Benner. Opal adsorbs and stabilizes RNA—a hierarchy of prebiotic silica minerals. *Synlett*, 28(01):84–88, 2017.
- [14] G. M. Blackburn, M. J. Gait, D. M. Williams, and D. Loakes. *Nucleic acids in chemistry and biology*. Royal Society of Chemistry, 2006.

- [15] J. C. Bowman, A. S. Petrov, M. Frenkel-Pinter, P. I. Penev, and L. D. Williams. Root of the tree: the significance, evolution, and origins of the ribosome. *Chemical reviews*, 120(11):4848–4878, 2020.
- [16] B. R. Brooks, C. L. Brooks III, A. D. Mackerell Jr, L. Nilsson, R. J. Petrella, B. Roux, Y. Won, G. Archontis, C. Bartels, S. Boresch, et al. Charmm: the biomolecular simulation program. *Journal of computational chemistry*, 30(10):1545–1614, 2009.
- [17] D. Campisi, T. Lamberts, N. Y. Dzade, R. Martinazzo, I. L. Ten Kate, and A. G. Tielens. Adsorption of polycyclic aromatic hydrocarbons and c60 onto forsterite: C–h bond activation by the schottky vacancy. *ACS Earth and Space Chemistry*, 6(8):2009–2023, 2022.
- [18] T. R. Cech. A model for the RNA-catalyzed replication of rna. *Proceedings of the National Academy of Sciences*, 83(12):4360–4363, 1986.
- [19] T. R. Cech. The RNA worlds in context. *Cold Spring Harbor perspectives in biology*, 4(7):a006742, 2012.
- [20] X. Chen, B. Minofar, P. Jungwirth, and H. C. Allen. Interfacial molecular organization at aqueous solution surfaces of atmospherically relevant dimethyl sulfoxide and methanesulfonic acid using sum frequency spectroscopy and molecular dynamics simulation. *The Journal of Physical Chemistry B*, 114(47):15546–15553, 2010.
- [21] F. Ciciriello, G. Costanzo, C. Crestini, R. Saladino, and E. Di Mauro. Origin

- of informational polymers and the search for non-terran life: protection of the polymeric state of dna by phosphate minerals. *Astrobiology*, 7(4):616–630, 2007.
- [22] R. company. Robotshop, n.d.. URL <https://ca.robotshop.com/products/acoustic-levitator-kit>.
- [23] S.-M. B. company. Synth-med biotechnology, n.d.. URL <https://synth-med.com/>.
- [24] G. Costanzo, S. Pino, A. M. Timperio, J. E. Šponer, J. Šponer, O. Nováková, O. Šedo, Z. Zdráhal, and E. Di Mauro. Non-enzymatic oligomerization of 3', 5'cyclic amp. *PLoS One*, 11(11):e0165723, 2016.
- [25] G. Costanzo, A. Giorgi, A. Scipioni, A. M. Timperio, C. Mancone, M. Tripodi, M. Kapralov, E. Krasavin, H. Kruse, J. Šponer, et al. Nonenzymatic oligomerization of 3 , 5 -cyclic cmp induced by proton and uv irradiation hints at a nonfastidious origin of rna. *ChemBioChem*, 18(15):1535–1543, 2017.
- [26] L. Da Silva, M.-C. Maurel, and D. Deamer. Salt-promoted synthesis of RNA-like molecules in simulated hydrothermal conditions. *Journal of molecular evolution*, 80(2):86–97, 2015.
- [27] B. Damer and D. Deamer. Coupled phases and combinatorial selection in fluctuating hydrothermal pools: a scenario to guide experimental approaches to the origin of cellular life. *Life*, 5(1):872–887, 2015.
- [28] B. Damer and D. Deamer. The hot spring hypothesis for an origin of life. *Astrobiology*, 20(4):429–452, 2020.

- [29] C. Darwin. The theory of x-ray reflection. *Philos. Mag.*, 27:315–333 & 675–690, 1914.
- [30] C. Darwin. *On the origin of species, 1859*. Routledge, 2004.
- [31] A. V. Dass, S. Wunnava, J. Langlais, B. von der Esch, M. Krusche, L. Ufer, N. Chrisam, R. C. Dubini, F. Gartner, S. Angerpointner, et al. RNA oligomerisation without added catalyst from 2 , 3 -cyclic nucleotides by drying at air-water interfaces. *ChemSystemsChem*, 5(1):e202200026, 2023.
- [32] D. Deamer. Liquid-crystalline nano structures: organizing matrices for non-enzymatic nucleic acid polymerization. *Chem. Soc. Rev.*, 41:5375–5379, 2012.
- [33] D. Deamer. Where did life begin? testing ideas in prebiotic analogue conditions. *Life*, 11(2):134, 2021.
- [34] D. Deamer, B. Damer, and V. Kompanichenko. Hydrothermal chemistry and the origin of cellular life. *Astrobiology*, 19(12):1523–1537, 2019.
- [35] D. W. Deamer. *First life : discovering the connections between stars, cells, and how life began*. University of California Press, Berkeley, 2011. ISBN 0520258320.
- [36] D. W. Deamer and C. D. Georgiou. Hydrothermal conditions and the origin of cellular life. *Astrobiology*, 15(12):1091–1095, 2015.
- [37] V. DeGuzman, W. Vercoutere, H. Shenasa, and D. Deamer. Generation of oligonucleotides under hydrothermal conditions by non-enzymatic polymerization. *Journal of Molecular Evolution*, 78(5):251–262, 2014.

- [38] T. Djokic, M. J. Van Kranendonk, K. A. Campbell, M. R. Walter, and C. R. Ward. Earliest signs of life on land preserved in ca. 3.5 ga hot spring deposits. *Nature communications*, 8(1):1–9, 2017.
- [39] C. M. Dobson, G. B. Ellison, A. F. Tuck, and V. Vaida. Atmospheric aerosols as prebiotic chemical reactors. *Proceedings of the National Academy of Sciences*, 97(22):11864–11868, 2000.
- [40] D. Donaldson and V. Vaida. The influence of organic films at the air- aqueous boundary on atmospheric processes. *Chemical reviews*, 106(4):1445–1461, 2006.
- [41] A. Dujardin, S. Himbert, R. Pudritz, and M. C. Rheinstädter. The Formation of RNA Pre-Polymers in the Presence of Different Prebiotic Mineral Surfaces Studied by Molecular Dynamics Simulations. *Life*, 13(1):112, 2022.
- [42] E. H. Eklund and D. P. Bartel. RNA-catalysed RNA polymerization using nucleoside triphosphates. *Nature*, 382(6589):373–376, 1996.
- [43] A. D. Ellington and J. W. Szostak. In vitro selection of RNA molecules that bind specific ligands. *nature*, 346(6287):818–822, 1990.
- [44] G. B. Ellison, A. F. Tuck, and V. Vaida. Atmospheric processing of organic aerosols. *Journal of Geophysical Research: Atmospheres*, 104(D9):11633–11641, 1999.
- [45] G. Ertem and J. P. Ferris. Synthesis of RNA oligomers on heterogeneous templates. *Nature*, 379(6562):238–240, 1996.
- [46] J. P. Ferris. Mineral catalysis and prebiotic synthesis: montmorillonite-catalyzed formation of rna. *Elements*, 1(3):145–149, 2005.

- [47] J. P. Ferris. Montmorillonite-catalysed formation of RNA oligomers: the possible role of catalysis in the origins of life. *Philosophical Transactions of the Royal Society B: Biological Sciences*, 361(1474):1777–1786, 2006.
- [48] J. P. Ferris and G. Ertem. Oligomerization of ribonucleotides on montmorillonite: reaction of the 5'-phosphorimidazolide of adenosine. *Science*, 257(5075):1387–1389, 1992.
- [49] S. Fox, H. L. Pleyer, and H. Strasdeit. An automated apparatus for the simulation of prebiotic wet–dry cycles under strictly anaerobic conditions. *International Journal of Astrobiology*, 18(1):60–72, 2019.
- [50] M. Frenkel-Pinter, J. W. Haynes, A. M. Mohyeldin, A. B. Sargon, A. S. Petrov, R. Krishnamurthy, N. V. Hud, L. D. Williams, and L. J. Leman. Mutually stabilizing interactions between proto-peptides and rna. *Nature Communications*, 11(1):3137, 2020.
- [51] K. Fukuda, Y. Shibasaki, H. Nakahara, and M.-h. Liu. Spontaneous formation of polypeptides in the interfacial thin films of amphiphilic amino acid esters: acceleration of the polycondensation and control of the structure of resultant polymers. *Advances in colloid and interface science*, 87(2-3):113–145, 2000.
- [52] W. D. Fuller, R. A. Sanchez, and L. E. Orgel. Studies in prebiotic synthesis: Vi. synthesis of purine nucleosides. *Journal of molecular biology*, 67(1):25–33, 1972.
- [53] P.-M. Gassin, L. Girard, G. Martin-Gassin, D. Brusselle, A. Jonchere, O. Diat,

- C. Viñas, F. Teixidor, and P. Bauduin. Surface activity and molecular organization of metallacarboranes at the air–water interface revealed by nonlinear optics. *Langmuir*, 31(8):2297–2303, 2015.
- [54] W. Gilbert. Origin of life: The RNA world. *nature*, 319(6055):618–618, 1986.
- [55] T. Greicius. Perseverance mars rover, 2021. URL <https://www.nasa.gov/perseverance>.
- [56] E. C. Griffith and V. Vaida. In situ observation of peptide bond formation at the water–air interface. *Proceedings of the National Academy of Sciences*, 109(39):15697–15701, 2012.
- [57] J. Gu. *Li Lab SOP Manual*. Li Lab, McMaster University, 2018.
- [58] M. Gull, M. A. Mojica, F. M. Fernández, D. A. Gaul, T. M. Orlando, C. L. Liotta, and M. A. Pasek. Nucleoside phosphorylation by the mineral schreibersite. *Scientific reports*, 5(1):17198, 2015.
- [59] M. Hargrave, S. K. Thompson, and D. Deamer. Computational models of polymer synthesis driven by dehydration/rehydration cycles: repurination in simulated hydrothermal fields. *Journal of molecular evolution*, 86(8):501–510, 2018.
- [60] T. Hassenkam, B. Damer, G. Mednick, and D. Deamer. Viroid-sized rings self-assemble from mononucleotides through wet-dry cycling: implications for the origin of life. *bioRxiv*, 2020.
- [61] R. M. Hazen and D. A. Sverjensky. Mineral surfaces, geochemical complexities,

- and the origins of life. *Cold Spring Harbor perspectives in biology*, 2(5):a002162, 2010.
- [62] B. Hess. P-lincs: A parallel linear constraint solver for molecular simulation. *Journal of chemical theory and computation*, 4(1):116–122, 2008.
- [63] P. G. Higgs. The effect of limited diffusion and wet–dry cycling on reversible polymerization reactions: implications for prebiotic synthesis of nucleic acids. *Life*, 6(2):24, 2016.
- [64] S. Himbert, M. Chapman, D. W. Deamer, and M. C. Rheinstädter. Organization of nucleotides in different environments and the formation of pre-polymers. *Scientific reports*, 6(1):1–12, 2016.
- [65] W. G. Hoover. Canonical dynamics: Equilibrium phase-space distributions. *Physical review A*, 31(3):1695, 1985.
- [66] W. Huang and J. P. Ferris. One-step, regioselective synthesis of up to 50-mers of RNA oligomers by montmorillonite catalysis. *Journal of the American Chemical Society*, 128(27):8914–8919, 2006.
- [67] N. V. Hud, B. J. Cafferty, R. Krishnamurthy, and L. D. Williams. The origin of RNA and “my grandfather’s axe”. *Chemistry & biology*, 20(4):466–474, 2013.
- [68] T. Inoue and L. Orgel. Oligomerization of (guanosine 5 -phosphor)-2-methylimidazolide on poly (c): an RNA polymerase model. *Journal of molecular biology*, 162(1):201–217, 1982.

- [69] R. V. Jadhav, S. M. Hivarkar, and V. B. Khyade. Millard reaction: The foundation of science of cooking established by millard. *International Journal of Biochemistry and Biomolecules*, 6(1):15–25, 2020.
- [70] C. A. Jerome, H.-J. Kim, S. J. Mojzsis, S. A. Benner, and E. Biondi. Catalytic synthesis of polyribonucleic acid on prebiotic rock glasses. *Astrobiology*, 2022.
- [71] S. Jo, T. Kim, V. G. Iyer, and W. Im. Charmm-gui: a web-based graphical user interface for charmm. *Journal of computational chemistry*, 29(11):1859–1865, 2008.
- [72] T. Jo, K. Tsuru, T. Hirohara, and H. Yamanaka. Warm temperature and alkaline conditions accelerate environmental RNA degradation. *Environmental DNA*, 2022.
- [73] G. F. Joyce. Forty years of in vitro evolution. *Angewandte Chemie International Edition*, 46(34):6420–6436, 2007.
- [74] E. V. Koonin and A. S. Novozhilov. Origin and evolution of the universal genetic code. *Annual review of genetics*, 51:45–62, 2017.
- [75] M. Kreysing, L. Keil, S. Lanzmich, and D. Braun. Heat flux across an open pore enables the continuous replication and selection of oligonucleotides towards increasing length. *Nature chemistry*, 7(3):203–208, 2015.
- [76] J. K. Kumar and J. S. Oliver. Proximity effects in monolayer films: Kinetic analysis of amide bond formation at the air- water interface using 1h nmr spectroscopy. *Journal of the American Chemical Society*, 124(38):11307–11314, 2002.

- [77] J. Lee, X. Cheng, J. M. Swails, M. S. Yeom, P. K. Eastman, J. A. Lemkul, S. Wei, J. Buckner, J. C. Jeong, Y. Qi, et al. Charmm-gui input generator for namd, gromacs, amber, openmm, and charmm/openmm simulations using the charmm36 additive force field. *Journal of chemical theory and computation*, 12(1):405–413, 2016.
- [78] H. Lehrach, D. Diamond, J. M. Wozney, and H. Boedtker. RNA molecular weight determinations by gel electrophoresis under denaturing conditions, a critical reexamination. *Biochemistry*, 16(21):4743–4751, 1977.
- [79] O. Leslie E. Prebiotic chemistry and the origin of the RNA world. *Critical reviews in biochemistry and molecular biology*, 39(2):99–123, 2004.
- [80] G. Macleod, C. McKeown, A. J. Hall, and M. J. Russell. Hydrothermal and oceanic pH conditions of possible relevance to the origin of life. *Origins of Life and Evolution of the Biosphere*, 24(1):19–41, 1994.
- [81] W. Martin, J. Baross, D. Kelley, and M. J. Russell. Hydrothermal vents and the origin of life. *Nature Reviews Microbiology*, 6(11):805–814, 2008.
- [82] C. B. Mast, S. Schink, U. Gerland, and D. Braun. Escalation of polymerization in a thermal gradient. *Proceedings of the National Academy of Sciences*, 110(20):8030–8035, 2013.
- [83] Y. Matsuzawa, S. Yokokawa, and K. Ichimura. Molecular organization of aminimides with long-alkyl chains on water surface. *Colloids and Surfaces A: Physicochemical and Engineering Aspects*, 198:165–172, 2002.

- [84] L. E. Mayhew, E. Ellison, T. McCollom, T. Trainor, and A. Templeton. Hydrogen generation from low-temperature water–rock reactions. *Nature Geoscience*, 6(6):478–484, 2013.
- [85] T. M. McCollom. Miller-urey and beyond: what have we learned about prebiotic organic synthesis reactions in the past 60 years? *Annual Review of Earth and Planetary Sciences*, 41:207–229, 2013.
- [86] C. P. McKay. What is life—and how do we search for it in other worlds? *PLoS biology*, 2(9):e302, 2004.
- [87] C. Menor-Salván and M. R. Marín-Yaseli. Prebiotic chemistry in eutectic solutions at the water–ice matrix. *Chemical Society Reviews*, 41(16):5404–5415, 2012.
- [88] A. M. Middlebrook, D. M. Murphy, and D. S. Thomson. Observations of organic material in individual marine particles at cape grim during the first aerosol characterization experiment (ace 1). *Journal of Geophysical Research: Atmospheres*, 103(D13):16475–16483, 1998.
- [89] S. L. Miller. Current status of the prebiotic synthesis of small molecules. *Chemica Scripta*, 26:5–11, 1986.
- [90] P.-A. Monnard, A. Kanavarioti, and D. W. Deamer. Eutectic phase polymerization of activated ribonucleotide mixtures yields quasi-equimolar incorporation of purine and pyrimidine nucleobases. *Journal of the American Chemical Society*, 125(45):13734–13740, 2003.

- [91] M. Morasch, C. B. Mast, J. K. Langer, P. Schilcher, and D. Braun. Dry polymerization of 3 , 5 -cyclic gmp to long strands of rna. *ChemBioChem*, 15(6): 879–883, 2014.
- [92] S. N. Moreno and R. Docampo. Polyphosphate and its diverse functions in host cells and pathogens. *PLoS pathogens*, 9(5):e1003230, 2013.
- [93] C. V. Mungi and S. Rajamani. Characterization of RNA-like oligomers from lipid-assisted nonenzymatic synthesis: implications for origin of informational molecules on early earth. *Life*, 5(1):65–84, 2015.
- [94] D. Murphy, D. Thomson, and M. Mahoney. In situ measurements of organics, meteoritic material, mercury, and other elements in aerosols at 5 to 19 kilometers. *Science*, 282(5394):1664–1669, 1998.
- [95] I. Nam, J. K. Lee, H. G. Nam, and R. N. Zare. Abiotic production of sugar phosphates and uridine ribonucleoside in aqueous microdroplets. *Proceedings of the National Academy of Sciences*, 114(47):12396–12400, 2017.
- [96] I. Nam, H. G. Nam, and R. N. Zare. Abiotic synthesis of purine and pyrimidine ribonucleosides in aqueous microdroplets. *Proceedings of the National Academy of Sciences*, 115(1):36–40, 2018.
- [97] S. Nosé. A molecular dynamics method for simulations in the canonical ensemble. *Molecular physics*, 52(2):255–268, 1984.
- [98] S. Nosé. A unified formulation of the constant temperature molecular dynamics methods. *The Journal of chemical physics*, 81(1):511–519, 1984.

- [99] F. Olasagasti and S. Rajamani. Lipid-assisted polymerization of nucleotides. *Life*, 9(4):83, 2019.
- [100] H. Ooka, S. E. McGlynn, and R. Nakamura. Electrochemistry at deep-sea hydrothermal vents: utilization of the thermodynamic driving force towards the autotrophic origin of life. *ChemElectroChem*, 6(5):1316–1323, 2019.
- [101] A. I. Oparin et al. The origin of life on the earth. *The origin of life on the earth.*, (3rd Ed), 1957.
- [102] J. Oró, B. Basile, S. Cortes, C. Shen, and T. Yamrom. The prebiotic synthesis and catalytic role of imidazoles and other condensing agents. *Origins of life*, 14:237–242, 1984.
- [103] M. Parrinello and A. Rahman. Polymorphic transitions in single crystals: A new molecular dynamics method. *Journal of Applied physics*, 52(12):7182–7190, 1981.
- [104] B. K. Pearce. *The Emergence of the RNA World on the Early Earth*. PhD thesis, McMaster University, 2017.
- [105] B. K. Pearce and R. E. Pudritz. Meteorites and the RNA world: A thermodynamic model of nucleobase synthesis within planetesimals. *Astrobiology*, 16(11):853–872, 2016.
- [106] C. Ponnampereuma and R. Mack. Nucleotide synthesis under possible primitive earth conditions. *Science*, 148(3674):1221–1223, 1965.
- [107] C. Ponnampereuma, R. Mariner, and C. Sagan. Formation of adenosine by

- ultra-violet irradiation of a solution of adenine and ribose. *Nature*, 198(4886): 1199–1200, 1963.
- [108] C. Ponnamperna, C. Sagan, and R. Mariner. Synthesis of adenosine triphosphate under possible primitive earth conditions. *Nature*, 199:222–226, 1963.
- [109] R. Porecha and D. Herschlag. RNA radiolabeling. In *Methods in Enzymology*, volume 530, pages 255–279. Elsevier, 2013.
- [110] M. W. Powner, B. Gerland, and J. D. Sutherland. Synthesis of activated pyrimidine ribonucleotides in prebiotically plausible conditions. *Nature*, 459(7244): 239–242, 2009.
- [111] L. Pray. Discovery of dna structure and function: Watson and crick. *Nature Education*, 1(1):100, 2008.
- [112] S. Rajamani, A. Vlassov, S. Benner, A. Coombs, F. Olasagasti, and D. Deamer. Lipid-assisted synthesis of RNA-like polymers from mononucleotides. *Origins of Life and Evolution of Biospheres*, 38(1):57–74, 2008.
- [113] A. Rich. On the problems of evolution and biochemical information transfer. *Horizons in biochemistry*, pages 103–126, 1962.
- [114] D. L. Robertson and G. F. Joyce. Selection in vitro of an RNA enzyme that specifically cleaves single-stranded dna. *Nature*, 344(6265):467–468, 1990.
- [115] D. S. Ross and D. Deamer. Dry/wet cycling and the thermodynamics and kinetics of prebiotic polymer synthesis. *Life*, 6(3):28, 2016.

- [116] F. Scappini, F. Casadei, R. Zamboni, M. Franchi, E. Gallori, and S. Monti. Protective effect of clay minerals on adsorbed nucleic acid against uv radiation: possible role in the origin of life. *International Journal of Astrobiology*, 3(1):17–19, 2004.
- [117] W. G. Scott, A. Szöke, J. Blaustein, S. M. O’rourke, and M. P. Robertson. RNA catalysis, thermodynamics and the origin of life. *Life*, 4(2):131–141, 2014.
- [118] V. Sojo, B. Herschy, A. Whicher, E. Camprubi, and N. Lane. The origin of life in alkaline hydrothermal vents. *Astrobiology*, 16(2):181–197, 2016.
- [119] J. W. Szostak. The narrow road to the deep past: in search of the chemistry of the origin of life. *Angewandte Chemie International Edition*, 56(37):11037–11043, 2017.
- [120] J. W. Szostak. The origin of life on earth and the design of alternative life forms. *Molecular Frontiers Journal*, 1(02):121–131, 2017.
- [121] H. Tervahattu, J. Juhanoja, and K. Kupiainen. Identification of an organic coating on marine aerosol particles by tof-sims. *Journal of Geophysical Research: Atmospheres*, 107(D16):ACH–18, 2002.
- [122] L. Toppozini, H. Dies, D. W. Deamer, and M. C. Rheinstädter. Adenosine monophosphate forms ordered arrays in multilamellar lipid matrices: insights into assembly of nucleic acid for primitive life. *PloS one*, 8(5):e62810, 2013.
- [123] H. Trinks, W. Schröder, and C. K. Biebricher. Ice and the origin of life. *Origins of life and evolution of biospheres*, 35(5):429–445, 2005.

- [124] C. Tuerk and L. Gold. Systematic evolution of ligands by exponential enrichment: RNA ligands to bacteriophage t4 dna polymerase. *science*, 249(4968):505–510, 1990.
- [125] I. Velikyan, S. Acharya, A. Trifonova, A. Földesi, and J. Chattopadhyaya. The p k a's of 2 '-hydroxyl group in nucleosides and nucleotides. *Journal of the American Chemical Society*, 123(12):2893–2894, 2001.
- [126] G. Wächtershäuser. Evolution of the first metabolic cycles. *Proceedings of the National Academy of Sciences*, 87(1):200–204, 1990.
- [127] P. Walde, H. Umakoshi, P. Stano, and F. Mavelli. Emergent properties arising from the assembly of amphiphiles. artificial vesicle membranes as reaction promoters and regulators. *Chemical Communications*, 50(71):10177–10197, 2014.
- [128] T. Walton, W. Zhang, L. Li, C. P. Tam, and J. W. Szostak. The mechanism of nonenzymatic template copying with imidazole-activated nucleotides. *Angewandte Chemie International Edition*, 58(32):10812–10819, 2019.
- [129] H. B. White. Coenzymes as fossils of an earlier metabolic state. *Journal of molecular evolution*, 7(2):101–104, 1976.
- [130] C. R. Woese. The genetic code: The molecular basis for genetic expression. Technical report, 1967.
- [131] W. Zhang, A. Pal, A. Ricardo, and J. W. Szostak. Template-directed nonenzymatic primer extension using 2-methylimidazole-activated morpholino derivatives of guanosine and cytidine. *Journal of the American Chemical Society*, 141(30):12159–12166, 2019.